



Global or regional? Constraining the origins of the middle Bambuí carbon cycle anomaly in Brazil

Huan Cui^{a,b,*}, Lucas Veríssimo Warren^c, Gabriel J. Uehlein^d, Juliana Okubo^c, Xiao-Ming Liu^e, Rebecca E. Plummer^f, Jean-Marc Baele^g, Steven Goderis^{a,b}, Philippe Claeys^{a,b}, Fei Li^h

^a Analytical, Environmental and Geo- Chemistry Group, Vrije Universiteit Brussel, Brussels, Belgium

^b ET-HOME (Evolution and Tracers of the Habitability of Mars and Earth) Astrobiology Research Consortium, Belgium

^c Department of Geology, Institute of Geosciences and Exact Sciences, São Paulo State University (Unesp), Rio Claro, SP, Brazil

^d Centro de Pesquisas Manoel Teixeira da Costa, Instituto de Geociências, Universidade Federal de Minas Gerais, Pampulha, Belo Horizonte, MG 31270-901, Brazil

^e Department of Geological Sciences, University of North Carolina, Chapel Hill, NC 27599, USA

^f Hydrology and Remote Sensing Laboratory, Beltsville Agricultural Research Center, US Department of Agriculture, Beltsville, MD 20705 USA

^g Department of Geology, Faculty of Engineering, University of Mons, Mons, Belgium

^h State Key Laboratory of Oil and Gas Reservoir Geology and Exploitation, School of Geoscience and Technology, Southwest Petroleum University, Chengdu 610500, China

ARTICLE INFO

Keywords:

Middle Bambuí Excursion (MIBE)
Carbon cycle
Sulfur cycle
Neoproterozoic
Chemostratigraphy
Biogeochemistry
Methanogenesis
Diagenesis
Geobiology
Ediacaran-Cambrian transition

ABSTRACT

The Ediacaran-Cambrian Bambuí Group in Brazil records an anomalously positive excursion in carbonate carbon isotopes ($\delta^{13}\text{C}_{\text{carb}}$) with a sustained plateau of ca. +15‰ (aka the Middle Bambuí Excursion–MIBE). Considering that the $\delta^{13}\text{C}_{\text{carb}}$ signals in Ediacaran-Cambrian seawaters do not typically exceed +6‰, the MIBE therefore represents a profound carbon cycle anomaly in Earth's history. Although intensive studies have been done on the Bambuí Group, origins of the MIBE remain enigmatic. In order to better constrain the biogeochemical carbon and sulfur cycles during the MIBE, high-resolution chemostratigraphic analysis was conducted for both the plateau (i.e., Lagoa do Jacaré Formation) and the recovery part (i.e., lower Serra da Saudade Formation) of the MIBE. Chemostratigraphic profiles reveal remarkably different values in $\delta^{13}\text{C}_{\text{carb}}$, $\delta^{13}\text{C}_{\text{org}}$, $\delta^{18}\text{O}_{\text{carb}}$, and $\delta^{34}\text{S}_{\text{pyrite}}$ between these two studied MIBE intervals. The new data show that the plateau of the MIBE is characterized by coupled higher $\delta^{13}\text{C}_{\text{carb}}$, higher $\delta^{13}\text{C}_{\text{org}}$, and higher $\delta^{34}\text{S}_{\text{pyrite}}$ signals compared with the recovery part of the MIBE. Based on multiple lines of sedimentological, geochemical, and model evidence, we propose that the possibilities of enhanced organic carbon burial and porewater methanogenesis are insufficient to explain the MIBE. Instead, local or regional controlling factors, including water-column methanogenesis, low-sulfate conditions, and enhanced carbonate recycling in a restricted basin may have played a role, independently or in unison, in generating this profound positive $\delta^{13}\text{C}_{\text{carb}}$ excursion. Therefore, the MIBE may reflect a regional event, instead of a global carbon cycle anomaly. We caution against the use of the MIBE in chemostratigraphic correlations on a global scale or any other attempt to infer global carbon cycling at that time. The biogeochemical landscape of the late Ediacaran-Cambrian basins and ocean margins may be more heterogeneous than previously thought.

1. Introduction

The Neoproterozoic Era (1000 to 541 Ma) witnessed multiple carbon cycle perturbations, which are recorded as large magnitude positive and negative excursions in carbonate carbon isotope abundances ($\delta^{13}\text{C}_{\text{carb}}$) (Knoll et al., 1986; Kaufman et al., 1997; Halverson et al., 2005; Kaufman et al., 2009; Shields-Zhou et al., 2012). Negative anomalies, like the Shuram Excursion, have been variably ascribed to meteoric water or burial diagenesis (Knauth and Kennedy, 2009; Derry,

2010b), or unusual oceanographic phenomenon related to the oxidation of dissolved organic carbon reservoirs by oxygen or sulfate (Fike et al., 2006; Shields et al., 2019; Zhang et al., 2019; Li et al., 2020) or the production of early authigenic carbonate (Schrag et al., 2013; Cui et al., 2017; Cui et al., 2019b; Cao et al., 2020). By contrast, less attention has been paid to positive $\delta^{13}\text{C}$ extremes, although they have been noted in the Neoproterozoic successions worldwide (Kaufman et al., 1997; Halverson et al., 2005; Kaufman et al., 2009; Cui et al., 2018; Moynihan et al., 2019). Both primary open ocean origins (Knoll et al., 1986;

* Corresponding author at: Department of Earth Sciences, University of Toronto, Toronto, Ontario, Canada.

E-mail address: huan.cui@vub.be (H. Cui).

<https://doi.org/10.1016/j.precamres.2020.105861>

Received 4 March 2020; Received in revised form 2 July 2020; Accepted 13 July 2020

Available online 17 July 2020

0301-9268/© 2020 Elsevier B.V. All rights reserved.

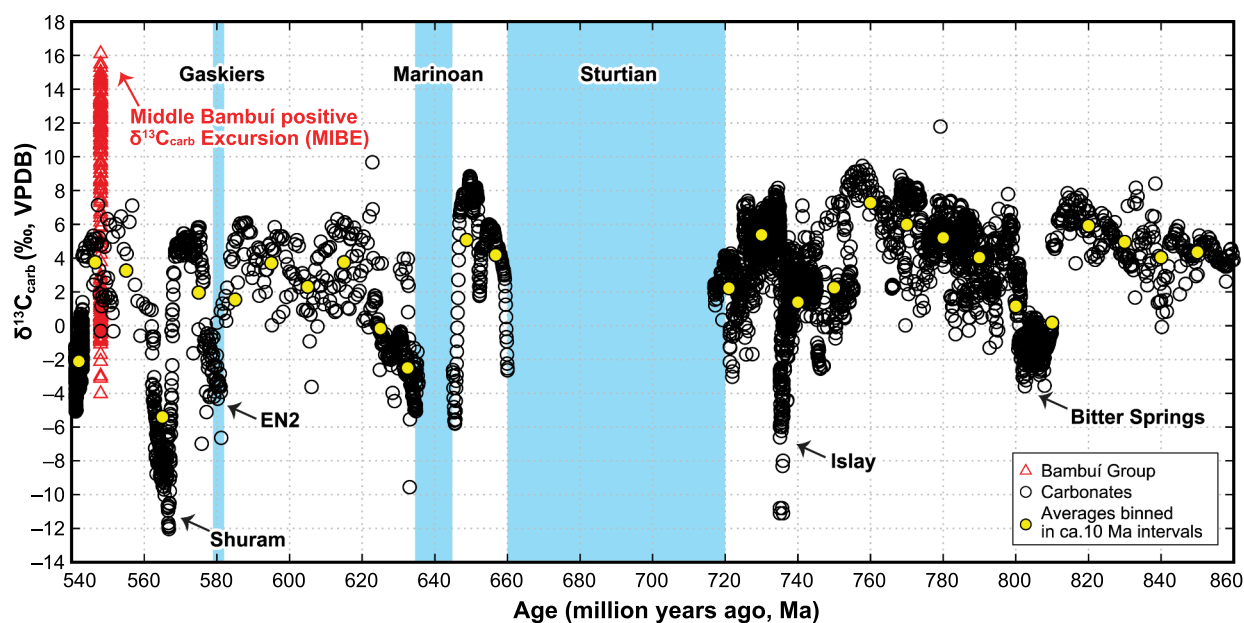


Fig. 1. Time-series compilation of $\delta^{13}\text{C}_{\text{carb}}$ for the time interval from 860 to 540 Ma. Yellow circles represent $\delta^{13}\text{C}_{\text{carb}}$ averages binned in mostly 10 million-year intervals. Data of the Bambiú Group, including the Middle Bambiú $\delta^{13}\text{C}_{\text{carb}}$ Excursion (MIBE), are shown as red triangles. The Sturtian, Marinoan, and Gaskiers glaciations are labelled in blue color. Note the remarkably high $\delta^{13}\text{C}_{\text{carb}}$ values (up to +16‰) from the MIBE. Source of the Bambiú $\delta^{13}\text{C}_{\text{carb}}$ data: (Iyer et al., 1995; Misi and Veizer, 1998; Uhlein et al., 2019; and this study). Source of all other $\delta^{13}\text{C}_{\text{carb}}$ data: (Canfield et al., 2020). Figure modified after Canfield et al. (2020). (For interpretation of the references to color in this figure legend, the reader is referred to the web version of this article.)

Halverson et al., 2005; Johnston et al., 2012) and local or regional origins (Ader et al., 2009; Frimmel, 2010; Cui et al., 2018; Hoffman and Lamothe, 2019; Uhlein et al., 2019; Caetano-Filho et al., 2020) have been proposed for Neoproterozoic positive $\delta^{13}\text{C}_{\text{carb}}$ anomalies, which hampers our understanding of the biogeochemical carbon cycles at that time.

Notably, a sustained positive $\delta^{13}\text{C}_{\text{carb}}$ excursion with values as high as +16‰ has been reported from the Ediacaran-Cambrian Bambiú Group, Brazil (Iyer et al., 1995; Martins and Lemos, 2007; Misi et al., 2007; Misi et al., 2011; Alvarenga et al., 2014; Paula-Santos et al., 2015; Guacaneme et al., 2017; Paula-Santos et al., 2017; Caetano-Filho et al., 2019; Hippert et al., 2019; Uhlein et al., 2019; Caetano-Filho et al., 2020), which has also been named as the Middle Bambiú Excursion–MIBE (Uhlein et al., 2019). Considering that the $\delta^{13}\text{C}_{\text{carb}}$ signals in Ediacaran-Cambrian seawaters do not typically exceed +6‰ (Prokoph et al., 2008; Halverson et al., 2010; Maloof et al., 2010a; Maloof et al., 2010b; Canfield et al., 2020), the MIBE therefore represents a profound carbon cycle anomaly in Earth's history (Fig. 1).

Studies of carbon isotope chemostratigraphy in the past four decades reveal increasingly complex interpretations. Carbon isotope signals of the sedimentary records can be affected by multiple controlling factors (Hayes, 1993; Shields et al., 2002). Potential factors that can lead to variations of $\delta^{13}\text{C}_{\text{carb}}$ signals include (but are not limited to) the rate of organic carbon burial (Knoll et al., 1986; Strauss et al., 1992), the atmospheric partial pressure of CO_2 (Kaufman and Xiao, 2003), syndepositional precipitation of early authigenic carbonate near sediment-water interface (Schrage et al., 2013; Sun and Turchyn, 2014; Cui et al., 2017), aerobic or anaerobic oxidation of organic carbon (including methane) (Jiang et al., 2003; Rothman et al., 2003; Kaufman et al., 2007; Lee et al., 2015; Cui et al., 2017; Shields et al., 2019), early marine diagenesis (Higgins et al., 2018), meteoric water diagenesis (Knauth and Kennedy, 2009; Oehlert and Swart, 2014; Dyer et al., 2017), burial diagenesis (Derry, 2010b), long-term tectonic events (Shields and Mills, 2017), volcanic activities (Paulsen et al., 2017), and preferential weathering of carbonates (Kump et al., 1999). Many of these factors are not mutually exclusive and may have played a role individually or in tandem in changing the $\delta^{13}\text{C}_{\text{carb}}$ signals. Since it is

impossible to evaluate all the above hypotheses in a single study, below we will focus on a few hypotheses that may reflect potential origins of the MIBE.

Canonical models of the global carbon cycle suggests that high $\delta^{13}\text{C}_{\text{carb}}$ signals likely result from an enhanced rate of organic carbon burial given that organic carbon is typically strongly enriched in ^{12}C (Broecker, 1970; Hayes et al., 1999; Kump and Arthur, 1999). Progressive burial of organic matter sequesters ^{12}C in sediments, resulting in the proportional enrichment of ^{13}C in both carbonates and organic matter in the oceans (Broecker, 1970; Derry et al., 1992; Des Marais et al., 1992; Summons and Hayes, 1992; Kump and Arthur, 1999; Ripperdan, 2001). Based on this model, positive $\delta^{13}\text{C}_{\text{carb}}$ excursions in sedimentary records have been widely regarded as indicators of oxygenation events in Earth history (Broecker, 1970; Knoll et al., 1986; Planavsky et al., 2012; Cui et al., 2018).

Alternatively, highly positive $\delta^{13}\text{C}_{\text{carb}}$ signals can also be explained by the occurrence of methanogenesis in porewaters or seawaters (Ader et al., 2009; Caetano-Filho et al., 2020; Petrov and Pokrovsky, 2020). This is possible considering that the residual alkalinity after fermentation (i.e., methanogenesis) is typically strongly enriched in ^{13}C after the ^{13}C -depleted methane gas is removed from the system (Claypool and Kaplan, 1974; Irwin et al., 1977; Talbot and Kelts, 1986; Meister et al., 2007; Wehrmann et al., 2011; Birgel et al., 2015; Pierre et al., 2016). Such a process occurs locally in the modern ocean, but could be widespread in the Precambrian ocean where the seawater was mostly anoxic and sulfate-depleted (Lyons et al., 2014; Sperling et al., 2015) and could therefore facilitate the occurrence of methanogenesis in marine environments.

In addition, local or regional environmental factors may also have played a role in generating positive $\delta^{13}\text{C}_{\text{carb}}$ anomalies. The coupled processes of methanogenesis and evaporation/degassing have been proposed for multiple terrestrial lakes in modern environments where extremely positive $\delta^{13}\text{C}_{\text{carb}}$ signals have been found (Stiller et al., 1985; Gomez et al., 2014; Birgel et al., 2015; Buongiorno et al., 2019). However, testing the evaporation/degassing hypothesis for deep-time $\delta^{13}\text{C}_{\text{carb}}$ anomalies still remains challenging given the dearth of direct geochemical proxies for these unusual hydrological conditions.

In this study, we explore the origins of the MIBE by testing multiple biogeochemical or diagenetic hypotheses. In order to utilize the inherent linkages between C and S cycles (Berner and Petsch, 1998; Berner, 1999; Planavsky et al., 2012; Cui et al., 2018; Shields et al., 2019), we conduct an integrated sedimentological and chemostratigraphic study of two different intervals of the MIBE. Both the plateau (represented by the carbonate-dominated KM7-14 section) and the recovery part (represented by the siliciclastic-dominated KM7-12 section) of the MIBE were investigated in this study. Distinct geochemical signals have been found between the two studied sections. Based on the new results, we evaluated multiple hypotheses that can potentially account for the MIBE.

2. Geological context

2.1. Sedimentology and stratigraphy

The Bambuí Group covers the São Francisco Craton in the central-eastern part of Brazil, encompassing a basal diamictite and overlying mixed carbonate-siliciclastic deposits of the Sete Lagoas, Serra de Santa Helena, Lagoa do Jacaré, Serra da Saudade, and Três Marias formations (Dardenne, 1978) (Figs. 2, 3). Originally, the Bambuí Group was interpreted to be entirely deposited in a foreland basin, in response to the uplift of the southern Brasília orogenic belt along the western margin of the São Francisco Craton (Alkmim and Martins-Neto, 2012; Reis and Suss, 2016; Reis et al., 2017; Uhlein et al., 2017). However, recent geochronologic and paleontological data (see Section 2.2 for details) indicate an Ediacaran age for the lower part of the Bambuí Group, which is substantially younger than the peak activity age of the Brasília belt, and therefore challenges the model of a foreland basin for the Bambuí Group. An alternative interpretation suggests a depositional environment of an epeiric ramp for the Sete Lagoas Formation (Drummond et al., 2015; Hippertt et al., 2019) with a transition to a foreland system toward the upper part of the Bambuí Group (Martins and Lemos, 2007).

Samples in this study were collected from the Lagoa do Jacaré and Serra da Saudade formations of the Bambuí Group in the São Francisco Craton, east-central Brazil (Figs. 2, 3; supplementary material). The Lagoa do Jacaré Formation is stratigraphically located above the Serra de Santa Helena Formation and below the Serra da Saudade Formation (Fig. 3). This unit comprises an up to ca. 140-m-thick mixed carbonate-siliciclastic succession of interbedded black shale, siltstone and carbonate (Dardenne, 1978; Uhlein et al., 2019) (Figs. 4, 5). The Lagoa do Jacaré Formation in the southern part of the Bambuí Basin has been poorly studied. However, in the northern part of the basin this unit can be informally divided into two stratigraphic intervals: an carbonate-dominated basal succession (~70 m) and a siliciclastic-dominated upper succession (~70 m) (Uhleim et al., 2019).

The basal part of the Lagoa do Jacaré Formation consists primarily of microbialite facies and domal or columnar stromatolites (dos Santos et al., 2018) (Fig. 4C–E). These microbial facies are commonly interbedded with massive mudstone and wave-ripple cross-laminated grainstone (Fig. 4G–L) with locally preserved syneresis cracks (Fig. 5A–D) (Iglesias and Uhlein, 2009). It is common to see tabular oolitic beds with hummocky cross-stratification in the basal Lagoa do Jacaré Formation (Uhleim et al., 2019). The presence of rip-up breccias (Fig. 4I–L), ooids (Fig. 4F), wave ripple and cross bedding (Fig. 4G–I) suggests an overall shallow and energetic environment. The occurrence of stromatolites and ooid deposits suggests that these shallow waters were saturated with respect to CaCO₃. The syneresis cracks in the Lagoa do Jacaré Formation (Fig. 5A–D) indicate the occurrence of sediment shrinkage without subaerial exposure, which typically results from abrupt changes in seawater salinity or earthquake-induced dewatering (Pratt, 1998).

The upper part of the Lagoa do Jacaré Formation contains a much higher proportion of fine-grained siliciclastic deposits composed of

siltstone, shale, carbonate mudstone and rare rhythmite (mudstone/shale) deposits. This part of the succession is interpreted as having been deposited above storm-wave base level during a regional sea level rise (Uhleim et al., 2019). The intercalation between siliciclastic and carbonate facies has been proposed to be related to high-frequency variations in sediment input controlled by climatic and tectonic factors (Uhleim et al., 2019).

2.2. Age constraints

The precise depositional age of the Bambuí Group is still uncertain. Both Cryogenian and Ediacaran ages have been proposed for the Bambuí Group. Largely based on the overall high $\delta^{13}\text{C}_{\text{carb}}$ values, low $^{87}\text{Sr}/^{86}\text{Sr}$ values (< 0.7080) (Misi et al., 2007; Kaufman et al., 2009), and a controversial Pb–Pb age of 740 ± 22 Ma (Babinski et al., 2007) for the Sete Lagoas cap carbonate, the Bambuí Group has been proposed to represent a sedimentary package of the Cryogenian (pre-Marinoan) Period (Misi et al., 2007; Kaufman et al., 2009). However, an increasing number of more recent studies on biostratigraphy (Warren et al., 2014; Perrella Júnior et al., 2017), geochronology (Rodrigues, 2008; Paula-Santos et al., 2015; Moreira et al., 2020; Tavares et al., 2020), and chemostratigraphy (Caxito et al., 2012; Alvarenga et al., 2014; Paula-Santos et al., 2015; Sial et al., 2016; Paula-Santos et al., 2017) argue that the Bambuí Group may be largely deposited in the late Ediacaran–Cambrian periods. It is notable that terminal Ediacaran index fossil *Cloudina* has been reported from the middle Sete Lagoas Formation (Warren et al., 2014; Perrella Júnior et al., 2017) (Fig. 2A, 3), though the fossil preservation is not ideal.

Published geochronological data suggest that the Lagoa do Jacaré and Serra da Saudade formations were largely deposited from the late Ediacaran to Cambrian Period (Fig. 3). Two independent studies of detrital zircon dating of the underlying Sete Lagoas Formation reveal the youngest U–Pb age of 610 Ma (Rodrigues, 2008) and 557 Ma (Paula-Santos et al., 2015), respectively, which are interpreted as the maximum depositional ages. In the overlying Serra da Saudade Formation and Três Marias Formation, a volcanic zircon age of 520.2 ± 5.3 Ma has been retrieved from a tuff layer (i.e., described as a “white mudstone” by Moreira et al., 2020) and the youngest detrital zircon age of 527 ± 4 Ma from a sandstone layer (Tavares et al., 2020) has been reported. These ages indicate a late Ediacaran, or even Cambrian age for the Lagoa do Jacaré Formation. Notably, in addition to the controversial Pb–Pb age of 740 ± 22 Ma (Babinski et al., 2007), a second Pb–Pb age of 608 ± 19 Ma (Caxito et al., 2018) was recently published from the Sete Lagoas cap carbonate, which challenges the earlier Cryogenian age and complicates the applications of Pb–Pb dating for carbonate samples.

An additional piece of evidence for a basal Ediacaran age of the Sete Lagoas cap carbonate comes from triple oxygen isotopes. Large triple oxygen isotope ($\Delta^{17}\text{O}$) anomalies down to -1.05‰ have been reported from the Sete Lagoas cap carbonate (Crockford et al., 2018). Such anomalous signals — also known as the Marinoan Oxygen-17 Depletion (MOSD) event — have thus far only been found in the Marinoan cap carbonates on a global scale (Bao et al., 2008; Zhou et al., 2010; Cao and Bao, 2013; Killingsworth et al., 2013; Bao, 2015; Crockford et al., 2018).

In summary, although the precise depositional age for the Bambuí Group is still controversial, the academic community working on the Neoproterozoic Era, in general, leans towards an Ediacaran–Cambrian age for the Bambuí Group. In this study, we assume a late Ediacaran–Cambrian age for the Lagoa do Jacaré and Serra da Saudade formations and hope more studies in the future can clarify this controversy.

2.3. Samples in this study

Outcrops of the MIBE in the studied region are generally limited to

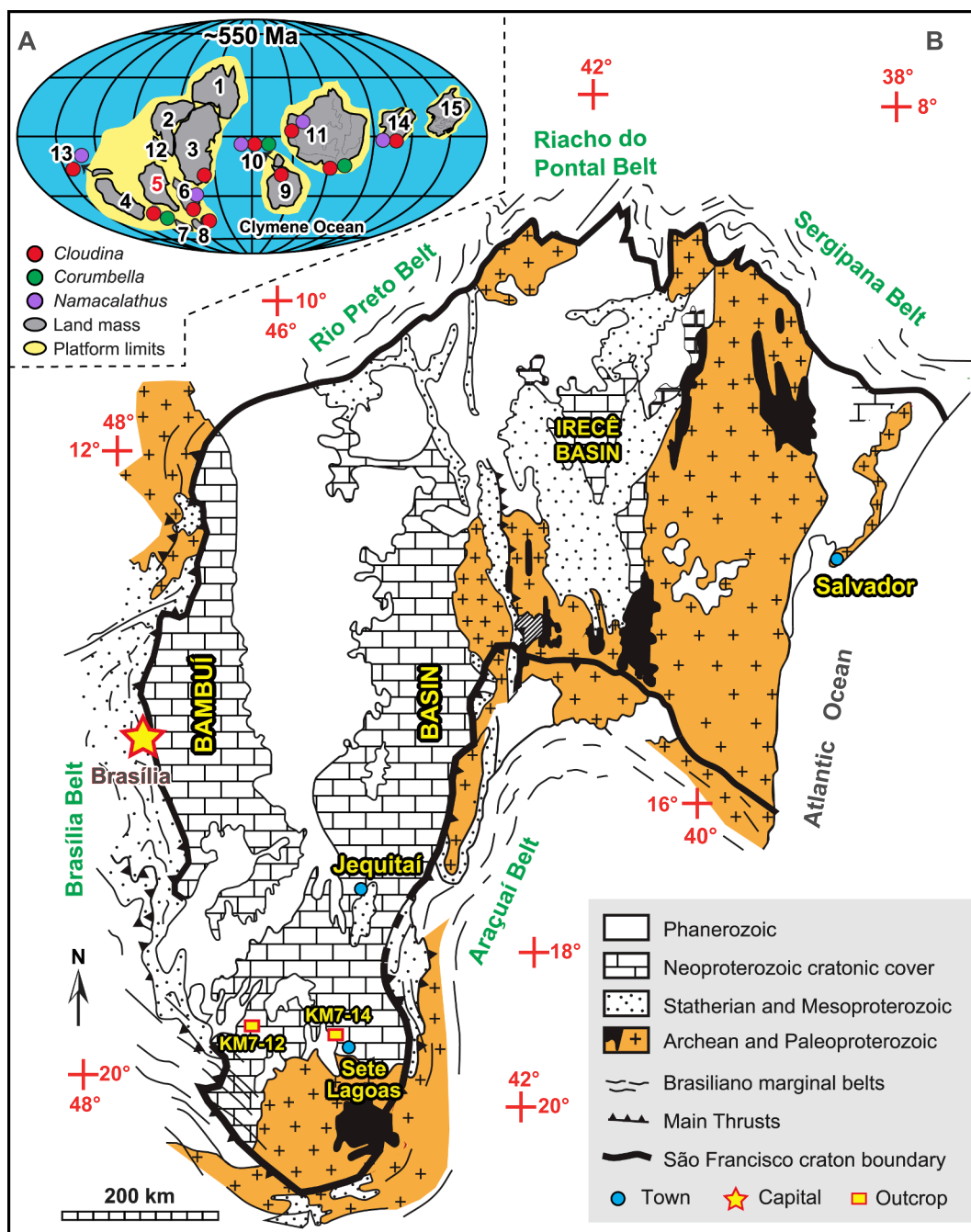


Fig. 2. (A) Paleogeographic reconstructions during ca. 550 Ma highlighting the *Cloudina*-bearing localities with, or without, *Corumbella* and *Namacalathus* occurrences. Note that the São Francisco craton (marked as number 5) was located in the center of the Gondwana paleo-continent. 1–Australia, 2–India, 3–Antarctica, 4–West Africa, 5–Congo–São Francisco, 6–Kalahari, 7–Paraná, 8–Rio de la Plata, 9–Amazonia, 10–Rio Apa, 11–Laurentia, 12–Madagascar, 13–Arabia–Nubia, 14–Siberia, 15–Baltica. Fossil data: (Germs, 1972; Yochelson and Stump, 1977; Grotzinger et al., 2000; Hagadorn and Waggoner, 2000; Hofmann and Mountjoy, 2001; Amthor et al., 2003; Gaucher et al., 2003; Kontorovich et al., 2008; Warren et al., 2011). Paleogeographic data: (Trindade et al., 2006; Li et al., 2008; Tohver et al., 2012). Image modified after (Warren et al., 2014; Warren et al., 2017). (B) Geological map of the São Francisco craton (modified after Paula-Santos et al., 2015; Reis and Suss, 2016; Paula-Santos et al., 2017). Chemostratigraphic analysis in this study was focused on the KM7-14 and KM7-12 sections. Detailed geological maps of the KM7-14 section and the KM7-12 section are available in the online supplementary material (Figs. S1, S2).

scattered quarries and roadcuts. The sections in this study include the KM7-14 section (Lagoa do Jacaré Formation, GMG quarry, S 19°15.089', W 44° 23.405', Fig. S1), the KM7-12 section (lower Serra da Saudade Formation, Abaeté Quarry, S 19°6.810', W 45° 43.061', Fig. S2), the KM 7-10 section (Lagoa do Jacaré Formation, Pedra do Chumbo quarry, S 19°46.670', W 45° 28.698'), and the KM7-13 section (Lagoa do Jacaré Formation, Cacau Quarry outside of Pompéu, S 19°11.152', W 44° 57.563').

Samples for chemostratigraphy were collected from the carbonate-dominated KM7-14 section (Lagoa do Jacaré Formation) and the siliciclastic-dominated KM7-12 section (lower Serra da Saudade Formation). In addition, one ooid grainstone/limestone (Fig. 6F, 10A–J) and two cross-bedded grainstone samples were collected from the Lagoa do Jacaré Formation at the KM7-13 section. A mudstone sample with planar lamination was also collected and analyzed from the KM 7-10 section. The complete sample list can be found in the

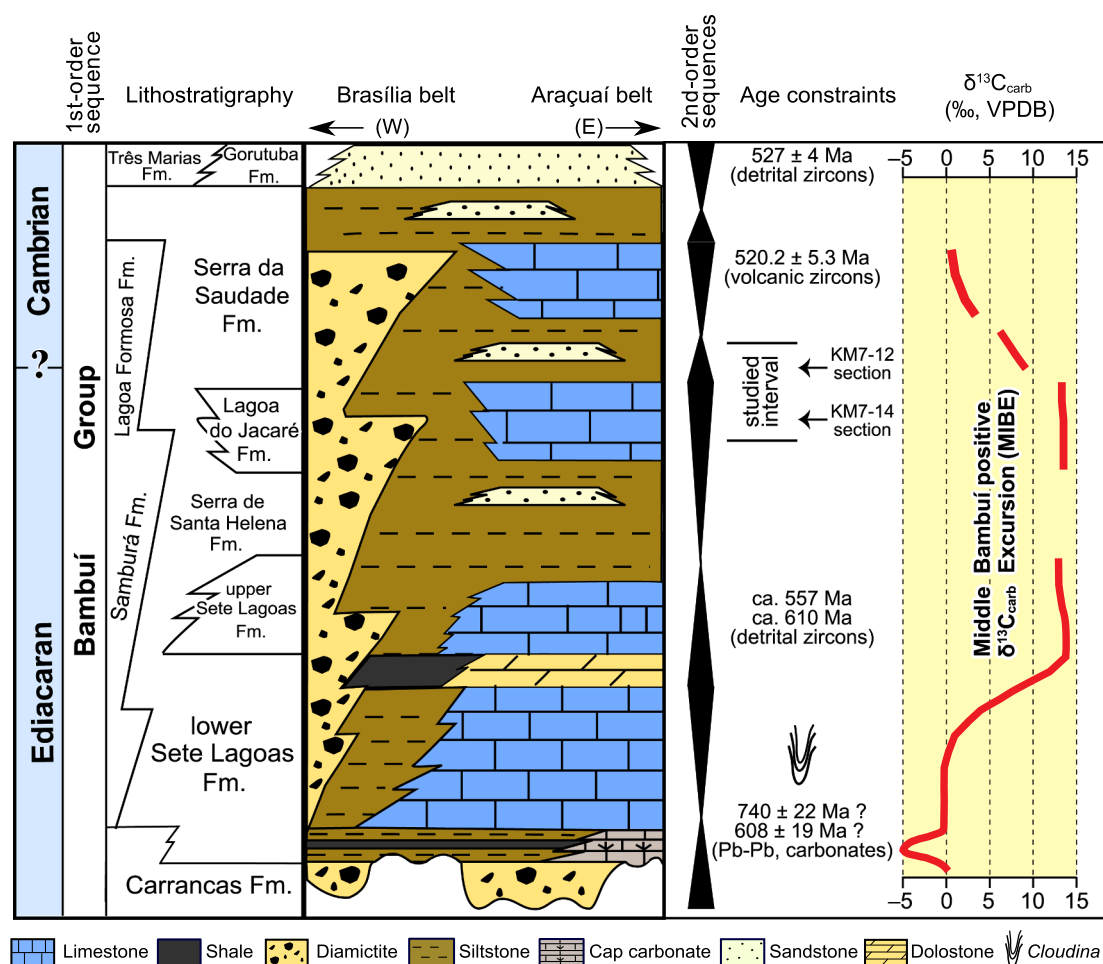


Fig. 3. A summary of the litho- and chemo-stratigraphy of the Ediacaran-Cambrian Bambuí Group, Brazil. Note the large positive $\delta^{13}\text{C}_{\text{carb}}$ excursion (aka Middle Bambuí Excursion–MIBE) (Uhlen et al., 2019). The Lagoa do Jacaré and Serra da Saudade formations are the focus of this study. Source of the fossil results: (Warren et al., 2014; Perrella Júnior et al., 2017). Sources of the geochronologic age constraints: U-Pb age of 527 ± 4 Ma from detrital zircons in the Três Marias Formation (Tavares et al., 2020); U-Pb age of 520.2 ± 5.3 Ma from volcanic zircons in the upper Serra da Saudade Formation (Moreira et al., 2020); U-Pb age of ca. 557 Ma from detrital zircons of the Sete Lagoas Formation (Paula-Santos et al., 2015); U-Pb age of ca. 610 Ma from detrital zircons of the Sete Lagoas Formation (Rodrigues, 2008); Pb-Pb age of 740 ± 22 Ma from Sete Lagoas cap carbonates (Babinski et al., 2007); Pb-Pb age of 608 ± 19 Ma from Sete Lagoas cap carbonates (Caxito et al., 2018). Based on the above age constraints, the Bambuí Group represents a transition from the Ediacaran to the Cambrian Period. Note the apparent inconsistency between the two published Pb-Pb age data from the Sete Lagoas cap carbonates, which challenges the credibility of the Pb-Pb technique in dating carbonates. Figure modified after Caetano-Filho et al. (2020).

online supplementary material.

3. Methods

Petrographic observations under both polarized light and cathodoluminescence were conducted at the Department of Geology, University of Mons, Belgium. The geochemical analyses in this study include paired carbonate carbon and oxygen isotopes ($\delta^{13}\text{C}_{\text{carb}}$, $\delta^{18}\text{O}_{\text{carb}}$), organic carbon isotopes ($\delta^{13}\text{C}_{\text{org}}$), total organic carbon content (TOC), the content of total sulfur in acidified residuals (TS), sulfur isotopes of pyrite ($\delta^{34}\text{S}_{\text{pyrite}}$ approximated by $\delta^{34}\text{S}_{\text{TS}}$) and carbonate-associated sulfate ($\delta^{34}\text{S}_{\text{CAS}}$), Sr isotope ratios ($^{87}\text{Sr}/^{86}\text{Sr}$), and concentrations of major (e.g., Ca, Mg, Sr, K, Fe) and trace (e.g., REE, Mn, Rb) elements. All the isotopic analyses were conducted in the Department of Geology, University of Maryland. Elemental concentrations were analyzed at the Carnegie Institution of Washington. Detailed methods have been published in previous papers (Cui et al., 2015; Cui et al., 2016a; Cui et al., 2016b; Liu et al., 2016), and are briefly summarized below.

3.1. Cathodoluminescence

Cathodoluminescence excitation was achieved with a cold cathode CITL CL system (Cambridge Image Technology - model Mk5, UK) at the Department of Geology, University of Mons, Belgium. The system was operated by using an acceleration voltage of 15 kV and a beam current of 500 μA . With these settings, the unfocused beam had a current density of about 8 $\mu\text{A}/\text{mm}^2$. CL images were captured with a Peltier-cooled digital color camera (Lumenera model Infinity 4, Canada), set from 0.1 to a few seconds exposure time depending on CL intensity and microscope magnification. Multiple frame averaging was used to reduce noise. Color calibration of the camera (white balance) was performed using the blue-filtered, tungsten-halogen light source of the microscope. This may result in CL colors that are slightly different from other equipment (especially around the yellow band, which is narrow) but can ensure more or less standardized observation conditions.

3.2. $\delta^{13}\text{C}_{\text{carb}}$ and $\delta^{18}\text{O}_{\text{carb}}$ analysis

Powders for $\delta^{13}\text{C}_{\text{carb}}$ and $\delta^{18}\text{O}_{\text{carb}}$ analyses were collected on polished slabs using a press micro-drill. Micro-drilling was guided by

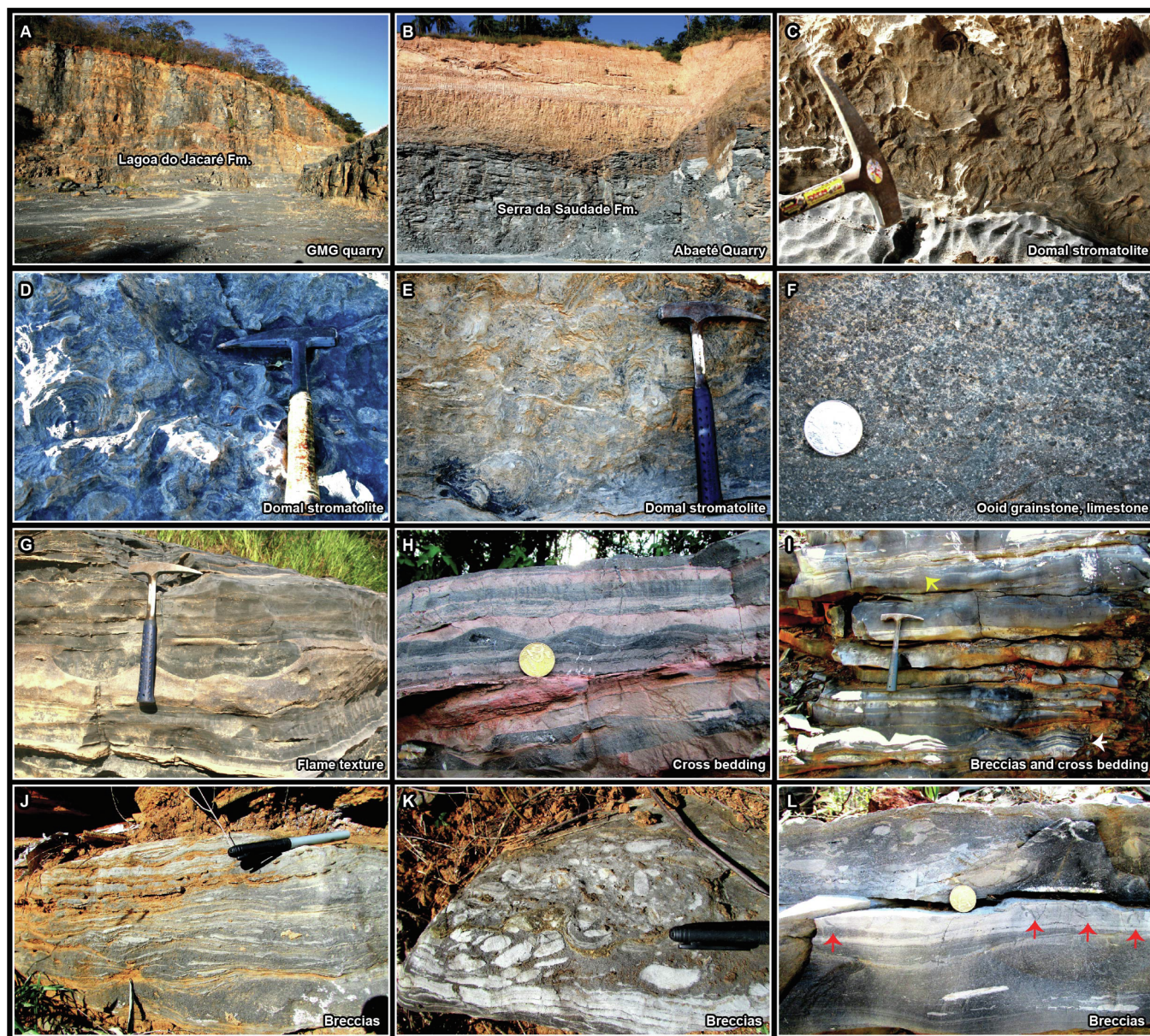


Fig. 4. Field observations of the middle Bambuí Group in the Bambuí Basin, Brazil. Except for image B that shows the Serra da Saudade Formation, all the other images show the Lagoa do Jacaré Formation. (A) Outcrop overview showing black limestone facies of the Lagoa do Jacaré Formation, GMG Quarry (B) Outcrop showing the Serra da Saudade Formation, Abaeté Quarry. (C–E) Domal stromatolites. (F) Massive oolitic grainstone/limestone facies from the Lagoa do Jacaré Formation. (G) Flame structures. (H) Bedded limestones with cross beddings. (I) Brecciated beds with cross beddings (white arrow) and cross beddings (yellow arrow). (J, K) Breccias and platy clasts. (L) Brecciated beds and syneresis cracks (lateral view, red arrows). Images A–G were taken in the southern part of the Bambuí Basin (see Section 2.3 for detailed locations); Images H–L were taken from a section close to the Januária city in the northern part of the Bambuí Basin, and the corresponding geochemical study in this area can be found in Uhlein et al. (2019). (For interpretation of the references to color in this figure legend, the reader is referred to the web version of this article.)

petrographic fabrics so that primary fabrics (e.g., ooids, marine cements, micrite) were sampled for further geochemical measurement. We indeed found few horizons with heavily recrystallized carbonate or veins, but those were strictly avoided during sampling. The precision for both carbon and oxygen isotopes based on repeated measurement of reference materials was routinely better than 0.1%.

3.3. $\delta^{13}\text{C}_{\text{org}}$ and $\delta^{34}\text{S}_{\text{pyrite}}$ analyses

The $\delta^{13}\text{C}_{\text{org}}$ and $\delta^{34}\text{S}_{\text{pyrite}}$ compositions of bulk powders were measured by combustion of decalcified residues to CO_2 or SO_2 with a Eurovector elemental analyzer in-line with an Elementar Isoprime isotope ratio mass spectrometer. Approximately 15 g of fresh rock chips

lacking secondary veins or weathered surfaces were crushed and repeatedly ($2 \times$ or more) acidified with 3 M HCl overnight to quantitatively remove carbonate. These residues were then washed with ultra-pure Milli-Q water repeatedly ($3 \times$ or more) to neutral pH, decanted, and dried in an 80 °C oven overnight for subsequent $\delta^{13}\text{C}_{\text{org}}$ and $\delta^{34}\text{S}_{\text{pyrite}}$ analyses. Total sulfur in the acidified residues was dominated by pyrite ($\delta^{34}\text{S}_{\text{pyrite}} \approx \delta^{34}\text{S}_{\text{TS}}$), although there may have also been trace amounts of organic sulfur. Uncertainties for $\delta^{13}\text{C}_{\text{org}}$ and $\delta^{34}\text{S}_{\text{pyrite}}$ measurements determined by multiple analyses of standard materials were better than 0.1% and 0.3%, respectively.

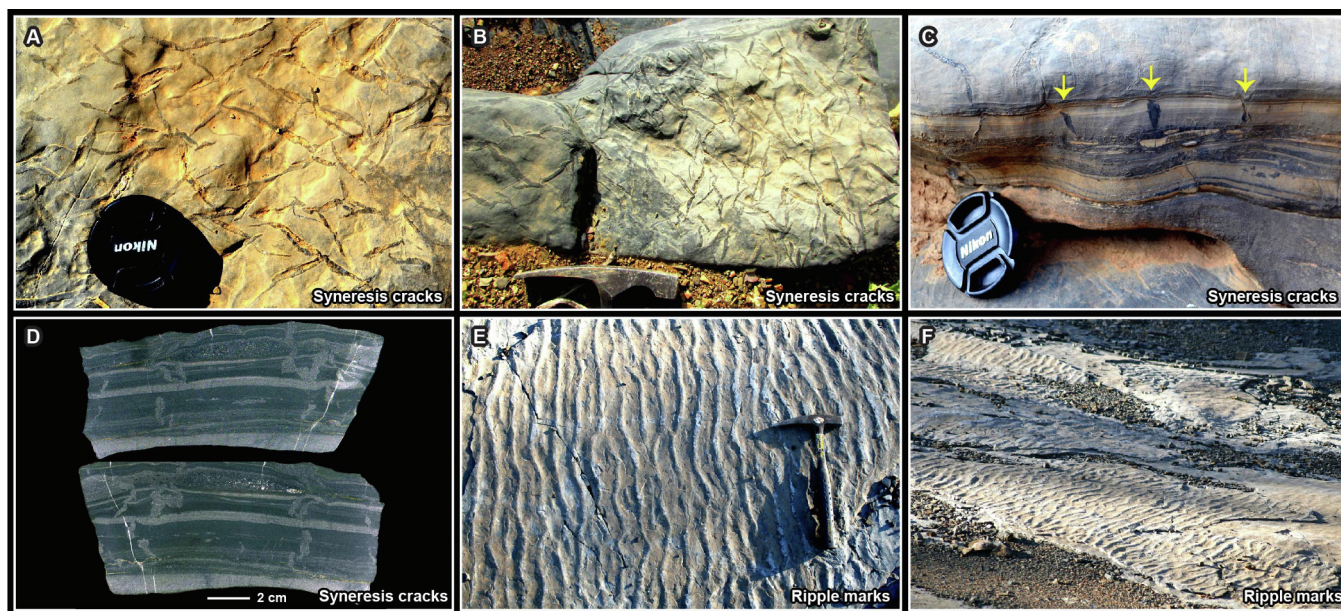


Fig. 5. Syneresis cracks and ripple marks in the Lagoa do Jacaré Formation, Brazil. (A, B) Top views of the syneresis cracks; (C, D) Lateral views of the syneresis cracks (yellow arrows). (E, F) Ripple marks, Pedra do Chumbo Quarry. (For interpretation of the references to color in this figure legend, the reader is referred to the web version of this article.)

3.4. $\delta^{34}\text{S}_{\text{CAS}}$ analysis

The $\delta^{34}\text{S}_{\text{CAS}}$ analysis was conducted by extracting carbonate-associated sulfate (CAS) of the samples and then convert the dissolved sulfate to barite before isotope analysis. To minimize the contamination of soluble non-CAS sulfate (Marengo et al., 2008; Wotte et al., 2012; Peng et al., 2014; Schobben et al., 2015), ~100 g of crushed bulk powders were leached by 10% NaCl solutions for at least 10 times with at least two hours for each time, and then washed with Milli-Q water for at least 3 times prior to acidification of the leached powders with 3 M HCl. CAS precipitates were then collected as BaSO_4 three days after BaCl_2 was added to the solution. The BaSO_4 precipitates were packed into folded tin cups with V_2O_5 for combustion to SO_2 in a Eurovector elemental analyzer in-line with a second Elementar Isoprime isotope ratio mass spectrometer, which measured isotope abundances. The precision for $\delta^{34}\text{S}_{\text{CAS}}$ measurements determined by multiple analyses of standard materials during analytical sessions is better than 0.3‰.

3.5. $^{87}\text{Sr}/^{86}\text{Sr}$ analysis

For $^{87}\text{Sr}/^{86}\text{Sr}$ analysis, micro-drilled powders (ca. 5–10 mg) were leached three times in 0.2 M ammonium acetate (pH ~8.2) to remove exchangeable Sr from non-carbonate minerals, and then rinsed three times with Milli-Q water. The leached powder was centrifuged, decanted, and acidified with doubly distilled 0.5 M acetic acid overnight to remove strontium from the carbonate crystal lattice. The supernatant was centrifuged to remove insoluble residues and then decanted, dried, and subsequently dissolved in 200 μl of 3 M HNO_3 . Strontium separation by cation exchange was carried out using a small polyethylene column containing ~1 cm thickness of Eichrom[®]Sr specific resin. The prepared filaments were measured using the VG Sector 54 thermal ionization mass spectrometer in the TIMS facility of the University of Maryland Geochemistry Laboratories. Final data have been corrected for fractionation using the standard value $^{86}\text{Sr}/^{88}\text{Sr} = 0.1194$. No corrections for Rb decay have been carried out given the very low Rb/Sr ratios in all the analyzed samples. Repeated analysis of the NBS SRM987 standard yields an average value of $^{87}\text{Sr}/^{86}\text{Sr} = 0.710245 \pm 0.000011$ (2σ) during the analytical window.

3.6. Major and trace elemental analysis

Major and trace elemental abundances of micro-drilled carbonates were analyzed for the carbonate-dominated KM7-14 section in order to evaluate the degree of diagenetic alteration and reconstruct redox conditions of the depositional environment. Aliquots of the micro-drilled carbonate powders were dissolved in 0.4 M HNO_3 , centrifuged, and only solutions were analyzed. Any clay fractions, if present, would not have been dissolved by the dilute acid, assuring that results represent elemental content of the carbonate phases. The resulting solutions were analyzed on a Thermo Scientific[®] iCAP-Q ICP-MS (Inductively Coupled Plasma – Mass Spectrometry) at the Carnegie Institution of Washington. Precision of these analyses as determined by repeated measurements of a house standard carbonate was < 5% (2σ) for major elements with high concentrations and < 10% (2σ) for trace elements and REEs.

4. Results

Integrated sedimentological and geochemical results are shown in Figs. 6–12. Samples from the Lagoa do Jacaré Formation show sedimentological textures of undulated lamination, planar lamination, or ooids (Fig. 6; supplementary material), suggesting an overall dynamic depositional environment. In contrast, samples from the Serra da Saudade Formation look very homogeneous (Fig. 7; supplementary material), suggesting a relatively quiet environment. Chemostratigraphic analysis was focused on the carbonate-dominated KM7-14 section (Lagoa do Jacaré Formation) and the siliciclastic-dominated KM7-12 section (Serra da Saudade Formation). These two sections show distinct values of $\delta^{13}\text{C}_{\text{carb}}$, $\delta^{13}\text{C}_{\text{org}}$, $\delta^{18}\text{O}_{\text{carb}}$, and $\delta^{34}\text{S}_{\text{pyrite}}$ (Figs. 11, S3, S4). Here we briefly summarize the results as below.

4.1. $\delta^{13}\text{C}_{\text{carb}}$ and $\delta^{18}\text{O}_{\text{carb}}$ data

The $\delta^{13}\text{C}_{\text{carb}}$ profile of the carbonate-dominated KM7-14 section shows anomalously positive values from +11.7‰ to +13.9‰ (mean: +12.6‰). In contrast, the $\delta^{13}\text{C}_{\text{carb}}$ profile of the siltstone-dominated KM7-12 section records relatively lower values between +5.1‰ to +9.0‰ (mean: +7.5‰) (Fig. 11B, 11L).

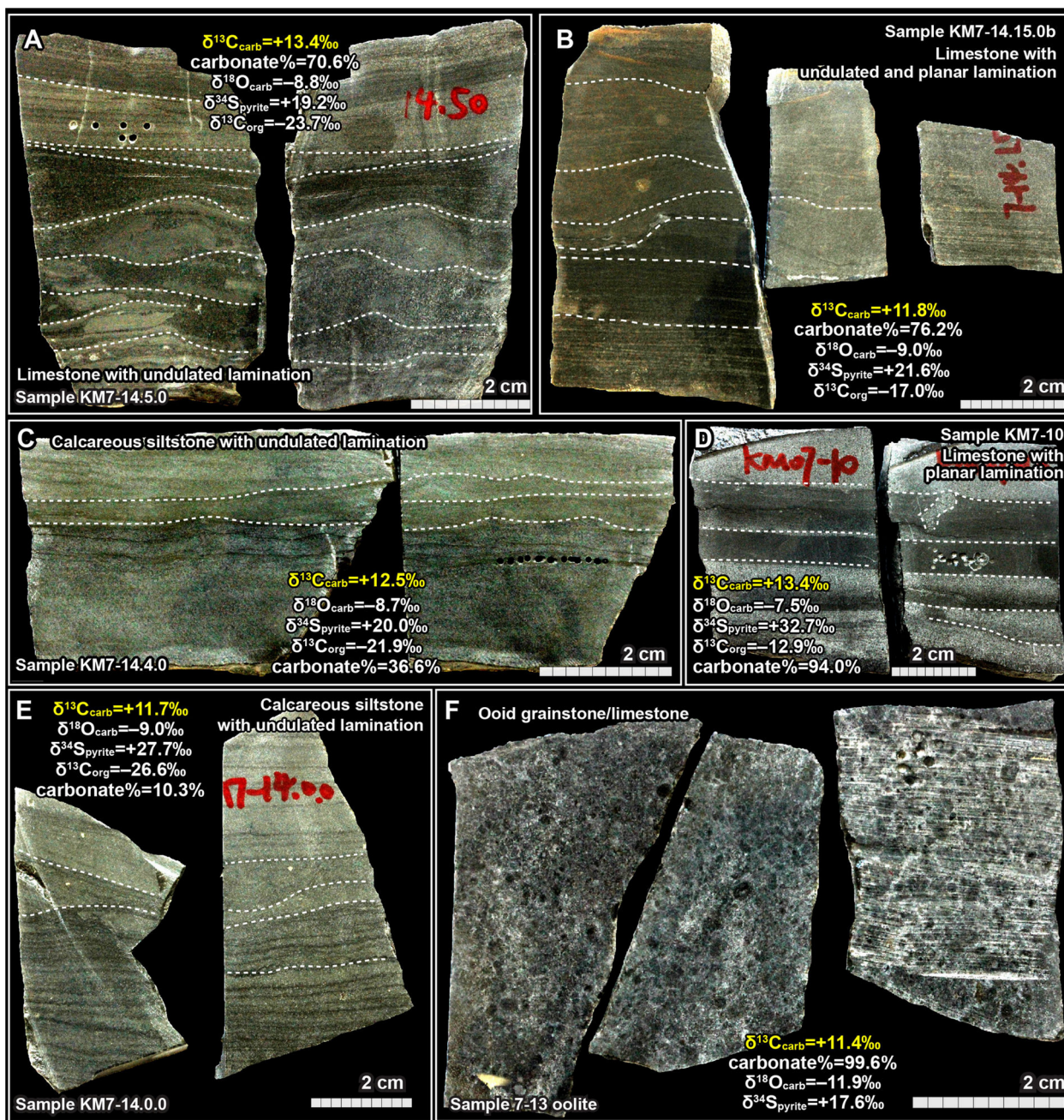


Fig. 6. Rock slabs and geochemical data of the Lagoa do Jacaré Formation at the KM7-14, KM7-13, and KM7-10 sections, Brazil. (A, B) Limestone samples with undulated laminations. (C) A calcareous siltstone sample with laminated beddings (microbial mats?). (D) A limestone sample with thinly interbedded layers. (E) A calcareous siltstone sample with laminated beddings (microbial mats?) (F) An ooid grainstone/limestone sample. Corresponding microscopic images of this sample can be found in Fig. 10A–J. The brightness and contrast of all the images have been enhanced in order to achieve the best view of detailed sedimentary textures. More sample slab images are available in the online supplementary materials.

The $\delta^{18}\text{O}_{\text{carb}}$ profile of the carbonate-dominated KM7-14 section also shows higher values than that of the siltstone-dominated KM7-12 section. The $\delta^{18}\text{O}_{\text{carb}}$ data reveal a range from -15.3‰ to -12.8‰ (mean: -13.9‰) at the KM7-12 section and a range from -9.7‰ to -6.7‰ (mean: -8.7‰) at the KM7-14 section (Fig. 11C, 11M).

4.2. $\delta^{13}\text{C}_{\text{org}}$ and $\Delta\delta^{13}\text{C}$ data

Interestingly, the organic matter extracted from the KM7-14 section also shows strong ^{13}C -enrichments compared with the ones from the KM7-12 section. The $\delta^{13}\text{C}_{\text{org}}$ values show a range from -26.6‰ up to -15.2‰ (mean: -20.2‰) at the KM7-14 section and a range from

-28.1‰ to -24.4‰ (mean: -25.8‰) at the KM7-12 section (Fig. 11D, 11N).

Although the paired $\delta^{13}\text{C}_{\text{carb}}$ and $\delta^{13}\text{C}_{\text{org}}$ profiles have distinct values at these two sections, the calculated $\Delta\delta^{13}\text{C}_{\text{carb-org}}$ ($=\delta^{13}\text{C}_{\text{carb}} - \delta^{13}\text{C}_{\text{org}}$) data are similar, with mean values of 33.4‰ at the KM7-12 section and 32.8‰ at the KM7-14 section (Fig. 11E, 11O).

4.3. Paired $\delta^{34}\text{S}_{\text{pyrite}}$ and $\delta^{34}\text{S}_{\text{CAS}}$ data

The $\delta^{34}\text{S}_{\text{pyrite}}$ profiles at both sections show distinct values. The $\delta^{34}\text{S}_{\text{pyrite}}$ data show a range from -3.9‰ to $+35.8\text{‰}$ (mean: $+13.7\text{‰}$) at the KM7-12 section and a range from -1.0‰ to $+29.1\text{‰}$

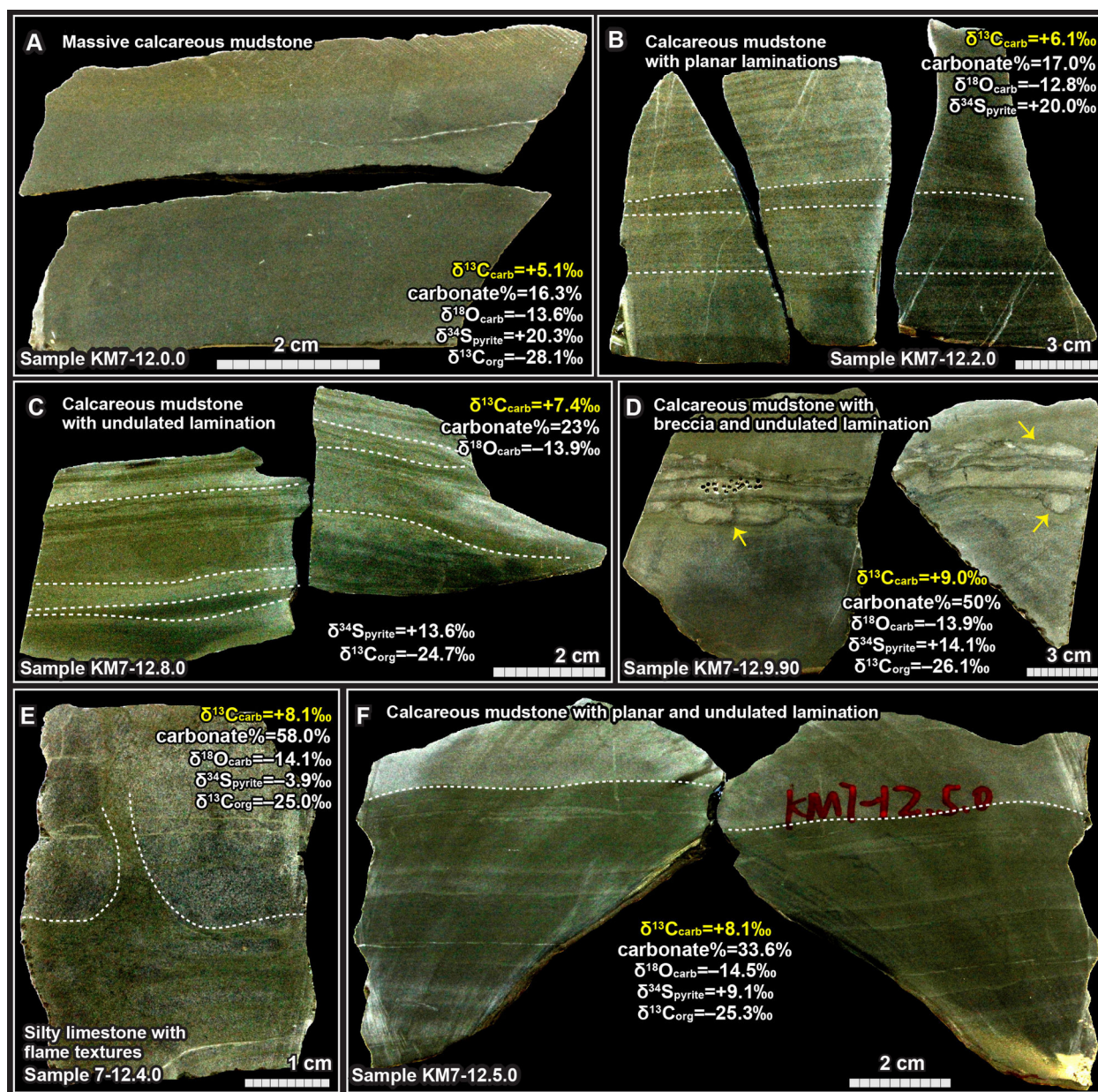


Fig. 7. Rock slabs and corresponding geochemical data of samples collected from the lower Serra da Saudade Formation at the siliciclastic-dominated KM7-12 section. (A) A calcareous siltstone sample with homogeneous textures. (B, C) Calcareous siltstone samples with undulated lamination. (D) A calcareous siltstone sample with undulated lamination and intraclasts. (E) A silty carbonate sample with possible flame textures. The corresponding microscopic image of this sample is shown in Fig. 9A, 9D, 9E. (F) A calcareous siltstone sample with planar and undulated laminations. The brightness and contrast of all the images have been enhanced in order to achieve the best view of detailed sedimentary textures. More sample slab images are available in the online supplementary materials.

(mean: +21.0‰) at the KM7-14 section (Fig. 11F, 11P).

The $\delta^{34}\text{S}_{\text{CAS}}$ data in this study are limited due to the fact that many samples (each processed with at least 100 g of powders) did not yield enough barite precipitate during CAS extraction. The limited $\delta^{34}\text{S}_{\text{CAS}}$ values show a range from +24.1‰ to +30.6‰ (mean: +26.9‰) at the KM7-12 section and a range from +14.8‰ to +25.5‰ (mean: +21.5‰) at the KM7-14 section (Fig. 11F, 11P).

Based on the sample-to-sample variation in stratigraphy, we noticed two $\delta^{34}\text{S}_{\text{pyrite}}$ outliers (−3.9‰ and +35.8‰) from the KM7-12 section and two $\delta^{34}\text{S}_{\text{pyrite}}$ outliers (−1.0‰ and +1.0‰ from the same sample) from the KM7-14 section, all of which are plotted beyond the scale and are shown as numbers in red color with arrows indicating their stratigraphic positions (Fig. 11F, 11P). Despite these four outliers, it is clear that the $\delta^{34}\text{S}_{\text{pyrite}}$ data of the KM7-12 section are overall less than 20‰ while the $\delta^{34}\text{S}_{\text{pyrite}}$ data of the KM7-14 section are mostly higher than

20‰.

4.4. $^{87}\text{Sr}/^{86}\text{Sr}$ data

Five limestone samples (three from the KM7-14 section and two from the KM7-12 section) were analyzed for $^{87}\text{Sr}/^{86}\text{Sr}$ compositions. The $^{87}\text{Sr}/^{86}\text{Sr}$ values measured from the KM7-14 section are 0.70738, 0.70730, and 0.70735 (mean: 0.70734) (Fig. 11T). In contrast, the $^{87}\text{Sr}/^{86}\text{Sr}$ values measured from the KM7-12 section are much higher (0.70853 and 0.70931) (Fig. 11J).

4.5. Elemental concentration data

In this study, only the carbonate-dominated KM7-14 section was analyzed for elemental concentrations (Fig. 12). The main goals of this

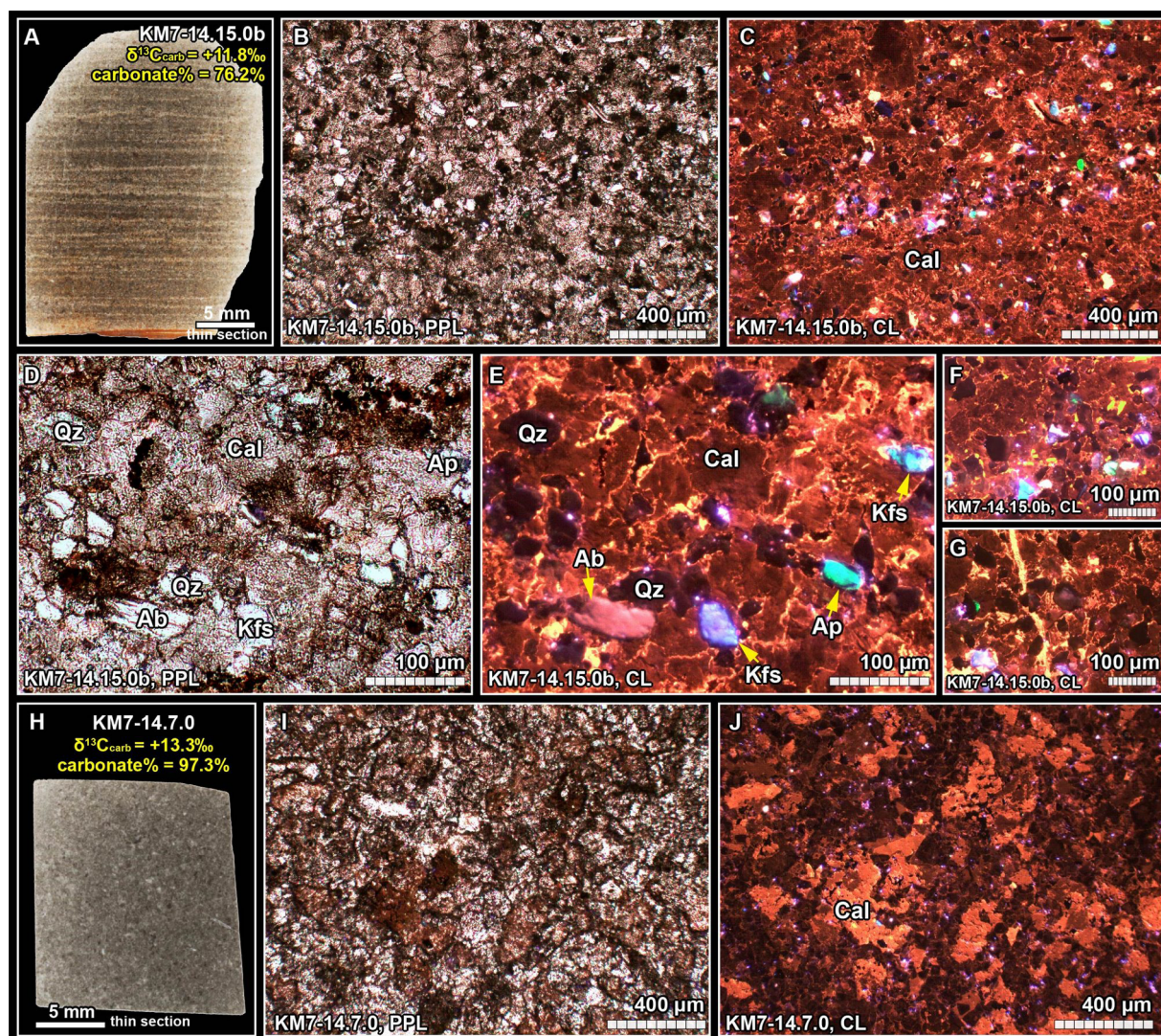


Fig. 8. Petrographic images of two samples from the Lagoa do Jacaré Formation at the KM7-14 section, Brazil. (A) Scanned thin section image of sample KM7-14.15.0b. (B–G) Microscopic views under plane polarized light and cathodoluminescence. B–C and D–E are paired petrographic images of the same views. Minerals under CL: orange = calcite, green = apatite, bright blue = K feldspar, pinkish = albite, black = quartz. Note the abundant angular-shaped quartz grains in dark color under CL and the clean quartz grains in white color under PPL, suggesting a significant detrital input during deposition. (H) Scanned thin section image of sample KM7-14.7.0. (I–J) Paired petrographic images of the same view. Note the patchy shape of the calcite under CL, suggesting the occurrence of carbonate recrystallization. Abbreviations: CL = cathodoluminescence, PPL = plane polarized light, Ap = Apatite, Cal = calcite, Qtz = quartz, Kfs = K-feldspar, Ab = Albite. (For interpretation of the references to color in this figure legend, the reader is referred to the web version of this article.)

analysis were to evaluate the diagenetic history of the samples (based on Rb/Sr, Mn/Sr, Mg/Ca ratios) and to reconstruct the redox conditions (based on the calculated Ce anomaly) of the depositional basin. Generally, the Rb/Sr, Mn/Sr, Mn/Ca ratios (ppm/ppm) are very low, except for a few outliers (Fig. 12F, 12G, 12H). The Ce anomaly (Ce/Ce^*) data were calculated based on the equation $Ce/Ce^* = C_{ePAAS}/([Pr]_{PAAS}^2/[Nd]_{PAAS})$, which show a range from 0.62 to 0.93 (mean: 0.83) at the KM7-14 section (Fig. 12D). We also calculated the Sr/Ca ratios (ppm/ppm) of the limestone samples collected from the KM7-14 section (Fig. 12E). The Sr/Ca ratios show a range from 0.013 to 0.043 (mean: 0.022).

5. Discussion

5.1. Diagenesis evaluation

Before discussing the detailed biogeochemical or diagenetic origins of the MIBE, an independent evaluation of the reliability of our geochemical data is necessary. Below we will evaluate the data and discuss

the potential influence of diagenesis on each individual data set.

5.1.1. Constraints from petrographic and trace element results

Petrographic observations under polarized light and CL were carried out based on seven thin sections. The thin sections were made from two samples at the carbonate-dominated KM7-14 section (Fig. 8), three samples at the siliciclastic-dominated KM7-12 section (Fig. 9), and two samples at the KM7-13 section (Fig. 10). Petrographic observations of these thin sections provide contextual information about the depositional environment and post-depositional diagenesis.

KM7-14 Section. A carbonate-dominated sample shows abundant detrital components comprised mostly of angular-shaped quartz grains, with a less amount of angular apatite, K-feldspar, and albite (Fig. 8A–G). These siliciclastic components suggest the involvement of detrital input during deposition. We also note that one carbonate sample shows a patchy texture with large calcite grains in the size of a few hundred μm under CL (Fig. 8H–J), which suggests the occurrence of recrystallization after deposition. No petrographic evidence for significant diagenetic alteration (e.g., late veins, replacement) has been

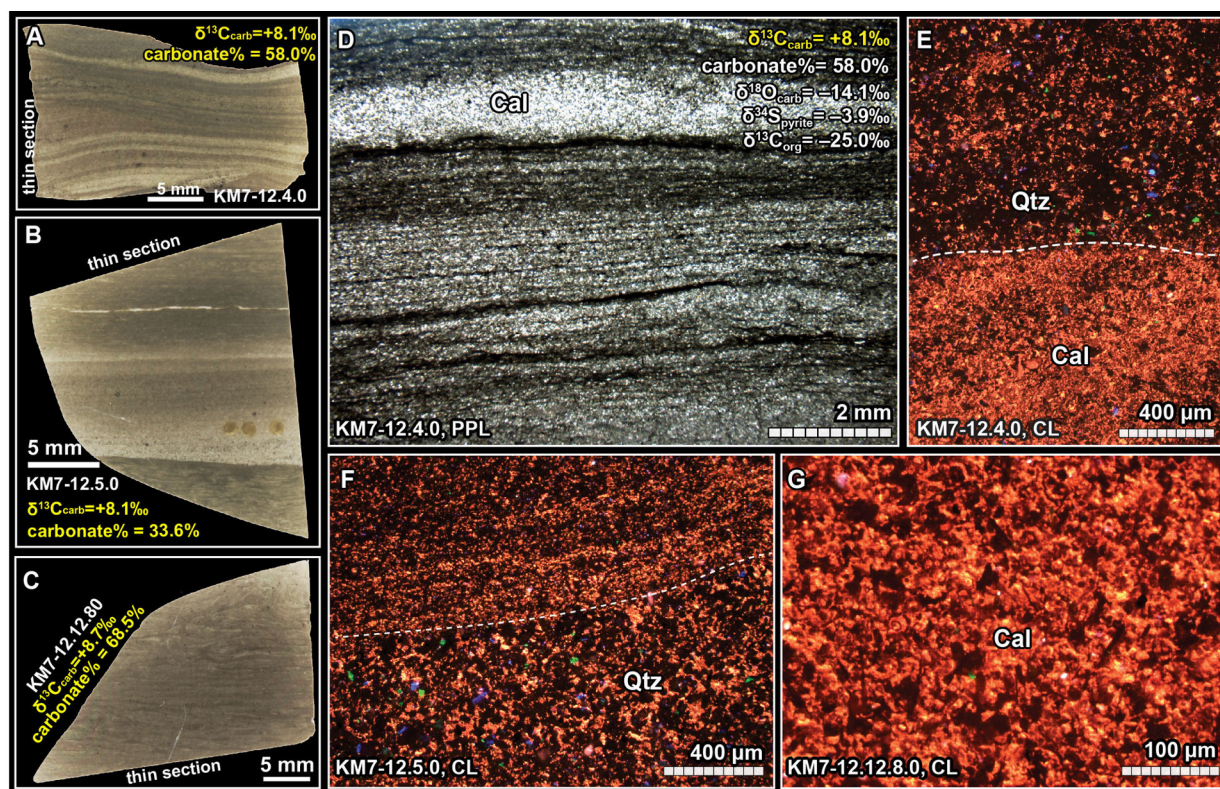


Fig. 9. Petrographic images of three samples from the lower Serra da Saudade Formation at the KM7-12 section, Brazil. (A–C) Scanned thin section images of sample KM7-12.4.0, sample KM7-12.5.0, and sample KM7-12.8.0 under plane polarized light. See Fig. 7E for the corresponding rock slab image. (E) Microscopic view of sample KM7-12.4.0 under cathodoluminescence. The dash line shows the boundary between an upper silicate-rich layer (dominated by quartz grains in black color) and a lower carbonate-rich layer (dominated by calcite grains in orange color). (F) Microscopic view of sample KM7-12.5.0 under cathodoluminescence. The dash line shows the boundary between an upper carbonate-rich layer (dominated by calcite grains in orange color) and a lower silicate-rich layer (dominated by quartz grains in black color). (G) Microscopic view of sample KM7-12.8.0 under cathodoluminescence. The abundant dark-colored angular-shaped grains under CL are mostly quartz. Abbreviations: CL = cathodoluminescence, PPL = plane polarized light, Cal = calcite, Qtz = quartz. (For interpretation of the references to color in this figure legend, the reader is referred to the web version of this article.)

found from the KM7-14 section. The elemental ratios of Rb/Sr, Mn/Sr, Mg/Ca are very low (mostly < 1) (Fig. 12), suggesting a limited influence of diagenetic alteration based on the empirical constraints in earlier studies (e.g., Kaufman and Knoll, 1995).

KM7-12 section. Three samples from the siltstone-dominated KM7-12 section have been investigated for thin section petrography. The samples show fine laminations in hand samples (Fig. 9A–C). Detailed microscopic observation reveals laminated quartz-dominated (in dark color under CL) and calcite-dominated layers (in orange color under CL) (Fig. 9D–G). No petrographic evidence for significant diagenetic alteration was found in the samples from this section.

KM7-13 section. The samples collected from the KM7-13 section are limited in this study. An ooid grainstone sample from the KM7-13 section has been investigated under the microscope. The ooids can be up to 2 mm in diameter and show concentric cortical fabrics with carbonate or quartz nuclei (Fig. 10A–D). CL images reveal an overall dark color in ooid cortices and a bright orange luminescence in cements and recrystallized calcite grains (Fig. 10E–J). It is notable that massive ooid fragments have been found in the CL images (Fig. 10E–J), which was possibly caused by early re-deposition or late burial diagenesis. The heterogeneous CL colors in the inner (Fig. 10G) or outer cortices (Fig. 10H) of some ooids suggest that they may have been partially altered by diagenesis. In addition, the other limestone sample from the KM7-13 section reveals a few dark-colored veins (Fig. 10K–M). CL images show a dark color in rhombohedral calcite grains and a bright orange color in calcite matrix, suggesting different Fe and Mn compositions between the grains and the matrix.

In summary, petrographic investigation of samples from the KM7-13

section reveals a certain degree of diagenetic alteration. However, no clear evidence for pervasive diagenetic alteration has been found in samples from the KM7-12 and KM7-14 sections, which are the main targets for chemostratigraphy in this study.

5.1.2. Assessing the $\delta^{13}\text{C}_{\text{carb}}$ and $\delta^{18}\text{O}_{\text{carb}}$ data

The covariation of $\delta^{13}\text{C}_{\text{carb}}$ and $\delta^{18}\text{O}_{\text{carb}}$ data have been widely used as a tool for the evaluation of diagenesis. Typically, the $\delta^{13}\text{C}_{\text{carb}}$ and $\delta^{18}\text{O}_{\text{carb}}$ values can be altered toward more negative values by progressive meteoric water diagenesis or burial diagenesis that is coupled with organic matter oxidation (Talbot and Kelts, 1986; Gischler et al., 2007; Knauth and Kennedy, 2009; Derry, 2010b; Bishop et al., 2014). These secondary processes could alter the primary $\delta^{13}\text{C}_{\text{carb}}$ and $\delta^{18}\text{O}_{\text{carb}}$ compositions toward more negative values. However, compared with the typical Ediacaran seawater values (Fig. 1), the $\delta^{13}\text{C}_{\text{carb}}$ of the MIBE evolves toward much more positive values. Such an evolving trend cannot be well explained by the secondary processes mentioned above. Therefore, we regard that meteoric water diagenesis and burial diagenesis have not played a tangible role in the $\delta^{13}\text{C}_{\text{carb}}$ and $\delta^{18}\text{O}_{\text{carb}}$ compositions during the MIBE.

5.1.3. Assessing the $\delta^{13}\text{C}_{\text{org}}$ data

Compared with published Ediacaran $\delta^{13}\text{C}_{\text{org}}$ data that typically range from -25‰ to -30‰ or even lower (Fike et al., 2006; McFadden et al., 2008; Cui et al., 2015; Cui et al., 2019c; Canfield et al., 2020), the organic matter in the MIBE appears to be much more enriched in ^{13}C , with $\delta^{13}\text{C}_{\text{org}}$ values up to -15.2‰ (Fig. 11N). One potential reason can be that the anomalously high $\delta^{13}\text{C}_{\text{org}}$ data are

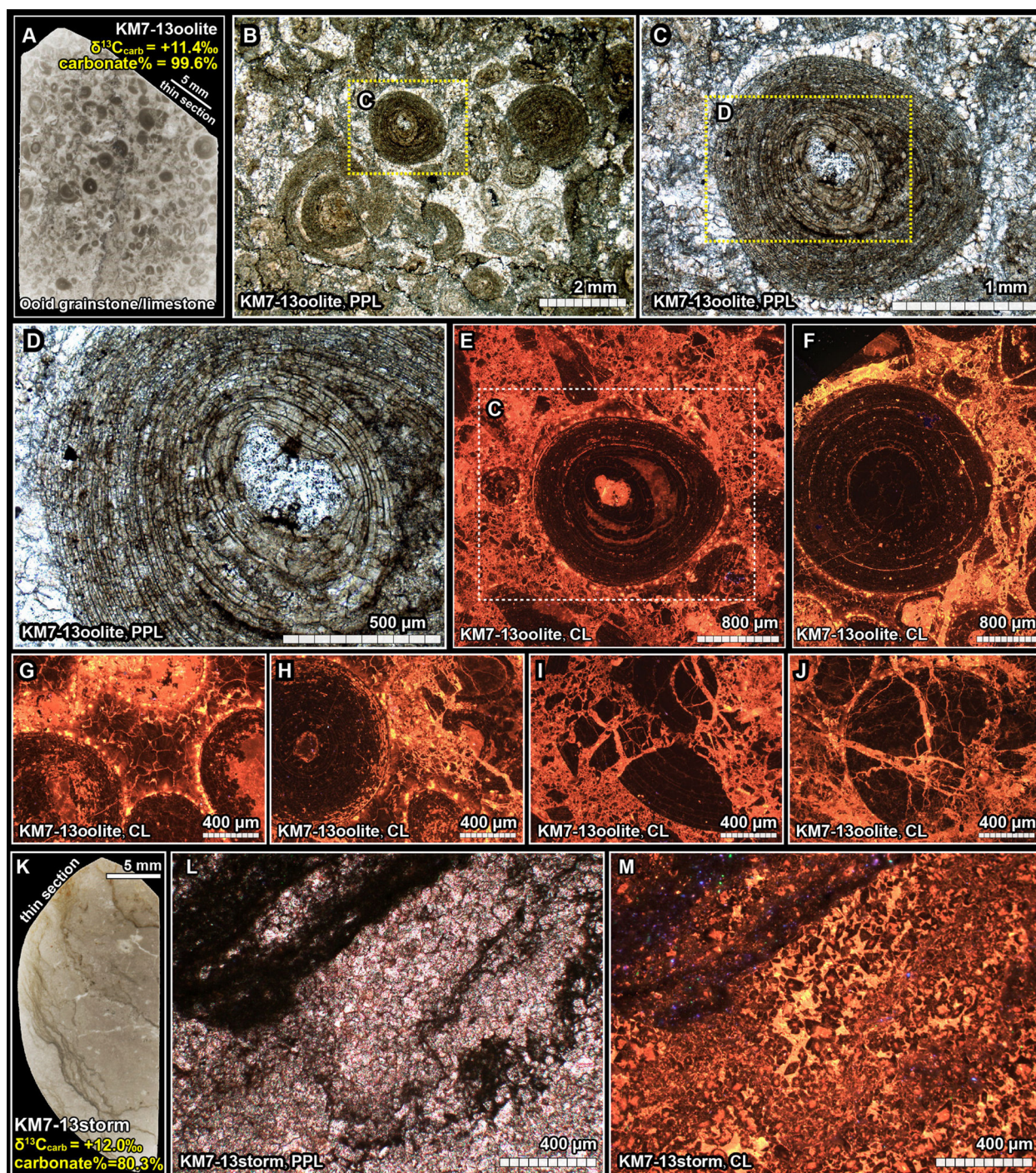


Fig. 10. Petrographic images of two samples from the KM7-13 section, Lagoa do Jacaré Formation, Brazil. (A) Scanned thin section image of an ooid grainstone (KM7-13oolite). (B–D) Petrographic images under plane polarized light. Dash line boxes in B, C and E represent the close-up view of C, D and C, respectively. Note the concentric laminar texture in each individual ooid. (E–J) CL images of the ooid grainstone sample. Note the ooids in dark color and the calcite matrix in bright orange color under CL. These CL images also show massive ooid fragments possibly caused by early re-deposition or late burial diagenesis. See Fig. 6F for the corresponding rock slab image. (K) Scanned thin section image of sample KM7-13storm. (L, M) Paired views under plane polarized light and cathodoluminescence. Abbreviations: CL = cathodoluminescence; PPL = plane polarized light. (For interpretation of the references to color in this figure legend, the reader is referred to the web version of this article.)

caused by mixed carbonates, resulting from incomplete acidification of the carbonate component. However, during the sample preparation, all the samples were acidified by using 3 M HCl until no more bubbles were produced. Additional precaution was taken by adding an extra amount of concentrated HCl acid after acidification in order to make sure complete acidification was achieved. Moreover, our $\delta^{13}\text{C}_{\text{org}}$ data from the KM7-14 section are in good agreement with the recently

published $\delta^{13}\text{C}_{\text{org}}$ values of the lower MIBE intervals in three different drill cores (Caetano-Filho et al., 2020). Therefore, we rule out the possibility of incomplete acidification as the cause of high $\delta^{13}\text{C}_{\text{org}}$ values in this study, and the measured $\delta^{13}\text{C}_{\text{org}}$ data should reflect depositional conditions.

Published studies have shown that high $\delta^{13}\text{C}_{\text{org}}$ signals can also be generated by progressive thermogenic breakdown of organic matter. In

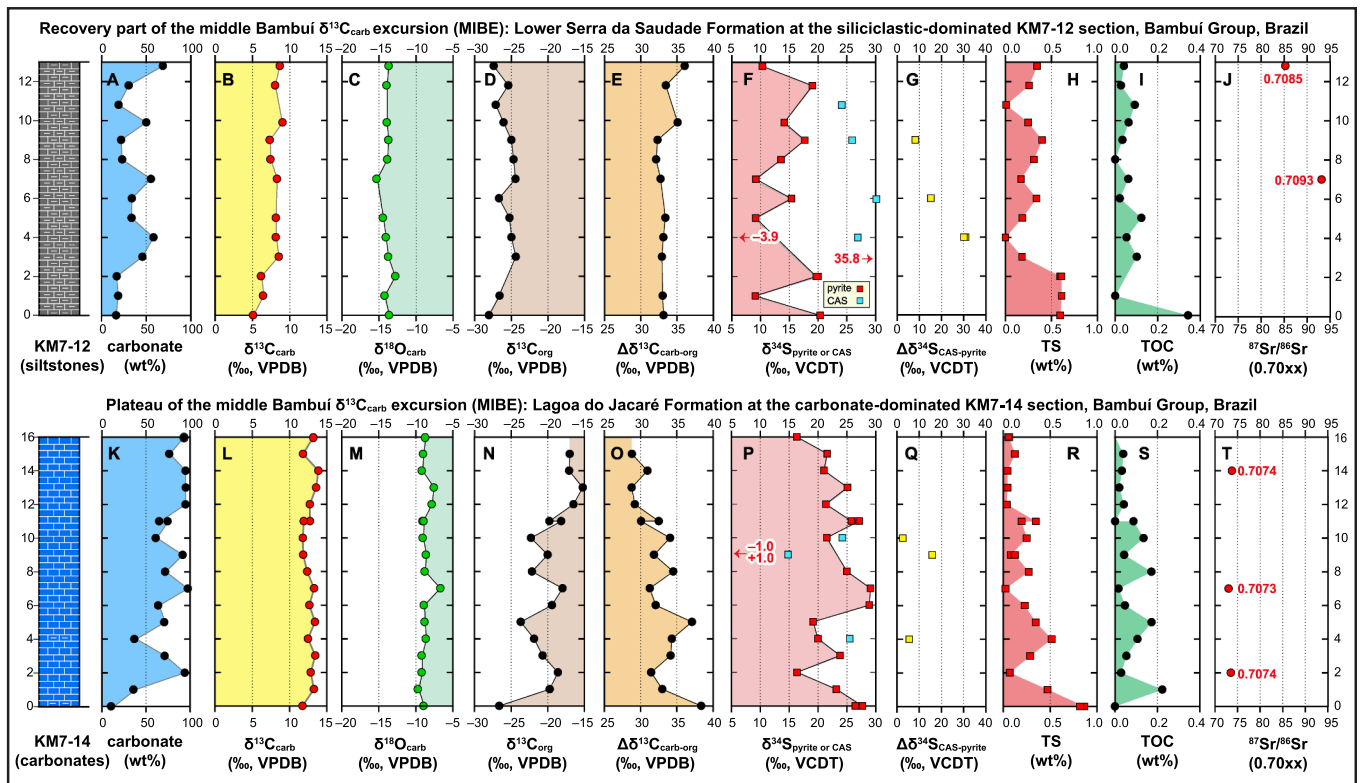


Fig. 11. Integrated chemostratigraphic profiles of two sections within the middle Bambuí $\delta^{13}\text{C}_{\text{carb}}$ excursion (MIBE). The siliclastic-dominated KM7-12 section represents the lower Serra da Saudade Formation (i.e., recovery part of the MIBE), while the carbonate-dominated KM7-14 section represents the Lagoa do Jacaré Formation (i.e., plateau of the MIBE). Geochemical profiles include (A, K) carbonate content (wt. %). (B, L) carbonate carbon isotopes ($\delta^{13}\text{C}_{\text{carb}}$, ‰ VPDB). (C, M) carbonate oxygen isotopes ($\delta^{18}\text{O}_{\text{carb}}$, ‰ VPDB). (D, N) organic carbon isotopes ($\delta^{13}\text{C}_{\text{org}}$, ‰ VPDB). (E, O) carbon isotope fractionations ($\Delta\delta^{13}\text{C}_{\text{carb-org}}$). (F, P) sulfur isotopes of total sulfur in acidified residuals ($\delta^{34}\text{S}_{\text{TS}} \approx \delta^{34}\text{S}_{\text{pyrite}}$, ‰ VCDT) and carbonate-associated sulfate ($\delta^{34}\text{S}_{\text{CAS}}$, ‰ VCDT). The $\delta^{34}\text{S}_{\text{CAS}}$ data are limited due to the fact that most of the samples (each processed with at least 100 g of powders) did not yield enough barite precipitate during CAS extraction. Note that the $\delta^{34}\text{S}_{\text{pyrite}}$ values of the KM7-12 section are mostly lower than + 20‰, while the $\delta^{34}\text{S}_{\text{pyrite}}$ values of the KM7-14 section are mostly higher than + 20‰. The four $\delta^{34}\text{S}_{\text{pyrite}}$ outliers with values beyond the plotted range are shown as numbers in red color with arrows pointing to their stratigraphic positions. (G, Q) sulfur isotope fractionations ($\Delta\delta^{34}\text{S}_{\text{CAS-pyrite}}$) between sulfate and sulfide. (H, R) total sulfur content (TS%, dominated by pyrite with trace amount of organic S) of decalcified residues. (I, S) total organic carbon content (TOC, wt%) of decalcified residues. (J, T) carbonate strontium isotope ratios ($^{87}\text{Sr}/^{86}\text{Sr}$). See detailed discussion in the main text. All the data can be found in the online supplementary material. (For interpretation of the references to color in this figure legend, the reader is referred to the web version of this article.)

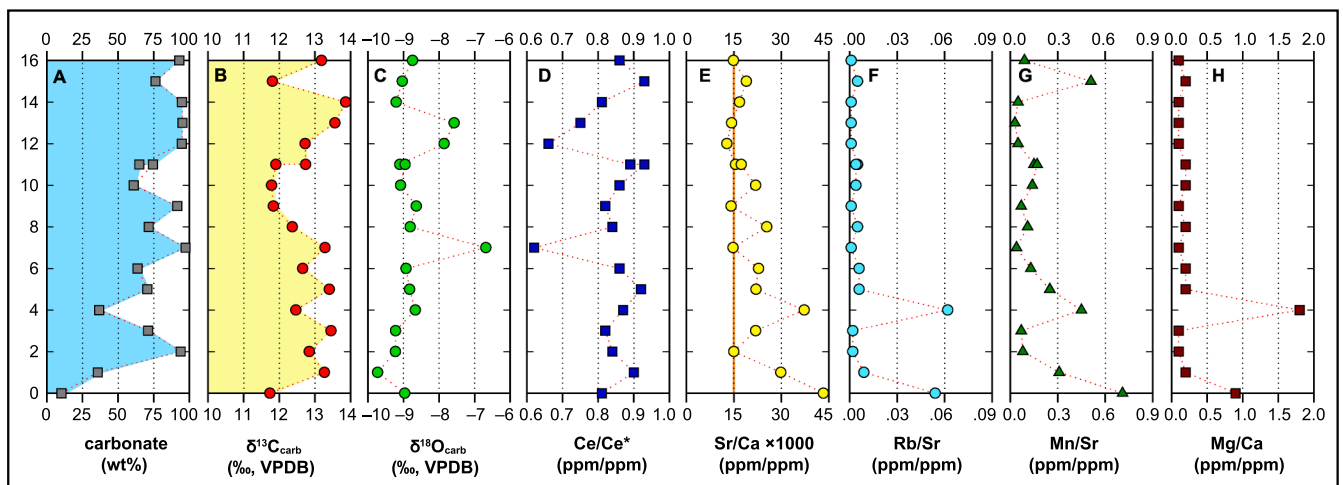


Fig. 12. Chemostratigraphic profiles of the Lagoa do Jacaré Formation at the carbonate-dominated KM7-14 section. Geochemical profiles include (A) carbonate content (wt. %). (B) carbonate carbon isotopes ($\delta^{13}\text{C}_{\text{carb}}$, ‰ VPDB). (C) carbonate oxygen isotopes ($\delta^{18}\text{O}_{\text{carb}}$, ‰ VPDB). (D) Ce anomaly (Ce/Ce^*) calculated using the formula $\text{Ce}/\text{Ce}^* = \text{Ce}_{\text{PAAS}} / ([\text{Pr}]_{\text{PAAS}}^2 / [\text{Nd}]_{\text{PAAS}})$ (Lawrence et al., 2006; Ling et al., 2013). (E) Sr/Ca ratios. For a comparison, the peak Sr/Ca value of the Ediacaran Gaojiashan Member of the Dengying Formation (Cui et al., 2016b; Cui et al., 2019c) is indicated as the orange line in E. (F) Rb/Sr ratios. (G) Mn/Sr ratios. (H) Mg/Ca ratios. The overall low elemental ratios (mostly < 1) of Rb/Sr, Mn/Sr, and Mg/Ca suggest a limited influence of diagenetic alteration. All the data can be found in the online supplementary material. (For interpretation of the references to color in this figure legend, the reader is referred to the web version of this article.)

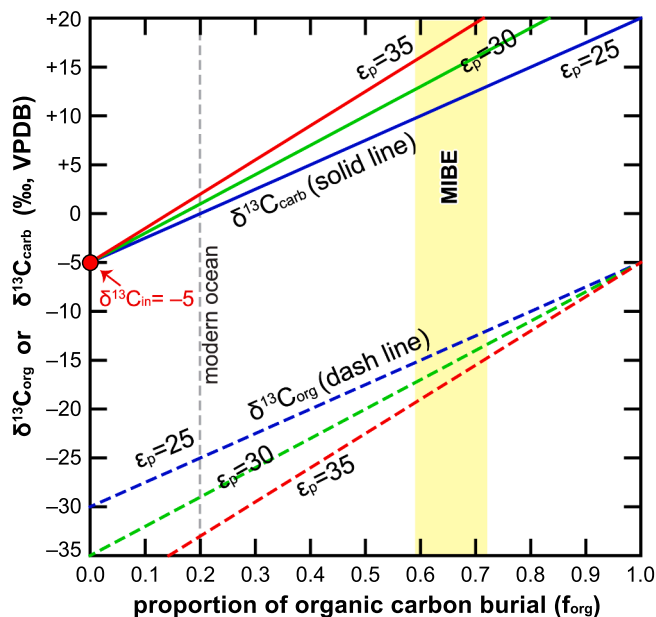


Fig. 13. Reconstructing the Middle Bambuí $\delta^{13}\text{C}_{\text{carb}}$ Excursion (MIBE) based on the conventional carbon cycle model. Yellow zone represents the MIBE. The canonical carbon cycle model includes two major sinks: carbonate carbon and organic carbon. The carbon source ($\delta^{13}\text{C}_{\text{in}}$) from the mantle via volcanic degassing has widely been assumed to be ca. -5‰ (Hayes, 1993; Kump and Arthur, 1999). In modern marine environment, to maintain a $\delta^{13}\text{C}_{\text{carb}}$ value of ca. 0‰ , assuming the fractionation factor ϵ_p of ca. $+30\text{‰}$, the invoked proportion of organic carbon burial should be around 20% (shown in gray dash line). In this model, to achieve the MIBE (i.e., $\delta^{13}\text{C}_{\text{carb}}$ = ca. $+15\text{‰}$), almost 70% of organic matter needs to be buried (yellow bar). See the main text for detailed discussion. (For interpretation of the references to color in this figure legend, the reader is referred to the web version of this article.)

this scenario, isotopically light carbon is preferentially released during thermogenic breakdown of organic matter (Sackett et al., 1968; Sackett, 1978), leading to progressively higher $\delta^{13}\text{C}_{\text{org}}$ values of the residual organic matter in the host rock (McKirdy and Powell, 1974; Hoefs and Frey, 1976; Simonet et al., 1981; Schwab et al., 2005). However, the cross plot of $\delta^{13}\text{C}_{\text{org}}$ vs TOC (Fig. S3) shows no correlation in this study. No clear evidence for hydrothermal diagenesis was found in this study. Therefore, the possibility that hydrothermal diagenesis caused the overall high $\delta^{13}\text{C}_{\text{org}}$ signals in the KM7-14 section is not likely.

5.1.4. Assessing the $^{87}\text{Sr}/^{86}\text{Sr}$ data

The $^{87}\text{Sr}/^{86}\text{Sr}$ data show higher values at the siliciclastic-dominated KM7-12 section and much lower values at the carbonate-dominated KM7-14 section (Fig. 11J, 11T). Assuming that the MIBE occurred during the late Ediacaran to Cambrian Period (see Section 2.2 for detailed reasoning), the anomalously low $^{87}\text{Sr}/^{86}\text{Sr}$ values around 0.7073 from the KM7-14 section (Fig. 11T) are uncommon given that the Ediacaran-Cambrian seawater $^{87}\text{Sr}/^{86}\text{Sr}$ values typically range from ca. 0.7080 to 0.7090 (Halverson et al., 2007; Sawaki et al., 2010; Cui et al., 2016a; Xiao et al., 2016; Cui et al., 2020). Since sedimentary diagenesis typically alter the primary $^{87}\text{Sr}/^{86}\text{Sr}$ signals towards higher values (Banner, 1995), such low values (down to 0.7073) cannot be easily explained by post-depositional diagenesis. Therefore, we regard that the anomalously low $^{87}\text{Sr}/^{86}\text{Sr}$ values around 0.7073 from the carbonate-dominated KM7-14 section reflect primary water-column signals in the restricted Bambuí Basin. However, we indeed found radiogenic $^{87}\text{Sr}/^{86}\text{Sr}$ values as high as 0.7093 from the siliciclastic-dominated KM7-12 section (Fig. 11J), which may be caused by the overprint of post-depositional Rb-rich fluids and are therefore largely porewater signals.

5.1.5. Assessing the $\delta^{34}\text{S}$ data

Most of the $\delta^{34}\text{S}_{\text{CAS}}$ data are within the range between 20‰ and 30‰ (Fig. 11F, 11P). There is one $\delta^{34}\text{S}_{\text{CAS}}$ outlier of 14.8‰, which also corresponds to a $\delta^{34}\text{S}_{\text{pyrite}}$ outlier of -1.0‰ in the KM7-14 section (Fig. 11P). Published studies have shown that CAS in marine carbonates can be affected by secondary processes related to pyrite oxidation (Marengo et al., 2008; Edwards et al., 2019) or the contamination of secondary atmospheric sulfate (Peng et al., 2014). Therefore, we regard that it is possible that the $\delta^{34}\text{S}_{\text{CAS}}$ outlier of 14.8‰ was caused by late alteration.

Four $\delta^{34}\text{S}_{\text{pyrite}}$ outliers (shown as numbers and arrows in Fig. 11F, 11P) show large sample-to-sample variation. The detailed reason for this variation is unclear. It is possible that local environmental factors may have played a role (Fike et al., 2015; Lang et al., 2020). Regardless, the $\delta^{34}\text{S}_{\text{pyrite}}$ profiles of these two sections show a clear pattern that $\delta^{34}\text{S}_{\text{pyrite}}$ data of the KM7-14 section (mostly $>20\text{‰}$) are overall higher than the $\delta^{34}\text{S}_{\text{pyrite}}$ values of the KM7-12 section (mostly $<20\text{‰}$), indicating different sulfur cycles in these two depositional stages.

5.2. Models of marine carbon cycles

5.2.1. Conventional carbon cycle model

Before discussing the origins of the MIBE, a brief introduction of the conventional carbon cycle model is needed. Conventional steady-state carbon cycle model includes one carbon source from the mantle via volcanic outgassing and two major carbon sinks (i.e., carbonate carbon and organic carbon) (Schidlowski, 1987; Des Marais et al., 1992; Kump and Arthur, 1999). The isotopic value of the source ($\delta^{13}\text{C}_{\text{in}}$) has widely been assumed to be ca. -5‰ (Hayes, 1993; Kump and Arthur, 1999). Based on a simple mass balance view, the relationship between the source and sinks can be expressed as the following:

$$\delta^{13}\text{C}_{\text{in}} = \delta^{13}\text{C}_{\text{carb}} * f_{\text{carb}} + \delta^{13}\text{C}_{\text{org}} * f_{\text{org}} \quad (1)$$

where f_{org} and f_{carb} represent the proportion of burial as carbonate carbon and organic carbon, respectively, and the sum of these two equals to one (i.e., $f_{\text{carb}} + f_{\text{org}} = 1$).

The offset (i.e., C isotope fractionation, ϵ_p) between carbonate carbon and organic carbon is mainly controlled by the carbon isotope fractionation during photosynthesis (Hayes, 1993), which can be expressed as $\epsilon_p = \delta^{13}\text{C}_{\text{carb}} - \delta^{13}\text{C}_{\text{org}}$. Thus, Eq. (1) can be rearranged with $\delta^{13}\text{C}_{\text{carb}}$ and $\delta^{13}\text{C}_{\text{org}}$ as the subject, respectively:

$$\delta^{13}\text{C}_{\text{carb}} = \delta^{13}\text{C}_{\text{in}} + \epsilon_p * f_{\text{org}} \quad (2)$$

$$\delta^{13}\text{C}_{\text{org}} = \delta^{13}\text{C}_{\text{carb}} - \epsilon_p \quad (3)$$

A few implications can be drawn from this model (Fig. 13). First, $\delta^{13}\text{C}_{\text{carb}}$ data co-vary with $\delta^{13}\text{C}_{\text{org}}$ data with a fixed fractionation. This co-varying nature has been widely used as an approach to evaluate the fidelity of chemostratigraphic $\delta^{13}\text{C}_{\text{carb}}$ record (e.g., Knoll et al., 1986; Shields et al., 1997; Derry, 2010a; Kump et al., 2011; Jiang et al., 2012; Johnston et al., 2012; see also Oehlert and Swart, 2014 for a different view). Second, as the proportion of organic carbon burial (f_{org}) increases, both $\delta^{13}\text{C}_{\text{carb}}$ and $\delta^{13}\text{C}_{\text{org}}$ data evolve to higher values simultaneously. Considering that organic carbon is typically enriched in ^{12}C due to preferential incorporation of the light isotope during photosynthesis, different proportions of organic carbon burial (f) would have a coupled effect on both $\delta^{13}\text{C}_{\text{carb}}$ and $\delta^{13}\text{C}_{\text{org}}$ signals. Therefore, based on this steady-state model, higher burial rates of organic carbon could lead to more sequestration of light carbon in sediments, leaving the ocean reservoir more enriched in ^{13}C . In this scenario, the depositional carbonates should record a positive $\delta^{13}\text{C}_{\text{carb}}$ anomaly.

Based on the conventional model, to achieve the MIBE (i.e., positive $\delta^{13}\text{C}_{\text{carb}}$ anomaly up to $+15\text{‰}$), it is expected that almost 70% of organic carbon must be buried in the sediments (yellow bar in Fig. 13), which is over 3 times the current amount (i.e., ca. 20% of organic carbon burial in the modern oceans; gray line in Fig. 13).

However, such an extremely high organic carbon burial event has not been evidenced by the sedimentary record of the Bambuí Group or any equivalent Ediacaran-Cambrian strata on a global scale. No high-TOC intervals have been found directly associated with the MIBE in the studied basin. Moreover, organic matter burial is self-limiting through the production of O₂ (and derived electron acceptors), creating a negative feedback through enhanced respiration. Therefore, we regard that the conventional model lacks sufficient geological evidence for the MIBE.

It is notable that a giant graphite deposit has been found in the Jequitinhonha Complex of the Araçuaí Belt (SE Brazil), which represents a depositional event with a large amount of organic matter burial (Pacheco et al., 2020). The recent age constraints based on the youngest grains of detrital zircons suggest that the maximum depositional age of this organic carbon burial event is ca. 630–609 Ma (Pacheco et al., 2020), and the maximum age of the regional metamorphic event is ca. 570–550 Ma (Pedrosa-Soares et al., 2011). Although it remains possible that the organic carbon burial event associated with this Jequitinhonha graphite deposit coincided with the MIBE, more geological and geochronological evidence is still needed to fully test the causal link between these two events.

5.2.2. Revised carbon cycle model with authigenic carbonate as a third sink

Largely based on the conventional dual-sink carbon cycle model (see Section 5.2.1), a revised triple-sink model with authigenic carbonate as a third sink in global carbon cycle has been proposed (Schrag et al., 2013). In this model, the carbon sinks include carbonate carbon, organic carbon, and early authigenic carbonate that precipitated near the sediment-water interface. Based on a mass balance view, the relationship between source and sinks can be expressed as the following:

$$\delta^{13}\text{C}_{\text{in}} = (\delta^{13}\text{C}_{\text{DIC}} - \varepsilon_{\text{p}})f_{\text{org}} + (1 - f_{\text{org}})[(\delta^{13}\text{C}_{\text{DIC}} - \varepsilon_{\text{ac}})f_{\text{ac}} + (\delta^{13}\text{C}_{\text{DIC}} - \varepsilon_{\text{mc}})(1 - f_{\text{ac}})] \quad (4)$$

or solving for $\delta^{13}\text{C}_{\text{DIC}}$ as:

$$\delta^{13}\text{C}_{\text{DIC}} = \delta^{13}\text{C}_{\text{in}} + f_{\text{org}}[\varepsilon_{\text{p}} - \varepsilon_{\text{mc}} - f_{\text{ac}}(\varepsilon_{\text{ac}} - \varepsilon_{\text{mc}})] + f_{\text{ac}}(\varepsilon_{\text{ac}} - \varepsilon_{\text{mc}}) \quad (5)$$

where $\delta^{13}\text{C}_{\text{in}}$ and $\delta^{13}\text{C}_{\text{DIC}}$ represent the carbon isotope composition of the carbon source and dissolved inorganic carbon (DIC), respectively; ε_{p} , ε_{ac} and ε_{mc} represent different $\delta^{13}\text{C}$ fractionation factors between seawater DIC and organic carbon (ε_{p}), authigenic carbonate (ε_{ac}) and normal marine carbonate (ε_{mc}), respectively; f_{org} and f_{ac} represent the burial proportion of carbon as organic carbon and authigenic carbonates, respectively.

Since this revised triple-sink model was published, multiple case studies have demonstrated that authigenic carbonate that formed during early diagenesis may have indeed played a role — at least on a local scale — in some ancient $\delta^{13}\text{C}_{\text{carb}}$ excursions (Wohlwend et al., 2016; Zhou et al., 2016; Cui et al., 2017; Xiao et al., 2019; Cao et al., 2020; Xiao et al., 2020). However, whether authigenic carbonate represents a *major* sink in the carbon cycle remains uncertain (Canfield and Kump, 2013). Notably, a recent study argues that clastic sedimentary rocks were not a major sink for ^{13}C -depleted carbonate during the Neoproterozoic Era (Canfield et al., 2020), which challenges the significance of authigenic carbonate in deep-time marine carbon cycles. Although authigenic carbonate appears to be a hypothesized sink that is not well demonstrated in the global sedimentary record, we will explore how this potential sink could have affected the genesis of the MIBE in this study (see Section 5.5 for details).

5.3. Testing the methanogenic origin for the MIBE

5.3.1. Porewater methanogenesis?

In modern marine environments, $\delta^{13}\text{C}_{\text{carb}}$ signals as high as +15‰ are typically limited to authigenic carbonates within methanogenic

zones, where light carbon is removed from the porewater system by methane production (Meister et al., 2007; Pierre et al., 2016). Therefore, anomalously high $\delta^{13}\text{C}_{\text{carb}}$ signals in the deep-time sedimentary records have commonly been interpreted as authigenic carbonate formed in ancient methanogenic zones (Irwin et al., 1977; Ader et al., 2009; Birgel et al., 2015).

However, multiple lines of sedimentological and geochemical evidence argue against the scenario of *porewater* methanogenesis for the MIBE. First, the MIBE has been recorded in well-preserved oolitic limestone in this study (Fig. 4F, 6F, 10A–J) and published literature (Misi and Veizer, 1998; Uhlein et al., 2019). Considering that ooids typically form under shallow and agitated water conditions (Siewers, 2003; Trower et al., 2017), this independent piece of sedimentological evidence suggests a water-column origin, instead of a porewater origin, for the MIBE.

Second, a comparison between the carbonate (i.e., KM7-14 section) and siltstone (i.e., KM7-12 section) facies of the MIBE suggests that the positive $\delta^{13}\text{C}_{\text{carb}}$ anomaly seems to be most obvious in carbonate facies (Fig. 11). It is worth mentioning that the underlying Serra de Santa Helena Formation and Sete Lagoas Formation at some sections also record similarly high $\delta^{13}\text{C}_{\text{carb}}$ and low $^{87}\text{Sr}/^{86}\text{Sr}$ ratios in carbonate facies (Alvarenga et al., 2014; Caetano-Filho et al., 2019; Uhlein et al., 2019), which is consistent with what we found in this study. This observation suggests that the MIBE may be limited to the shallow marine environment of the Bambuí Basin.

Third, the new data in this study, together with recently published work (Caetano-Filho et al., 2020), show a covariation in paired $\delta^{13}\text{C}_{\text{carb}}$ and $\delta^{13}\text{C}_{\text{org}}$ values toward more positive values during the plateau of the MIBE (Fig. 11D, 11N). Considering that no known diagenetic mechanisms in the Precambrian can alter paired carbon isotopes in the same direction (Knoll et al., 1986), the covariation of $\delta^{13}\text{C}_{\text{carb}}$ and $\delta^{13}\text{C}_{\text{org}}$ suggests a seawater origin, instead of a porewater origin, for the MIBE (Caetano-Filho et al., 2020).

Fourth, authigenic carbonate formed within porewaters of the methanogenesis zone are essentially local and diagenetic (Meister et al., 2007; Petrov and Pokrovsky, 2020). In contrast, the MIBE has been continuously and consistently recorded for tens to hundreds of meters in strata with little sample-to-sample variation at multiple localities across the basin (Misi et al., 2007; Paula-Santos et al., 2015; Uhlein et al., 2019). The steady and continuous stratigraphic expression on a basin scale is inconsistent with any post-depositional diagenetic event. Therefore, we regard that the porewater methanogenesis hypothesis cannot fully explain all the sedimentological and stratigraphic observations of the MIBE; instead, the MIBE may reflect water-column signals in the Bambuí Basin.

5.3.2. Water-column methanogenesis?

Although the *porewater* methanogenesis hypothesis has been regarded to be inconsistent with the sedimentological and geochemical observations from the MIBE, methanogenesis in water columns may still be possible for the MIBE. Notably, the hypothesis of a large epeiric methanogenic Bambuí sea in the center of Gondwana supercontinent has recently been proposed for the MIBE based on the covariation of paired carbon isotopes from the Bambuí Group (Caetano-Filho et al., 2020). In this hypothesis, methanogenesis occurs in water columns of a restricted Bambuí Basin, generating anomalous $\delta^{13}\text{C}_{\text{carb}}$ signals on a basin scale.

Supporting evidence for water-column methanogenesis during the MIBE also comes from the S isotope data in this study (Fig. 11F, 11P). Chemostratigraphic profiles of the two sections show that higher $\delta^{13}\text{C}_{\text{carb}}$ signals during the plateau of the MIBE (Fig. 11L) are also coupled with higher $\delta^{34}\text{S}_{\text{pyrite}}$ signals (Fig. 11P). The $\delta^{34}\text{S}_{\text{CAS}}$ and S isotope fractionation ($\Delta\delta^{34}\text{S}_{\text{CAS-pyrite}}$) data are limited in this study (Fig. 11F–G, 11P–Q) due to the fact that most of the samples did not yield enough barite precipitates during CAS extraction, even though each sample was processed with at least 100 g of powders. Regardless,

assuming that the sulfate S isotope composition remains similar during MIBE, higher $\delta^{34}\text{S}_{\text{pyrite}}$ signals during the plateau of the MIBE suggest smaller $\Delta\delta^{34}\text{S}_{\text{CAS-pyrite}}$. Considering that sulfate concentration can strongly dictate the magnitude of S isotope fractionation between sulfate and sulfide (Habicht et al., 2002; Fike et al., 2015), one possible interpretation for the coupled high $\delta^{13}\text{C}_{\text{carb}}$ and high $\delta^{34}\text{S}_{\text{pyrite}}$ signals is the occurrence of enhanced methanogenesis in sulfate-depleted water columns (Fig. 16A). In this scenario, ^{13}C -depleted methane flux formed via methanogenesis in water columns and was released from the system without being oxidized (Fig. 16B). The overall low concentration of seawater sulfate in the Bambuí Basin not only facilitated methane production, but also inhibited microbial sulfate reduction, anaerobic oxidation of methane, and S isotope fractionation between sulfate and sulfide during the MIBE. Our interpretation for the C and S isotope data is also consistent with the observation that methanogens are typically outcompeted for substrates (e.g. lactate and acetate) by sulfate reducers in modern environments (Jørgensen and Kasten, 2006), and therefore methanogenesis typically only occurs in sulfate-depleted conditions.

Could the redox conditions allow for water-column methanogenesis during the MIBE? Although direct redox results (e.g., U isotopes, Fe speciation) are not available, the Ce anomaly data measured from the KM7-14 section (Fig. 12D) indicate that the redox conditions may have fluctuated during the MIBE. Regardless, methanogenesis has been reported from both oxic and anoxic water columns (Bogard et al., 2014; Birgel et al., 2015). Therefore, we regard that water-column methanogenesis remains a possible process for the MIBE.

5.4. Testing the global vs. regional origins for the MIBE

5.4.1. Sedimentological and geochemical evidence for a regional MIBE

It is notable that anomalously high $\delta^{13}\text{C}_{\text{carb}}$ signals (up to +18‰) have been reported from microbialites or tufa in modern and ancient evaporative and hypersaline lakes (Valero-Garcés et al., 2000; Gomez et al., 2014; Guo and Chafetz, 2014; Birgel et al., 2015; Buongiorno et al., 2019; Beeler et al., 2020). Interestingly, a recent case study suggests that abiotic processes like evaporation and fast CO_2 degassing alone (without invoking any biotic process) can account for positive $\delta^{13}\text{C}_{\text{carb}}$ anomalies as high as +15‰ (Buongiorno et al., 2019; Beeler et al., 2020). These studies on positive $\delta^{13}\text{C}_{\text{carb}}$ anomalies in local or regional environments offer new insights to the origin of the MIBE.

Multiple lines of evidence suggest that the MIBE may reflect a carbon cycle anomaly in a regionally restricted basin, instead of an open ocean. First, abundant oolites and stromatolites (Figs. 4, 6, 10) have been found in the MIBE (Misi and Veizer, 1998; Reis and Suss, 2016; Paula-Santos et al., 2017; dos Santos et al., 2018; Caetano-Filho et al., 2019; this study). Published studies suggest that ooid formation typically occurs in local environments with carbonate saturated, normal to elevated salinity, warm and agitated aqueous conditions (> 20 °C) (Lees, 1975; Paul and Peryt, 2000; Siewers, 2003; Lehrmann et al., 2012; Trower et al., 2017). Additionally, the occurrence of syneresis cracks and ripple marks (Fig. 5) indicates a shallow (not necessarily with subaerial exposure) condition with changing salinity in a restricted basin. These sedimentological observations (i.e., oolite, stromatolite, syneresis cracks) suggest a restricted basin with a CaCO_3 -saturated condition in upper water columns.

Second, the anomalously low $^{87}\text{Sr}/^{86}\text{Sr}$ values during the MIBE echo the scenario of a restricted basin. Published studies of the late Ediacaran strata suggest that the open ocean $^{87}\text{Sr}/^{86}\text{Sr}$ composition at that time was ca. 0.7085 to 0.7090 (Halverson et al., 2007; Jiang et al., 2007; Sawaki et al., 2010; Xiao et al., 2016; Cui et al., 2019c; Cui et al., 2020). Assuming a late Ediacaran age for the Lagoa do Jacaré Formation (see Section 2.2 for details), the anomalously low $^{87}\text{Sr}/^{86}\text{Sr}$ values (down to 0.7073) measured from the well-preserved limestone samples in this study (Fig. 11T), together with many other published $^{87}\text{Sr}/^{86}\text{Sr}$ values from the Bambuí Group (Kawashita, 1998; Misi and Veizer,

1998; Lima, 2011; Caxito et al., 2012; Alvarenga et al., 2014; Paula-Santos et al., 2015; Paula-Santos et al., 2017), indicate a restricted Bambuí Basin that was decoupled from the Ediacaran open ocean.

Third, paleogeographic studies suggest that the Bambuí Basin was located in the center of the Gondwana supercontinent, therefore representing a highly restricted basin (Fig. 2A) (Paula-Santos et al., 2017; Uhlein et al., 2019). The reconstructed orogenic belts surrounding the São Francisco Craton include the Brasília Belt in the west, the Araçuaí Belt in the east, and the Sergipana, Riacho do Pontal and Rio Preto belts in the north, all developed during the southwest Gondwana collage during the Ediacaran-Cambrian period. Such a geotectonic framework may have facilitated the formation of a restricted basin. In light of this, the low $^{87}\text{Sr}/^{86}\text{Sr}$ signals have been proposed to result from the weathering and recycling of older carbonate units surrounding the Bambuí Basin (Uhlein et al., 2019).

Fourth, the Sr/Ca ratios measured from the carbonate facies (Fig. 12E) also offer valuable information about the environmental conditions of the MIBE. Considering that different concentrations of acid used during sample dissolution can yield different Sr concentrations or Sr/Ca ratios for the same sample, it is not always feasible to compare the published Sr concentration data or Sr/Ca ratios from different studies. Regardless, multiple chemostratigraphic positive anomalies in Sr concentrations or Sr/Ca ratios have been reported from the terminal Ediacaran strata (Ries et al., 2009; Sawaki et al., 2010; Paula-Santos et al., 2015; Cui et al., 2016b; Paula-Santos et al., 2017; Caetano-Filho et al., 2019; Cui et al., 2019a; Cui et al., 2019c), suggesting a period with enhanced alkalinity and/or aragonite production (Cui et al., 2016b; Cui et al., 2019c). In this study, we compared the new Sr/Ca ratios with the published data from the Dengying Formation at the Gaojiashan section (analyzed by using the same concentration of acid in the same lab) (Cui et al., 2016b). It is notable that most of the Sr/Ca data from the Lagoa do Jacaré carbonates are higher than the Sr/Ca ratios analyzed from the carbonates in the Gaojiashan Member (Fig. 12E). The latter has been proposed to represent a period with enhanced chemical weathering, seawater alkalinity, and aragonite production that may have triggered the onset of animal biomineralization (Cui et al., 2016b; Cui et al., 2019a; Cui et al., 2019c). Compared with the data in the Gaojiashan Member, the even higher Sr/Ca data from the Lagoa do Jacaré Formation may reflect a similarly high-alkalinity condition, which is consistent with the scenario of a restricted Bambuí Basin at that time.

In summary, based on multiple lines of sedimentological, paleogeographic, and geochemical evidence, we regard that the MIBE may reflect anomalous carbon cycles in a restricted basin, and therefore was decoupled from the late Ediacaran-Cambrian open ocean.

5.4.2. Enhanced carbonate weathering in a restricted basin?

It was recently proposed that enhanced carbonate weathering may have contributed to the MIBE (Uhlein et al., 2019). This hypothesis is supported by the reconstructed paleogeography of the Bambuí Basin (Fig. 2A). Based on paleomagnetic studies, the São Francisco craton was located in the center of the Gondwana supercontinent at ca. 550 Ma (Trindade et al., 2006; Li et al., 2008; Tohver et al., 2012), where restricted basins with enhanced alkalinity via carbonate weathering and recycling was possible. It is notable that petrographic results in this study (Fig. 8) show abundant detrital components, including angular-shaped quartz grains and a few apatite, K-feldspar, and albite grains (Fig. 8A–G). The occurrence of these low-maturity detrital components in carbonate samples indicates that the depositional basin was close to its sediment sources, which echoes the reconstructed paleogeography of the Bambuí Basin (Fig. 2A) (Paula-Santos et al., 2017; Uhlein et al., 2019).

In this study, we utilized both the canonical dual-sink model and the revised triple-sink model (Fig. 14) to test the role of a carbon source with a higher isotopic value ($\delta^{13}\text{C}_{\text{in}} > -5\text{‰}$) in generating the MIBE in a restricted basin. Although the $\delta^{13}\text{C}_{\text{in}}$ value has been widely assumed

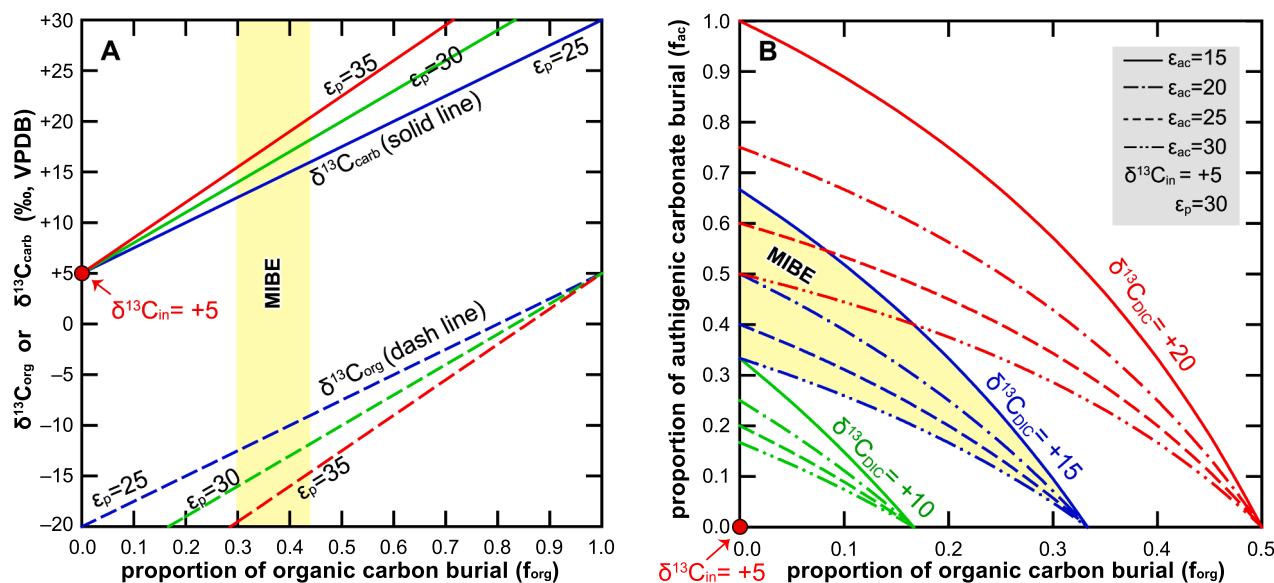


Fig. 14. Reconstructing the Middle Cambrian $\delta^{13}\text{C}_{\text{carb}}$ positive Excursion (MIBE) based on (A) the conventional dual-sink carbon cycle model and (B) the revised triple-sink carbon cycle model. In both models, we used an elevated isotopic value of the carbon source ($\delta^{13}\text{C}_{\text{in}}$) of +5‰, which is the typical backdrop $\delta^{13}\text{C}_{\text{carb}}$ value during the Neoproterozoic. Carbon cycle model in B includes ^{13}C -depleted authigenic carbonate as the third sink. Parameters f_{org} and f_{carb} represent the proportion of carbon burial as carbonate carbon and organic carbon, respectively. Fractionation factors ϵ_p , ϵ_{ac} and ϵ_{mc} represent the offset between seawater DIC and organic carbon (ϵ_p), authigenic carbonate (ϵ_{ac}) and normal marine carbonate (ϵ_{mc}), respectively. Yellow zones represent the MIBE. Abbreviation: DIC = dissolved inorganic carbon. See Section 5.4.2 for detailed discussion. (For interpretation of the references to color in this figure legend, the reader is referred to the web version of this article.)

to be -5‰ (Hayes, 1993; Kump and Arthur, 1999), an enhanced $\delta^{13}\text{C}_{\text{in}}$ — typically results from enhanced carbonate weathering — could lead to a considerable perturbation on the $\delta^{13}\text{C}_{\text{carb}}$ and $\delta^{13}\text{C}_{\text{org}}$ (Kump et al., 1999). To reconstruct the MIBE, we explored the possibility of $\delta^{13}\text{C}_{\text{in}} = +5\text{‰}$, which is the typical backdrop value of the Neoproterozoic $\delta^{13}\text{C}_{\text{carb}}$ record (Fig. 1) (Prokoph et al., 2008).

Several implications could be drawn from the models (Fig. 14). First, the variation of $\delta^{13}\text{C}_{\text{DIC}}$ is coupled with both f_{org} and f_{ac} ; and a larger fractionation induced by authigenesis could achieve the MIBE with smaller f_{org} and f_{ac} values. Second, with a higher $\delta^{13}\text{C}_{\text{in}}$ value, positive anomaly of $\delta^{13}\text{C}_{\text{DIC}}$ can be more easily achieved with certain proportions of burial in organic carbon and authigenic carbonate. Based on the dual-sink carbon model, to achieve the MIBE, around 30% to 40% of organic carbon must be buried (yellow band in Fig. 14A). Based on the triple-sink carbon model, assuming an organic carbon burial rate of 20% (i.e., current level in modern oceans), then to maintain the MIBE (yellow zone in Fig. 14B), at least 15% of ^{13}C -depleted authigenic carbonate burial is required. These calculations provide the first-order constraints of organic carbon burial during the MIBE, although more geological evidence for enhanced carbonate weathering is still needed.

5.5. Assessing the authigenic carbonate hypothesis for the MIBE

5.5.1. Carbon cycle with ^{13}C -depleted authigenic carbonate as the third sink

It has been proposed that the prolonged periods of high $\delta^{13}\text{C}_{\text{carb}}$ in the Neoproterozoic can be caused by persistent burial of a larger amount of ^{13}C -depleted authigenic carbonate, without invoking sustained high organic carbon burial (Schrag et al., 2013). This hypothesis has the potential to explain the MIBE. In the framework of the revised triple-sink carbon cycle model (see Section 5.2.2 for details), by assigning some basic assumptions ($\delta^{13}\text{C}_{\text{in}} = -5\text{‰}$, $\epsilon_p = +30\text{‰}$ and $\epsilon_{\text{mc}} = 0\text{‰}$) with varying $\delta^{13}\text{C}_{\text{DIC}}$ ($= 0\text{‰}$, $+5\text{‰}$, $+10\text{‰}$, $+15\text{‰}$) and ϵ_{ac} ($= +15\text{‰}$, $+20\text{‰}$, $+25\text{‰}$, $+30\text{‰}$), one could obtain the modeled results in Fig. 15A.

Several implications can be drawn from this model. First, the change of marine $\delta^{13}\text{C}_{\text{DIC}}$ is a function of both organic carbon burial (f_{org}) and authigenic carbonate burial (f_{ac}). An elevated $\delta^{13}\text{C}_{\text{DIC}}$ could

be maintained with an increase in authigenic carbonates burial even without any change in organic carbon burial. Second, to maintain a fixed $\delta^{13}\text{C}_{\text{DIC}}$ value, f_{org} and f_{ac} can be small if the $\delta^{13}\text{C}$ fractionation caused by authigenesis (ϵ_{ac}) is large enough. This is particularly meaningful if methane-derived authigenic carbonate — which is typically highly depleted in ^{13}C — is a considerable sink in carbon burial (see also a different view in Canfield et al., 2020), because the oxidation of methane typically leads to extremely large ϵ_{ac} . Given the above constraints, if we assume a burial rate of organic carbon that was similar to the modern value (i.e., 20%) at that time, then to achieve the MIBE, over 60% of authigenic carbonates ($\epsilon_{\text{ac}} = 30\text{‰}$) must be buried simultaneously. Alternatively, with a much higher proportion of organic carbon burial, a smaller proportion of authigenic carbonate burial is needed to achieve the MIBE based on this model. These calculations provide the first-order constraints about how the hypothesized sink of ^{13}C -depleted authigenic carbonate could potentially contribute to the MIBE, although detailed geological evidence for the existence of authigenic carbonate is still lacking.

5.5.2. Carbon cycle with ^{13}C -enriched authigenic carbonates as the third sink

It should be noted that all the discussion above is focused on ^{13}C -depleted authigenic carbonates with positive ϵ_{ac} ($= \delta^{13}\text{C}_{\text{DIC}} - \delta^{13}\text{C}_{\text{ac}}$) values. It is also possible that the sink of authigenic carbonates formed in the geological record are enriched in ^{13}C like what has been found in the methanogenesis zone of modern marine sediments (Meister et al., 2007; Birgel et al., 2015). This scenario may be particularly meaningful for the vast time of the Precambrian when the oxidant budget (e.g., O_2 , sulfate, or iron oxide) in the Earth's surface environment was depleted, and the methane flux may be directly released into the atmosphere without being oxidized (Catling et al., 2007; Ader et al., 2009; Bristow and Grotzinger, 2013; Li et al., 2015; Shen et al., 2016). It has been proposed that the overall high backdrop $\delta^{13}\text{C}_{\text{carb}}$ values (ca. $+6\text{‰}$) of the Ediacaran chemostratigraphy may reflect this scenario (Ader et al., 2009). Therefore, we also tested this scenario for the MIBE with negative ϵ_{ac} values in this study (Fig. 15B).

Modeled results in Fig. 15B suggest that, to maintain the MIBE with

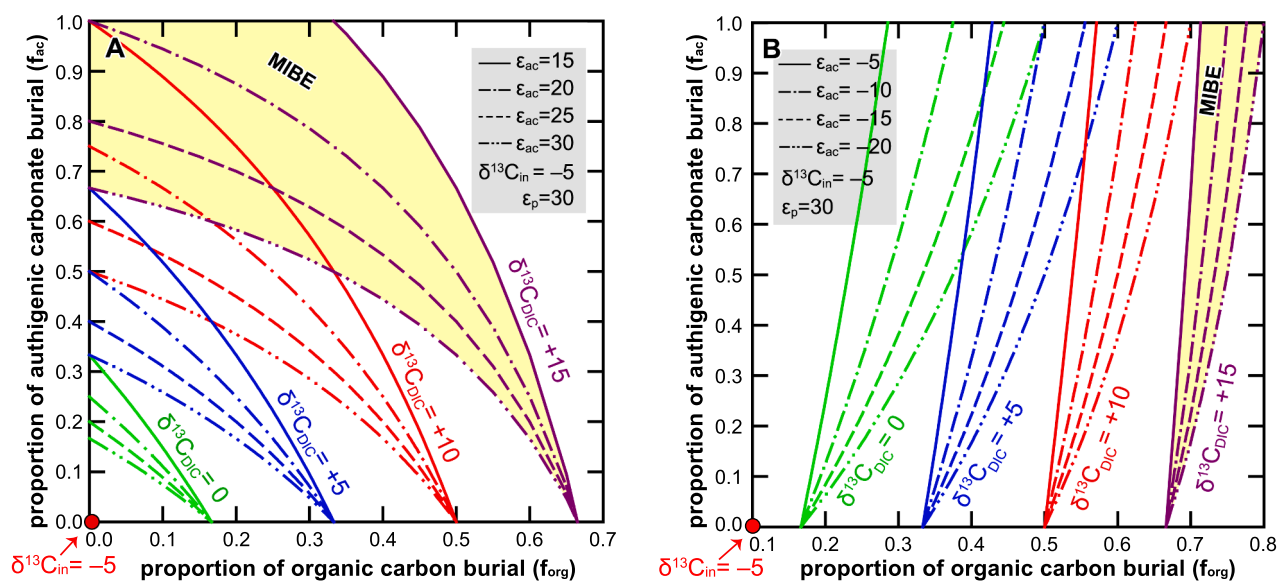


Fig. 15. Reconstructing the Middle Cambrian $\delta^{13}\text{C}_{\text{carb}}$ Excursion (MIBE) based on the triple-sink carbon cycle model. (A) Revised carbon cycle model with ^{13}C -depleted authigenic carbonates as the third sink. (B) Carbon cycle model with ^{13}C -enriched authigenic carbonates as the third sink. Parameters f_{org} and f_{carb} represent the proportion of carbon burial as carbonate carbon and organic carbon, respectively. Fractionation factors ϵ_p , ϵ_{ac} and ϵ_{mc} represent the offset between seawater DIC and organic carbon (org), authigenic carbonate (ac) and normal marine carbonate (mc), respectively. Yellow zones represent the MIBE. Abbreviation: DIC = dissolved inorganic carbon. See Section 5.5 for detailed discussion. (For interpretation of the references to color in this figure legend, the reader is referred to the web version of this article.)

a sink of ^{13}C -enriched authigenic carbonates, an organic carbon burial rate of at least 66% is required. This scenario appears to be rather unlikely due to the lack of supporting evidence in the geological record (e.g., strata with extremely high TOC in the Bambuí Basin; see Uhlein et al., 2019 for the TOC data). However, it should also be noted that this model is based on the assumption that MIBE (represented by $\delta^{13}\text{C}_{\text{DIC}} = +15\text{‰}$ in Fig. 15B) reflects primary seawater DIC signals in a steady state, which is not always necessarily true. Therefore, this model cannot rule out the possibility that local or regional environmental factors (e.g., water column methanogenesis and/or evaporation) may have contributed to the highly positive $\delta^{13}\text{C}_{\text{carb}}$ signals during the MIBE.

5.6. Biogeochemical context of the MIBE

Based on the integrated sedimentological, geochemical, and model results in this study, it is proposed that the MIBE may represent a carbon cycle anomaly in the water columns of a restricted Bambuí Basin (Fig. 16A). Several important observations and implications can be made for the MIBE in this study.

- (1) Based on the published work and the two new sections in this study, it appears that the MIBE is most obvious in carbonate facies (including oolitic limestones and cross-bedded limestones). These sedimentological results, together with the covariation of paired C isotope data (Caetano-Filho et al., 2020; this study) (Fig. 11D, 11N), suggest that the MIBE reflects water-column signals, instead of porewater signals (see Section 5.3 for details).
- (2) Based on the sulfur isotope data in this study (Fig. 11F, 11P), we speculate that the seawater in the Bambuí Basin may be depleted in sulfate, therefore facilitating methanogenesis in seawaters during the MIBE. Enhanced methanogenesis in the water columns of the Bambuí Basin may have generated a large amount of ^{13}C -depleted methane. If the methane flux was released from sediments and water columns without being oxidized, seawater DIC should record anomalously positive $\delta^{13}\text{C}_{\text{carb}}$ signals (Fig. 16A, 16B) (Caetano-Filho et al., 2020).
- (3) Enhanced carbonate weathering and recycling may have also contributed to the genesis of the MIBE (Uhlain et al., 2019). Our models

demonstrate that elevated isotopic values of the carbon input ($\delta^{13}\text{C}_{\text{in}}$) to the Bambuí basin can facilitate the genesis of higher $\delta^{13}\text{C}_{\text{carb}}$ in seawaters (Fig. 14).

- (4) Whether authigenic carbonate — an overlooked major sink hypothesized by Schrag et al. (2013) — has played a role in the MIBE remains uncertain. We provide the first-order constraints for the MIBE in the framework of the triple-sink carbon cycle model (Fig. 15). However, direct geological evidence for the occurrence of authigenic carbonate mineralization during the MIBE is still lacking.
- (5) Based on the biogeochemical model proposed in this study (Fig. 16), the anomalously high $\delta^{13}\text{C}_{\text{carb}}$ signals (up to $+16\text{‰}$) and anomalously low $^{87}\text{Sr}/^{86}\text{Sr}$ signals (down to 0.7073) in the MIBE may be largely limited to the restricted Bambuí Basin, and therefore was decoupled from the Ediacaran-Cambrian open ocean. In the open ocean, Ediacaran-Cambrian seawaters with higher sulfate concentration, lower $\delta^{13}\text{C}_{\text{carb}}$ signals of ca. $+5\text{‰}$, and higher $^{87}\text{Sr}/^{86}\text{Sr}$ signals of ca. 0.7084 (Fig. 16C) may coexist with the MIBE (Fig. 16A, 16B) at that time.

5.7. Implications on the $\delta^{13}\text{C}_{\text{carb}}$ chemostratigraphy

Largely based on carbon and strontium isotopic chemostratigraphy (including the positive $\delta^{13}\text{C}_{\text{carb}}$ excursions and the lowest $^{87}\text{Sr}/^{86}\text{Sr}$ values of ca. 0.7073), the MIBE in Brazil and a similar positive $\delta^{13}\text{C}_{\text{carb}}$ anomaly (aka the Hüttenberg anomaly) in the Hüttenberg Formation of northern Namibia have been considered as equivalent Cryogenian strata right before the Marinoan glaciation (Kaufman and Knoll, 1995; Kaufman et al., 1997; Misi et al., 2007; Kaufman et al., 2009). This stratigraphic scheme is tempting given that many other remarkably positive $\delta^{13}\text{C}_{\text{carb}}$ anomalies have also been found preceding the Marinoan glaciation on a global scale, including the Keele Formation ($\delta^{13}\text{C}_{\text{carb}}$ up to ca. $+10\text{‰}$) in Canada (Narbonne et al., 1994; Kaufman et al., 1997), the Etina Formation ($\delta^{13}\text{C}_{\text{carb}}$ up to ca. $+10\text{‰}$) in Australia (Walter et al., 2000; McKirdy et al., 2001; Swanson-Hysell et al., 2010; Rose et al., 2012), and the Tayshir Formation ($\delta^{13}\text{C}_{\text{carb}}$ up to ca. $+12\text{‰}$) in Mongolia (Brasier et al., 1996a; Brasier et al., 1996b; Shields et al., 1997; Shields et al., 2002; Macdonald et al., 2009; Bold et al.,

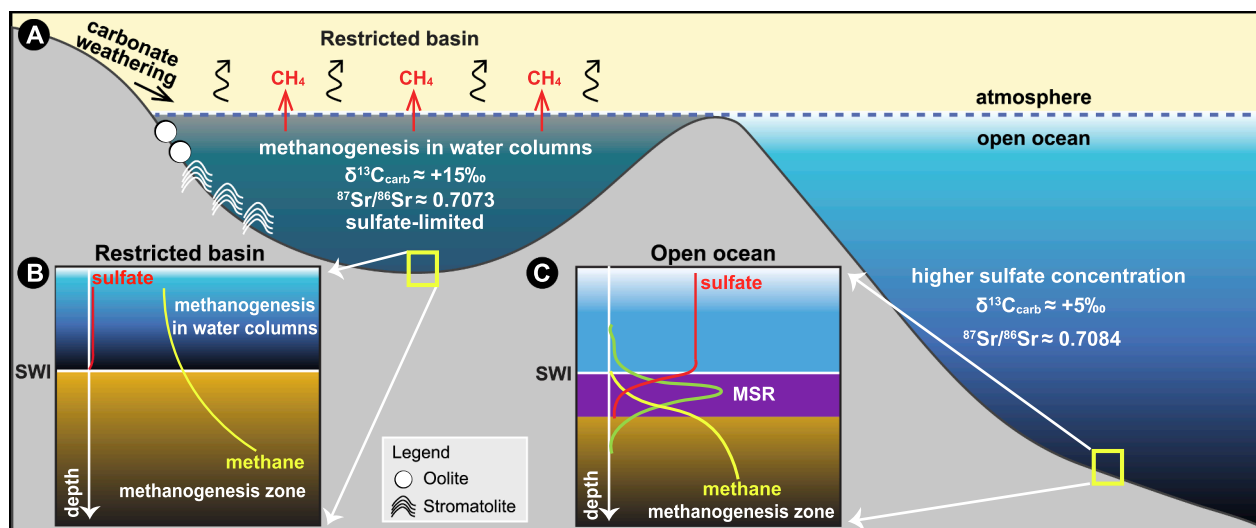


Fig. 16. Biogeochemical model for the Middle Bambuí $\delta^{13}\text{C}_{\text{carb}}$ Excursion (MIBE). (A) The MIBE represents a regional carbon cycle anomaly in a restricted Bambuí Basin that was disconnected from the Ediacaran-Cambrian open ocean. Local or regional environmental factors like water-column methanogenesis, carbonate weathering and recycling, and/or evaporation may have played a role in the generating the MIBE. See Sections 5.3, 5.4 and 5.6 for detailed discussion. (B) Schematic model for the redox zonation across the sediment–water interface of the restricted Bambuí Basin during the MIBE. (C) Schematic model for the redox zonation across the sediment–water interface of the Ediacaran-Cambrian open ocean. Abbreviations: MSR = microbial sulfate reduction; SWI = sediment–water interface. See the main text for a further discussion.

2016). By correlating the MIBE and the Hüttenberg anomaly with the many other pre-Marinoan positive $\delta^{13}\text{C}_{\text{carb}}$ anomalies, one has to also place the associated diamictite intervals to the Sturtian, instead of the Marinoan, realm (Misi et al., 2007; Kaufman et al., 2009).

However, the above correlation scheme appears to be in conflict with multiple lines of published geochronological and paleontological evidence, including the ca. 635 Ma age for the Ghaub diamictite in Namibia (Hoffmann et al., 2004; Prave et al., 2016), the preservation of *Cloudina* fossil in the lower Sete Lagoas Formation (Warren et al., 2014; Perrella Júnior et al., 2017), and the detrital zircon ages throughout the Bambuí Group (see Section 2.2 for details). Without the solid evidence to falsify these published results at the moment, correlating the MIBE and the Hüttenberg anomaly to other Cryogenian strata is still problematic.

Alternatively, our study suggests that the MIBE may represent a regional, instead of a global, carbon cycle anomaly during the Ediacaran-Cambrian transition. The global open ocean origin for many positive $\delta^{13}\text{C}_{\text{carb}}$ anomalies has been widely assumed but increasingly challenged in the stratigraphic correlation of the Precambrian strata (Frimmel, 2010; Hoffman and Lamothe, 2019). Although this study cannot fully test all the potential hypotheses for the MIBE, constraints from the sedimentological and geochemical results indicate that neither the conventional carbon cycle model nor the porewater methanogenesis hypothesis is valid. Instead, local or regional factors like water-column methanogenesis and carbonate recycling may have played a role independently or in tandem during the MIBE.

The recognition of local controlling factors in large positive $\delta^{13}\text{C}_{\text{carb}}$ excursions may fundamentally undermine their applications in global correlations. Our study suggests that some of the Neoproterozoic carbon cycle anomalies may not be a reliable record of global carbon cycles. In light of this, we caution against the use of the MIBE in chemostratigraphic correlations on a global scale or any attempt to infer global carbon cycling at that time. Many other similarly positive $\delta^{13}\text{C}_{\text{carb}}$ anomalies in the Neoproterozoic Era (Halverson et al., 2005; Kaufman et al., 2009; Halverson et al., 2010; Cui et al., 2018) and beyond should also be carefully evaluated before being used for chemostratigraphic correlations.

6. Conclusions

In order to constrain the origins of the middle Bambuí $\delta^{13}\text{C}_{\text{carb}}$ excursion (MIBE) in Brazil, we conducted a detailed sedimentological and chemostratigraphic investigation for the plateau (i.e., Lagoa do Jacaré Formation at the KM7-14 section) and the recovery part (i.e., lower Serra da Saudade Formation at the KM7-12 section) of the MIBE. The carbonate-dominated KM7-14 section shows $\delta^{13}\text{C}_{\text{carb}}$ values up to +13.9‰, while the siliciclastic-dominated KM7-12 section shows lower $\delta^{13}\text{C}_{\text{carb}}$ values (mean +7.5‰). It is notable that these two different sections show distinct $\delta^{13}\text{C}_{\text{carb}}$, $\delta^{13}\text{C}_{\text{org}}$, $\delta^{18}\text{O}_{\text{carb}}$, and $\delta^{34}\text{S}_{\text{pyrite}}$ signals (Fig. 11; Fig. S4). The plateau of the MIBE is characterized by higher $\delta^{13}\text{C}_{\text{carb}}$, higher $\delta^{13}\text{C}_{\text{org}}$, and higher $\delta^{34}\text{S}_{\text{pyrite}}$ signals in this study (Fig. 11L, 11N, 11P).

Based on integrated results, we propose that neither the conventional carbon cycle model nor the porewater methanogenesis hypothesis can sufficiently explain the MIBE. Instead, regional controlling factors like water-column methanogenesis and carbonate recycling may have played a role in the MIBE. The anomalously high $\delta^{13}\text{C}_{\text{carb}}$ signals (up to +16‰) and anomalously low $^{87}\text{Sr}/^{86}\text{Sr}$ signals (down to 0.7073) during the MIBE may be largely limited to the restricted Bambuí Basin, and therefore was decoupled from the Ediacaran-Cambrian open ocean (Fig. 16).

In light of this study, we caution against the use of the MIBE in chemostratigraphic correlations on a global scale, or any other attempt to infer global carbon cycling at that time. The biogeochemical landscape of the late Ediacaran-Cambrian basins and ocean margins may be more heterogeneous than previously thought.

Declaration of Competing Interest

The authors declare that they have no known competing financial interests or personal relationships that could have appeared to influence the work reported in this paper.

Acknowledgements

This paper is a contribution to the special issue “Neoproterozoic Earth-Life System”. The paper was handled by Frances Westall (editor)

and Feifei Zhang (guest editor). This paper has been significantly improved by constructive reviews by Paul Hoffman (Harvard & Victoria), Zhenbing She (CUG-Wuhan), and the anonymous reviewers. The authors thank Aroldo Misi, Alan Jay Kaufman, Kristen (Miller) Slawter, and Manoel Tuller for assistance in the field sampling; Richard Walker and Igor Puchtel for their guide in Sr isotope analysis; Zakri Siegel for assistance in CAS extraction; Aroldo Misi, Alan Jay Kaufman, and Shuhai Xiao for helpful comments.

This study was partly funded by AJK's FESD grant (NSF-EAR 13-38810), AM's CNPq grants (CNPq-486416/2006-2), LW's FAPESP grant (2018/26230-6), and GU's grants (CNPq-447449/2014-1 and FAPEMIG-APQ-01711-14). LW is a fellow of the CNPq. SG and PhC acknowledge support by the Belgian Science Policy (BELSPO), the Research Foundation - Flanders (FWO), and the VUB strategic program. HC acknowledges support from the ET-HOME (Evolution and Tracers of the Habitability of Mars and Earth) astrobiology research consortium during his postdoc in Brussels, Belgium.

Appendix A. Supplementary data

Supplementary data to this article can be found online at <https://doi.org/10.1016/j.precamres.2020.105861>.

References

- Ader, M., Macouin, M., Trindade, R.I.F., Hadrien, M.-H., Yang, Z., Sun, Z., Besse, J., 2009. A multilayered water column in the Ediacaran Yangtze platform? insights from carbonate and organic matter paired $\delta^{13}\text{C}$. *Earth Planet. Sci. Lett.* 288, 213–227. <https://doi.org/10.1016/j.epsl.2009.09.024>.
- Alkmim, F.F., Martins-Neto, M.A., 2012. Proterozoic first-order sedimentary sequences of the São Francisco craton, eastern Brazil. *Mar. Pet. Geol.* 33, 127–139. <https://doi.org/10.1016/j.marpetgeo.2011.08.011>.
- Alvarenga, C.J.S., Santos, R.V., Vieira, L.C., Lima, B.A.F., Mancini, L.H., 2014. Meso-Neoproterozoic isotope stratigraphy on carbonates platforms in the Brasília Belt of Brazil. *Precamb. Res.* 251, 164–180. <https://doi.org/10.1016/j.precamres.2014.06.011>.
- Amthor, J.E., Grotzinger, J.P., Schröder, S., Bowring, S.A., Ramezani, J., Martin, M.W., Matter, A., 2003. Extinction of *Cloudina* and *Namacalathus* at the Precambrian-Cambrian boundary in Oman. *Geology* 31, 431–434. [https://doi.org/10.1130/0091-7613\(2003\)031<0431:eocana>2.0.co;2](https://doi.org/10.1130/0091-7613(2003)031<0431:eocana>2.0.co;2).
- Babinski, M., Vieira, L.C., Trindade, R.I.F., 2007. Direct dating of the Sete Lagoas cap carbonate (Bambuú Group, Brazil) and implications for the Neoproterozoic glacial events. *Terra Nova* 19, 401–406. <https://doi.org/10.1111/j.1365-3121.2007.00764.x>.
- Banner, J.L., 1995. Application of the trace element and isotope geochemistry of strontium to studies of carbonate diagenesis. *Sedimentology* 42, 805–824. <https://doi.org/10.1111/j.1365-3091.1995.tb00410.x>.
- Bao, H., Lyons, J., Zhou, C., 2008. Triple oxygen isotope evidence for elevated CO_2 levels after a Neoproterozoic glaciation. *Nature* 453, 504–506. <https://doi.org/10.1038/nature06959>.
- Bao, H., 2015. Sulfate: a time capsule for Earth's O_2 , O_3 , and H_2O . *Chem. Geol.* 395, 108–118. <https://doi.org/10.1016/j.chemgeo.2014.11.025>.
- Beeler, S.R., Gomez, F.J., Bradley, A.S., 2020. Controls of extreme isotopic enrichment in modern microbialites and associated abiogenic carbonates. *Geochim. Cosmochim. Acta* 269, 136–149. <https://doi.org/10.1016/j.gca.2019.10.022>.
- Berner, R.A., Petsch, S.T., 1998. The sulfur cycle and atmospheric oxygen. *Science* 282, 1426–1427. <https://doi.org/10.1126/science.282.5393.1426>.
- Berner, R.A., 1999. Atmospheric oxygen over Phanerozoic time. *Proc. Natl. Acad. Sci.* 96, 10955–10957. <https://doi.org/10.1073/pnas.96.20.10955>.
- Birgel, D., Meister, P., Lundberg, R., Horath, T.D., Bontognali, T.R.R., Bahniuk, A.M., de Rezende, C.E., Vasconcelos, C., McKenzie, J.A., 2015. Methanogenesis produces strong ^{13}C enrichment in stromatolites of Lagoa Salgada, Brazil: a modern analogue for Palaeo-/Neoproterozoic stromatolites? *Geobiology* 13, 245–266. <https://doi.org/10.1111/gbi.12130>.
- Bishop, J.W., Osleger, D.A., Montañez, I.P., Sumner, D.Y., 2014. Meteoric diagenesis and fluid-rock interaction in the Middle Permian Carbonian backreef Yates Formation, Slaughter Canyon, New Mexico. *AAPG Bull.* 98, 1495–1519. <https://doi.org/10.1306/052013111158>.
- Bogard, M.J., del Giorgio, P.A., Boutet, L., Chaves, M.C.G., Prairie, Y.T., Merante, A., Derry, A.M., 2014. Oxidic water column methanogenesis as a major component of aquatic CH_4 fluxes. *Nat. Commun.* 5, 5350. <https://doi.org/10.1038/ncomms6350>.
- Bold, U., Smith, E.F., Rooney, A.D., Bowring, S.A., Buchwaldt, R., Dudás, F.Ö., Ramezani, J., Crowley, J.L., Schrag, D.P., Macdonald, F.A., 2016. Neoproterozoic stratigraphy of the Zavkhan terrane of Mongolia: the backbone for Cryogenian and early Ediacaran chemostratigraphic records. *Am. J. Sci.* 316, 1–63. <https://doi.org/10.2475/01.2016.01>.
- Brasier, M.D., Dorjnamjaa, D., Lindsay, J., 1996a. The Neoproterozoic to early Cambrian in southwest Mongolia: an introduction. *Geol. Mag.* 133, 365–369. <https://doi.org/10.1017/s0016756800007548>.
- Brasier, M.D., Shields, G., Kuleshov, V.N., Zhegallo, E.A., 1996b. Integrated chemo- and biostratigraphic calibration of early animal evolution: Neoproterozoic–early Cambrian of southwest Mongolia. *Geol. Mag.* 133, 445–485. <https://doi.org/10.1017/s0016756800007603>.
- Bristow, T.F., Grotzinger, J.P., 2013. Sulfate availability and the geological record of cold-seep deposits. *Geology* 41, 811–814. <https://doi.org/10.1130/g34265.1>.
- Broecker, W.S., 1970. A boundary condition on the evolution of atmospheric oxygen. *J. Geophys. Res.* 75, 3553–3557. <https://doi.org/10.1029/JC075i018p03553>.
- Buongiorno, J., Gomez, F.J., Fike, D.A., Kah, L.C., 2019. Mineralized microbialites as archives of environmental evolution, Laguna Negra, Catamarca Province, Argentina. *Geobiology* 17, 199–222. <https://doi.org/10.1111/gbi.12327>.
- Caetano-Filho, S., Macedo Paula-Santos, G., Guacaneme, C., Babinski, M., Bedoya-Rueda, C., Peloso, M., Amorim, K., Afonso, J., Kuchenbecker, M., Reis, H., Trindade, R.I.F., 2019. Sequence stratigraphy and chemostratigraphy of an Ediacaran-Cambrian foreland-related carbonate ramp (Bambuú Group, Brazil). *Precamb. Res.* 331, 105365. <https://doi.org/10.1016/j.precamres.2019.105365>.
- Caetano-Filho, S., Sansjofre, P., Ader, M., Paula-Santos, G., Guacaneme, C., Babinski, M., Bedoya-Rueda, C., Kuchenbecker, M., Reis, H.L.S., Trindade, R.I.F., 2020. A large epeiric methanogenic Bambuí sea in the core of Gondwana supercontinent? *Geosci. Front.* <https://doi.org/10.1016/j.gsf.2020.04.005>. In press.
- Canfield, D.E., Kump, L.R., 2013. Carbon cycle makeover. *Science* 339, 533–534. <https://doi.org/10.1126/science.1231981>.
- Canfield, D.E., Knoll, A.H., Poulton, S.W., Narbonne, G.M., Dunning, G.R., 2020. Carbon isotopes in clastic rocks and the Neoproterozoic carbon cycle. *Am. J. Sci.* 320, 97–124. <https://doi.org/10.2475/02.2020.01>.
- Cao, M., Daines, S.J., Lenton, T.M., Cui, H., Algeo, T.J., Dahl, T.W., Shi, W., Chen, Z.-Q., Anbar, A., Zhou, Y.-Q., 2020. Comparison of Ediacaran platform and slope $\delta^{238}\text{U}$ records in South China: implications for global-ocean oxygenation and the origin of the Shuram Excursion. *Geochim. Cosmochim. Acta.* <https://doi.org/10.1016/j.gca.2020.04.035>. In press.
- Cao, X., Bao, H., 2013. Dynamic model constraints on oxygen-17 depletion in atmospheric O_2 after a snowball Earth. *Proc. Natl. Acad. Sci.* 110, 14546–14550. <https://doi.org/10.1073/pnas.1302972110>.
- Catling, D.C., Claire, M.W., Zahnle, K.J., 2007. Anaerobic methanotrophy and the rise of atmospheric oxygen. *Philos. Trans. R. Soc. A* 365, 1867–1888. <https://doi.org/10.1098/rsta.2007.2047>.
- Caxito, F.A., Halverson, G.P., Uhlein, A., Stevenson, R., Dias, T.G., Uhlein, G.J., 2012. Marinoan glaciation in east central Brazil. *Precamb. Res.* 200, 38–58. <https://doi.org/10.1016/j.precamres.2012.01.005>.
- Caxito, F.A., Frei, R., Uhlein, G.J., Dias, T.G., Ártng, T.B., Uhlein, A., 2018. Multiproxy geochemical and isotope stratigraphy records of a Neoproterozoic Oxygenation Event in the Ediacaran Sete Lagoas cap carbonate, Bambuí Group, Brazil. *Chem. Geol.* 481, 119–132. <https://doi.org/10.1016/j.chemgeo.2018.02.007>.
- Claypool, G.E., Kaplan, I., 1974. The origin and distribution of methane in marine sediments. In: Kaplan, I.R. (Ed.), *Natural Gases in Marine Sediments*. Springer, Boston, MA, pp. 99–139. https://doi.org/10.1007/978-1-4684-2757-8_8.
- Crockford, P.W., Hodgskiss, M.S.W., Uhlein, G.J., Caxito, F., Hayes, J.A., Halverson, G.P., 2018. Linking paleocontinents through triple oxygen isotope anomalies. *Geology* 46, 179–182. <https://doi.org/10.1130/G39470.1>.
- Cui, H., Kaufman, A.J., Xiao, S., Zhu, M., Zhou, C., Liu, X.-M., 2015. Redox architecture of an Ediacaran ocean margin: integrated chemostratigraphic ($\delta^{13}\text{C}$ - $\delta^{34}\text{S}$ - $\delta^{87}\text{Sr}$ - $\delta^{86}\text{Sr}$ -Ce/Ce⁺) correlation of the Doushantuo Formation, South China. *Chem. Geol.* 405, 48–62. <https://doi.org/10.1016/j.chemgeo.2015.04.009>.
- Cui, H., Grazhdankin, D.V., Xiao, S., Peek, S., Rogov, V.I., Bykova, N.V., Sievers, N.E., Liu, X.-M., Kaufman, A.J., 2016a. Redox-dependent distribution of early macro-organisms: evidence from the terminal Ediacaran Khatyspyt Formation in Arctic Siberia. *Palaeogeogr. Palaeoclimatol. Palaeoecol.* 461, 122–139. <https://doi.org/10.1016/j.palaeo.2016.08.015>.
- Cui, H., Kaufman, A.J., Xiao, S., Peek, S., Cao, H., Min, X., Cai, Y., Siegel, Z., Liu, X.-M., Peng, Y., Schiffbauer, J.D., Martin, A.J., 2016b. Environmental context for the terminal Ediacaran biomineralization of animals. *Geobiology* 14, 344–363. <https://doi.org/10.1111/gbi.12178>.
- Cui, H., Kaufman, A.J., Xiao, S., Zhou, C., Liu, X.-M., 2017. Was the Ediacaran Shuram Excursion a globally synchronized early diagenetic event? insights from methane-derived authigenic carbonates in the uppermost Doushantuo Formation, South China. *Chem. Geol.* 450, 59–80. <https://doi.org/10.1016/j.chemgeo.2016.12.010>.
- Cui, H., Kaufman, A.J., Peng, Y., Liu, X.-M., Plummer, R.E., Lee, E.I., 2018. The Neoproterozoic Hüttenberg $\delta^{13}\text{C}$ anomaly: genesis and global implications. *Precamb. Res.* 313, 242–262. <https://doi.org/10.1016/j.precamres.2018.05.024>.
- Cui, H., Kaufman, A.J., Xiao, S., Grazhdankin, D.V., Peek, S., Martin, A.J., Bykova, N.V., Rogov, V.I., Liu, X.-M., Zhang, F., Romaniello, S.J., Anbar, A.D., Peng, Y., Cai, Y., Schiffbauer, J.D., Meyer, M., Gilleaudeau, G.J., Plummer, R.E., Sievers, N.E., Goderis, S., Claeys, P., 2019a. Recent advances in understanding the terminal Ediacaran Earth-life system in South China and Arctic Siberia. *International Meeting on the Ediacaran System and the Ediacaran–Cambrian Transition, Guadalupe, Extremadura, Spain*, <https://doi.org/10.3989/eegeol.43586.552>.
- Cui, H., Orland, I.J., Kitajima, K., Xiao, S., Kaufman, A.J., Fournelle, J.H., Baele, J.-M., Goderis, S., Claeys, P., Valley, J.W., 2019b. Probing an atypical Shuram Excursion by SIMS. *Geological Society of America Abstracts with Programs*. Vol. 51, No. 5, Phoenix, Arizona, USA, <https://doi.org/10.1130/abs/2019AM-332454>.
- Cui, H., Xiao, S., Cai, Y., Peek, S., Plummer, R.E., Kaufman, A.J., 2019c. Sedimentology and chemostratigraphy of the terminal Ediacaran Dengying Formation at the Gaojiaoshan section, South China. *Geol. Mag.* 156, 1924–1948. <https://doi.org/10.1017/S0016756819000293>.
- Cui, H., Kaufman, A.J., Zou, H., Kattan, F.H., Trusler, P., Smith, J., Ivantsov, Yu.A., Rich, T.H., Al Qubani, A., Yazed, A., Liu, X.-M., Johnson, P., Goderis, S., Claeys, P., Vickers-Rich, P., 2020. Primary or secondary? a dichotomy of the strontium isotope anomalies in the Ediacaran carbonates of Saudi Arabia. *Precamb. Res.* 105720. <https://doi.org/10.1016/j.precamres.2020.105720>.
- Dardenne, M.A., 1978. *Síntese sobre a estratigrafia do Grupo Bambuí no Brasil Central*. Congresso Brasil. Geol. 597–610.
- Derry, L.A., Kaufman, A.J., Jacobsen, S.B., 1992. Sedimentary cycling and environmental

- change in the Late Proterozoic: evidence from stable and radiogenic isotopes. *Geochim. Cosmochim. Acta* 56, 1317–1329. [https://doi.org/10.1016/0016-7037\(92\)90064-p](https://doi.org/10.1016/0016-7037(92)90064-p).
- Derry, L.A., 2010a. On the significance of $\delta^{13}\text{C}$ correlations in ancient sediments. *Earth Planet. Sci. Lett.* 296, 497–501. <https://doi.org/10.1016/j.epsl.2010.05.035>.
- Derry, L.A., 2010b. A burial diagenesis origin for the Ediacaran Shuram-Wonoka carbon isotope anomaly. *Earth Planet. Sci. Lett.* 294, 152–162. <https://doi.org/10.1016/j.epsl.2010.03.022>.
- Des Marais, D.J., Strauss, H., Summons, R.E., Hayes, J.M., 1992. Carbon isotope evidence for the stepwise oxidation of the Proterozoic environment. *Nature* 359, 605–609. <https://doi.org/10.1038/359605a0>.
- dos Santos, D.M., Sanchez, E.A., Santucci, R.M., 2018. Morphological and petrographic analysis of newly identified stromatolitic occurrences in the Lagoa do Jacaré Formation, Bambuí Group, State of Minas Gerais, Brazil. *Rev. Brasil. Paleontol.* 21, 195–207. <https://doi.org/10.4072/rbp.2018.3.01>.
- Drummond, J.B.R., Pufahl, P.K., Porto, C.G., De Souza Carvalho, M., 2015. Neoproterozoic phosporite from the Sete Lagoas Formation (Brazil) and the Precambrian phosphorus cycle. *Sedimentology* 62, 1978–2008. <https://doi.org/10.1111/sed.12214>.
- Dyer, B., Higgins, J.A., Maloof, A.C., 2017. A probabilistic analysis of meteorically altered $\delta^{13}\text{C}$ chemostratigraphy from late Paleozoic ice age carbonate platforms. *Geology* 45, 135–138. <https://doi.org/10.1130/g38513.1>.
- Edwards, C.T., Fike, D.A., Saltzman, M.R., 2019. Testing carbonate-associated sulfate (CAS) extraction methods for sulfur isotope stratigraphy: a case study of a Lower-Middle Ordovician carbonate succession, Shingle Pass, Nevada, USA. *Chem. Geol.* 119297. <https://doi.org/10.1016/j.chemgeo.2019.119297>.
- Fike, D.A., Grotzinger, J.P., Pratt, L.M., Summons, R.E., 2006. Oxidation of the Ediacaran ocean. *Nature* 444, 744–747. <https://doi.org/10.1038/nature05345>.
- Fike, D.A., Bradley, A.S., Rose, C.V., 2015. Rethinking the ancient sulfur cycle. *Annu. Rev. Earth Planet. Sci.* 43, 593–622. <https://doi.org/10.1146/annurev-earth-060313-054802>.
- Frimmel, H.E., 2010. On the reliability of stable carbon isotopes for Neoproterozoic chemostratigraphic correlation. *Precamb. Res.* 182, 239–253. <https://doi.org/10.1016/j.precamres.2010.01.003>.
- Gaucher, C., Boggiani, P., Sprechmann, P., Sial, A., Fairchild, T., 2003. Integrated correlation of the Vendian to Cambrian Arroyo del Soldado and Corumbá Groups (Uruguay and Brazil): palaeogeographic, palaeoclimatic and palaeobiologic implications. *Precamb. Res.* 120, 241–278. [https://doi.org/10.1016/s0301-9268\(02\)00140-7](https://doi.org/10.1016/s0301-9268(02)00140-7).
- Germs, G.J., 1972. New shelly fossils from Nama Group, South West Africa. *Am. J. Sci.* 272, 752–761. <https://doi.org/10.2475/ajs.272.8.752>.
- Gischler, E., Swart, P.K., Lomando, A.J., 2007. Stable isotopes of carbon and oxygen in modern sediments of carbonate platforms, barrier reefs, atolls and ramps: patterns and implications. In: K., S.P., P., E.G., A., M.J., Jarvis, I., Stevens, T. (Eds.), *Perspectives in Carbonate Geology: A Tribute to the Career of Robert Nathan Ginsburg*, pp. 61–74. <https://doi.org/10.1002/9781444312065.ch5>.
- Gomez, F.J., Kah, L.C., Bartley, J.K., Astini, R.A., 2014. Microbialites in a high-altitude Andean lake: multiple controls in carbonate precipitation and lamina accretion. *Palaios* 29, 233–249. <https://doi.org/10.2110/palo.2013.049>.
- Grotzinger, J.P., Watters, W.A., Knoll, A.H., 2000. Calcified metazoans in thrombolite-stromatolite reefs of the terminal Proterozoic Nama Group, Namibia. *Paleobiology* 26, 334–359. [https://doi.org/10.1666/0094-8373\(2000\)026<0334:cmitsr>2.0.co;2](https://doi.org/10.1666/0094-8373(2000)026<0334:cmitsr>2.0.co;2).
- Guacaneme, C., Babinski, M., Paula-Santos, G.M.d., Pedrosa-Soares, A.C., 2017. C, O, and Sr isotopic variations in Neoproterozoic-Cambrian carbonate rocks from Sete Lagoas Formation (Bambuí Group), in the Southern São Francisco Basin, Brazil. *Braz. J. Geol.* 47, 521–543. <https://doi.org/10.1590/2317-4889201720160126>.
- Guo, X., Chafetz, H.S., 2014. Trends in $\delta^{18}\text{O}$ and $\delta^{13}\text{C}$ values in lacustrine tufa mounds: Palaeohydrology of Searles Lake, California. *Sedimentology* 61, 221–237. <https://doi.org/10.1111/sed.12085>.
- Habicht, K.S., Gade, M., Thamdrup, B., Berg, P., Canfield, D.E., 2002. Calibration of sulfate levels in the Archean ocean. *Science* 298, 2372–2374. <https://doi.org/10.1126/science.1078265>.
- Hagadorn, J.W., Waggoner, B., 2000. Ediacaran fossils from the southwestern Great Basin, United States. *J. Paleontol.* 74. [https://doi.org/10.1666/0022-3360\(2000\)074<0349:eftsg>2.0.co;2](https://doi.org/10.1666/0022-3360(2000)074<0349:eftsg>2.0.co;2).
- Halverson, G.P., Hoffman, P.F., Schrag, D.P., Maloof, A.C., Rice, A.H.N., 2005. Toward a Neoproterozoic composite carbon-isotope record. *Geol. Soc. Am. Bull.* 117, 1181–1207. <https://doi.org/10.1130/b25630.1>.
- Halverson, G.P., Dudás, F.Ö., Maloof, A.C., Bowring, S.A., 2007. Evolution of the $^{87}\text{Sr}/^{86}\text{Sr}$ composition of Neoproterozoic seawater. *Palaeogeogr. Palaeoclimatol. Palaeoecol.* 256, 103–129. <https://doi.org/10.1016/j.palaeo.2007.02.028>.
- Halverson, G.P., Wade, B.P., Hurtgen, M.T., Barovich, K.M., 2010. Neoproterozoic chemostratigraphy. *Precamb. Res.* 182, 337–350. <https://doi.org/10.1016/j.precamres.2010.04.007>.
- Hayes, J.M., 1993. Factors controlling ^{13}C contents of sedimentary organic compounds: Principles and evidence. *Mar. Geol.* 113, 111–125. [https://doi.org/10.1016/0025-3227\(93\)90153-m](https://doi.org/10.1016/0025-3227(93)90153-m).
- Hayes, J.M., Strauss, H., Kaufman, A.J., 1999. The abundance of ^{13}C in marine organic matter and isotopic fractionation in the global biogeochemical cycle of carbon during the past 800 Ma. *Chem. Geol.* 161, 103–125. [https://doi.org/10.1016/s0009-2541\(99\)00083-2](https://doi.org/10.1016/s0009-2541(99)00083-2).
- Higgins, J.A., Blättler, C.L., Lundstrom, E.A., Santiago-Ramos, D.P., Akhtar, A.A., Crüger Ahm, A.S., Bialik, O., Holmden, C., Bradbury, H., Murray, S.T., Swart, P.K., 2018. Mineralogy, early marine diagenesis, and the chemistry of shallow-water carbonate sediments. *Geochim. Cosmochim. Acta* 220, 512–534. <https://doi.org/10.1016/j.gca.2017.09.046>.
- Hippert, J.P., Caxito, F.A., Uehlein, G.J., Nalini, H.A., Sial, A.N., Abreu, A.T., Nogueira, L.B., 2019. The fate of a Neoproterozoic intracratonic marine basin: Trace elements, TOC and IRON speciation geochemistry of the Bambuí Basin, Brazil. *Precamb. Res.* 330, 101–120. <https://doi.org/10.1016/j.precamres.2019.05.001>.
- Hoefs, J., Frey, M., 1976. The isotopic composition of carbonaceous matter in a metamorphic profile from the Swiss Alps. *Geochim. Cosmochim. Acta* 40, 945–951.
- Hoffman, P.F., Lamothe, K.G., 2019. Seawater-buffered diagenesis, destruction of carbon isotope excursions, and the composition of DIC in Neoproterozoic oceans. *Proc. Natl. Acad. Sci.* 116, 18874–18879. <https://doi.org/10.1073/pnas.1909570116>.
- Hoffmann, K.-H., Condon, D.J., Bowring, S.A., Crowley, J.L., 2004. U-Pb zircon date from the Neoproterozoic Ghaub Formation, Namibia: constraints on Marinoan glaciation. *Geology* 32, 817–820. <https://doi.org/10.1130/g20519.1>.
- Hofmann, H.J., Mountjoy, E.W., 2001. *Namacalathus-Cloudina* assemblage in Neoproterozoic Miette Group (Byng Formation), British Columbia: Canada's oldest shelly fossils. *Geology* 29, 1091–1094. [https://doi.org/10.1130/0091-7613\(2001\)029<1091:ncaimn>2.0.co;2](https://doi.org/10.1130/0091-7613(2001)029<1091:ncaimn>2.0.co;2).
- Iglesias, M., Uehlein, A., 2009. Estratigrafia do Grupo Bambuí e coberturas fanerozóicas no vale do rio São Francisco, norte de Minas Gerais. *Rev. Brasil. Geoci.* 39, 256–266.
- Irwin, H., Curtis, C., Coleman, M., 1977. Isotopic evidence for source of diagenetic carbonates formed during burial of organic-rich sediments. *Nature* 269, 209–213. <https://doi.org/10.1038/269209a0>.
- Iyer, S.S., Babinski, M., Krouse, H.R., Chemale Jr, F., 1995. Highly ^{13}C -enriched carbonate and organic matter in the Neoproterozoic sediments of the Bambuí Group, Brazil. *Precamb. Res.* 73, 271–282. [https://doi.org/10.1016/0301-9268\(94\)00082-3](https://doi.org/10.1016/0301-9268(94)00082-3).
- Jiang, G., Kennedy, M.J., Christie-Blick, N., 2003. Stable isotopic evidence for methane seeps in Neoproterozoic postglacial cap carbonates. *Nature* 426, 822–826. <https://doi.org/10.1038/nature02201>.
- Jiang, G., Kaufman, A.J., Christie-Blick, N., Zhang, S., Wu, H., 2007. Carbon isotope variability across the Ediacaran Yangtze platform in South China: Implications for a large surface-to-deep ocean $\delta^{13}\text{C}$ gradient. *Earth Planet. Sci. Lett.* 261, 303–320. <https://doi.org/10.1016/j.epsl.2007.07.009>.
- Jiang, G., Wang, X., Shi, X., Xiao, S., Zhang, S., Dong, J., 2012. The origin of decoupled carbonate and organic carbon isotope signatures in the early Cambrian (ca. 542–520Ma) Yangtze platform. *Earth Planet. Sci. Lett.* 317–318, 96–110. <https://doi.org/10.1016/j.epsl.2011.11.018>.
- Johnston, D.T., Macdonald, F.A., Gill, B.C., Hoffman, P.F., Schrag, D.P., 2012. Uncovering the Neoproterozoic carbon cycle. *Nature* 483, 320–323. <https://doi.org/10.1038/nature10854>.
- Jørgensen, B.B., Kastan, S., 2006. Sulfur cycling and methane oxidation. In: Schulz, H.D., Zabel, M. (Eds.), *Marine Geochemistry*. Springer-Verlag Berlin Heidelberg, Berlin, pp. 271–309. <https://doi.org/10.1007/3-540-32144-6>.
- Kaufman, A.J., Knoll, A.H., 1995. Neoproterozoic variations in the C-isotopic composition of seawater: stratigraphic and biogeochemical implications. *Precamb. Res.* 73, 27–49. [https://doi.org/10.1016/0301-9268\(94\)00070-8](https://doi.org/10.1016/0301-9268(94)00070-8).
- Kaufman, A.J., Knoll, A.H., Narbonne, G.M., 1997. Isotopes, ice ages, and terminal Proterozoic earth history. *Proc. Natl. Acad. Sci.* 94, 6600–6605.
- Kaufman, A.J., Xiao, S., 2003. High CO_2 levels in the Proterozoic atmosphere estimated from individual microfossils. *Nature* 425, 279–282. <https://doi.org/10.1038/nature01902>.
- Kaufman, A.J., Corsetti, F.A., Varni, M.A., 2007. The effect of rising atmospheric oxygen on carbon and sulfur isotope anomalies in the Neoproterozoic Johnnie Formation, Death Valley, USA. *Chem. Geol.* 237, 47–63. <https://doi.org/10.1016/j.chemgeo.2006.06.023>.
- Kaufman, A.J., Sial, A.N., Frimmel, H.E., Misi, A., 2009. Neoproterozoic to Cambrian palaeoclimatic events in southwestern Gondwana. In: Gaucher, C., Sial, A.N., Halverson, G.P., Frimmel, H.E. (Eds.), *Neoproterozoic-Cambrian Tectonics, Global Change and Evolution: a focus on southwestern Gondwana*. Developments in Precambrian Geology. Elsevier, Amsterdam, Netherlands, pp. 369–388. [https://doi.org/10.1016/s0166-2635\(09\)01626-0](https://doi.org/10.1016/s0166-2635(09)01626-0).
- Kawashita, K., 1998. *Rochas Carboníticas Neoproterozoicas da América do Sul: Idades e Inferências Químicoestratigráficas*. University of São Paulo, Brazil, pp. 126 pp.
- Killingsworth, B.A., Hayes, J.A., Zhou, C., Bao, H., 2013. Sedimentary constraints on the duration of the Marinoan Oxygen-17 Depletion (MODS) event. *Proc. Natl. Acad. Sci.* 110, 17686–17690. <https://doi.org/10.1073/pnas.1213154110>.
- Knauth, L.P., Kennedy, M.J., 2009. The late Precambrian greening of the Earth. *Nature* 460, 728–732. <https://doi.org/10.1038/nature08213>.
- Knoll, A.H., Hayes, J.M., Kaufman, A.J., Swett, K., Lambert, I.B., 1986. Secular variation in carbon isotope ratios from Upper Proterozoic successions of Svalbard and East Greenland. *Nature* 321, 832–838. <https://doi.org/10.1038/321832a0>.
- Kontorovich, A., Varlamov, A., Grazhdankin, D., Karlova, G., Klets, A., Kontorovich, V., Saraev, S., Terleev, A., Belyaev, S.Y., Varakina, I., 2008. A section of Vendian in the east of West Siberian Plate (based on data from the Borehole Vostok 3). *Russ. Geol. Geophys.* 49, 932–939. <https://doi.org/10.1016/j.rgg.2008.06.012>.
- Kump, L., Arthur, M., Patzkowsky, M., Gibbs, M., Pinkus, D., Sheehan, P., 1999. A weathering hypothesis for glaciation at high atmospheric pCO_2 during the Late Ordovician. *Palaeogeogr. Palaeoclimatol. Palaeoecol.* 152, 173–187. [https://doi.org/10.1016/s0031-0182\(99\)00046-2](https://doi.org/10.1016/s0031-0182(99)00046-2).
- Kump, L.R., Arthur, M.A., 1999. Interpreting carbon-isotope excursions: carbonates and organic matter. *Chem. Geol.* 161, 181–198. [https://doi.org/10.1016/s0009-2541\(99\)00086-8](https://doi.org/10.1016/s0009-2541(99)00086-8).
- Kump, L.R., Junium, C., Arthur, M.A., Brasier, A., Fallick, A., Melezhik, V., Lepland, A., CČrne, A.E., Luo, G., 2011. Isotopic evidence for massive oxidation of organic matter following the Great Oxidation Event. *Science* 334, 1694–1696. <https://doi.org/10.1126/science.1213999>.
- Lang, X., Tang, W., Ma, H., Shen, B., 2020. Local environmental variation obscures the interpretation of pyrite sulfur isotope records. *Earth Planet. Sci. Lett.* 533, 116056. <https://doi.org/10.1016/j.epsl.2019.116056>.
- Lawrence, M.G., Greig, A., Collerson, K.D., Kamber, B.S., 2006. Rare Earth Element and Yttrium variability in South East Queensland waterways. *Aquatic Geochem.* 12 (1), 39–72. <https://doi.org/10.1007/s10498-005-4471-8>.
- Lee, C., Love, G.D., Fischer, W.W., Grotzinger, J.P., Halverson, G.P., 2015. Marine organic matter cycling during the Ediacaran Shuram excursion. *Geology* 43, 1103–1106. <https://doi.org/10.1130/g37236.1>.

- Lees, A., 1975. Possible influence of salinity and temperature on modern shelf carbonate sedimentation. *Mar. Geol.* 19, 159–198. [https://doi.org/10.1016/0025-3227\(75\)90067-5](https://doi.org/10.1016/0025-3227(75)90067-5).
- Lehrmann, D.J., Minzioni, M., Li, X., Yu, M., Payne, J.L., Kelley, B.M., Schaal, E.K., Enos, P., 2012. Lower Triassic oolites of the Nanpanjiang Basin, south China: facies architecture, giant ooids, and diagenesis—implications for hydrocarbon reservoirs. *AAPG Bull.* 96, 1389–1414. <https://doi.org/10.1306/01231211148>.
- Li, C., Planavsky, N.J., Love, G.D., Reinhard, C.T., Hardisty, D., Feng, L., Bates, S.M., Huang, J., Zhang, Q., Chu, X., Lyons, T.W., 2015. Marine redox conditions in the middle Proterozoic ocean and isotopic constraints on authigenic carbonate formation: insights from the Chuanlinggou Formation, Yanshan Basin, North China. *Geochim. Cosmochim. Acta* 150, 90–105. <https://doi.org/10.1016/j.gca.2014.12.005>.
- Li, Z., Cao, M., Loyd, S.J., Algeo, T.J., Zhao, H., Wang, X., Zhao, L., Chen, Z.-Q., 2020. Transient and stepwise ocean oxygenation during the late Ediacaran Shuram Excursion: insights from carbonate $\delta^{238}\text{U}$ of northwestern Mexico. *Precamb. Res.* 344, 105741. <https://doi.org/10.1016/j.precambres.2020.105741>.
- Li, Z.X., Bogdanova, S.V., Collins, A.S., Davidson, A., De Waele, B., Ernst, R.E., Fitzsimons, I.C.W., Fuck, R.A., Gladkochub, D.P., Jacobs, J., Karlstrom, K.E., Lu, S., Natapov, L.M., Pease, V., Pisarevsky, S.A., Thrane, K., Vernikovsky, V., 2008. Assembly, configuration, and break-up history of Rodinia: a synthesis. *Precamb. Res.* 160, 179–210. <https://doi.org/10.1016/j.precambres.2007.04.021>.
- Lima, O.N.B.d., 2011. Estratigrafia isotópica e evolução sedimentar do Grupo Bambuí na borda ocidental do Cráton do São Francisco: implicação tectônica e paleo-ambiental. Ph.D. Dissertation, Instituto de Geociências, Universidade de Brasília, 114 pp.
- Ling, H.-F., Chen, X., Li, D., Wang, D., Shields-Zhou, G.A., Zhu, M., 2013. Cerium anomaly variations in Ediacaran–earliest Cambrian carbonates from the Yangtze Gorges area, South China: implications for oxygenation of coeval shallow seawater. *Precamb. Res.* 225, 110–127. <https://doi.org/10.1016/j.precambres.2011.10.011>.
- Liu, X.-M., Kah, L.C., Knoll, A.H., Cui, H., Kaufman, A.J., Shahar, A., Hazen, R.M., 2016. Tracing Earth's O_2 evolution using Zn/Fe ratios in marine carbonates. *Geochem. Perspect. Lett.* 2, 24–34. <https://doi.org/10.7185/geochemlet.1603>.
- Lyons, T.W., Reinhard, C.T., Planavsky, N.J., 2014. The rise of oxygen in Earth's early ocean and atmosphere. *Nature* 506, 307–315. <https://doi.org/10.1038/nature13068>.
- Macdonald, F.A., Jones, D.S., Schrag, D.P., 2009. Stratigraphic and tectonic implications of a newly discovered glacial diamictite-cap carbonate couplet in southwestern Mongolia. *Geology* 37, 123–126. <https://doi.org/10.1130/g24797a.1>.
- Malooof, A.C., Porter, S.M., Moore, J.L., Dudás, F.Ö., Bowring, S.A., Higgins, J.A., Fike, D.A., Eddy, M.P., 2010a. The earliest Cambrian record of animals and ocean geochemical change. *Geol. Soc. Am. Bull.* 122, 1731–1774. <https://doi.org/10.1130/B30346.1>.
- Malooof, A.C., Ramezani, J., Bowring, S.A., Fike, D.A., Porter, S.M., Mazouad, M., 2010b. Constraints on early Cambrian carbon cycling from the duration of the Nemakit-Daldynian–Tommotian boundary $\delta^{13}\text{C}$ shift, Morocco. *Geology* 38, 623–626. <https://doi.org/10.1130/g30726.1>.
- Marenco, P.J., Corsetti, F.A., Hammond, D.E., Kaufman, A.J., Bottjer, D.J., 2008. Oxidation of pyrite during extraction of carbonate associated sulfate. *Chem. Geol.* 247, 124–132. <https://doi.org/10.1016/j.chemgeo.2007.10.006>.
- Martins, M., Lemos, V.B., 2007. Stratigraphic analysis of the Neoproterozoic sedimentary sequences of the Sao Francisco Basin. *Rev. Brasil. Geocienc.* 37, 156–167.
- McFadden, K.A., Huang, J., Chu, X., Jiang, G., Kaufman, A.J., Zhou, C., Yuan, X., Xiao, S., 2008. Pulsed oxidation and biological evolution in the Ediacaran Doushantuo Formation. *Proc. Natl. Acad. Sci.* 105, 3197–3202. <https://doi.org/10.1073/pnas.0708336105>.
- McKirdy, D.M., Powell, T.G., 1974. Metamorphic alteration of carbon isotopic composition in ancient sedimentary organic matter: new evidence from Australia and South Africa. *Geology* 2, 591–595. [https://doi.org/10.1130/0091-7613\(1974\)2<591:MAOCIC>2.0.CO;2](https://doi.org/10.1130/0091-7613(1974)2<591:MAOCIC>2.0.CO;2).
- McKirdy, D.M., Burgess, J.M., Lemon, N.M., Yu, X., Cooper, A.M., Gostin, V.A., Jenkins, R.J.F., Both, R.A., 2001. A chemostratigraphic overview of the late Cryogenian interglacial sequence in the Adelaide Fold-Thrust Belt, South Australia. *Precamb. Res.* 106, 149–186. [https://doi.org/10.1016/S0301-9268\(00\)00130-3](https://doi.org/10.1016/S0301-9268(00)00130-3).
- Meister, P., McKenzie, J.A., Vasconcelos, C., Bernasconi, S., Frank, M., Gutjahr, M., Schrag, D.P., 2007. Dolomite formation in the dynamic deep biosphere: results from the Peru Margin. *Sedimentology* 54, 1007–1032. <https://doi.org/10.1111/j.1365-3091.2007.00870.x>.
- Misi, A., Veizer, J., 1998. Neoproterozoic carbonate sequences of the Una Group, Irecê Basin, Brazil: chemostratigraphy, age and correlations. *Precamb. Res.* 89, 87–100. [https://doi.org/10.1016/S0301-9268\(97\)00073-9](https://doi.org/10.1016/S0301-9268(97)00073-9).
- Misi, A., Kaufman, A.J., Veizer, J., Powis, K., Azmy, K., Boggiani, P.C., Gaucher, C., Teixeira, J.B.G., Sanches, A.L., Iyer, S.S., 2007. Chemostratigraphic correlation of Neoproterozoic successions in South America. *Chem. Geol.* 237, 143–167. <https://doi.org/10.1016/j.chemgeo.2006.06.019>.
- Misi, A., Kaufman, A.J., Azmy, K., Dardenne, M.A., Sial, A.N., de Oliveira, T.F., 2011. Neoproterozoic successions of the São Francisco Craton, Brazil: the Bambuí, Una, Vazante and Vaza Barris/Miaba groups and their glaciogenic deposits. In: Arnaud, E., Halverson, G.P., Shields-Zhou, G. (Eds.), *Geological Society, London, Memoirs*, pp. 509–522. <https://doi.org/10.1144/m36.48>.
- Moreira, D.S., Uhlein, A., Dussin, I.A., Uhlein, G.J., Misuzaki, A.M.P., 2020. A Cambrian age for the upper Bambuí Group, Brazil, supported by the first U-Pb dating of volcanoclastic bed. *J. S. Am. Earth Sci.* 99, 102503. <https://doi.org/10.1016/j.jsames.2020.102503>.
- Moynihán, D.P., Strauss, J.V., Nelson, L.L., Padgett, C.D., 2019. Upper Windermere Supergroup and the transition from rifting to continent-margin sedimentation, Nadaleen River area, northern Canadian Cordillera. *Bulletin* 131 (9–10), 1673–1701. <https://doi.org/10.1130/B32039.1>.
- Narbonne, G.M., Kaufman, A.J., Knoll, A.H., 1994. Integrated chemostratigraphy and biostratigraphy of the Windermere Supergroup, northwestern Canada: implications for Neoproterozoic correlations and the early evolution of animals. *Geol. Soc. Am. Bull.* 106, 1281–1292. [https://doi.org/10.1130/0016-7606\(1994\)106<1281:icabot>2.3.co;2](https://doi.org/10.1130/0016-7606(1994)106<1281:icabot>2.3.co;2).
- Oehlert, A.M., Swart, P.K., 2014. Interpreting carbonate and organic carbon isotope covariance in the sedimentary record. *Nat. Commun.* 5, 4672. <https://doi.org/10.1038/ncomms5672>.
- Pacheco, F.E.R.C., Caxito, F.D.A., Pedrosa-Soares, A.C., Dussin, I.A., Gonçalves-Dias, T., 2020. Detrital zircon U-Pb and Lu-Hf data for a kinizigite gneiss (Jequitinhonha Complex, Araçuaí Orogen, SE Brazil) constrain the age of a huge storage of Ediacaran carbon. *J. S. Am. Earth Sci.* <https://doi.org/10.1016/j.jsames.2020.102709>. 102709.
- Paul, J., Peryt, T., 2000. Kalkowsky's stromatolites revisited (Lower Triassic Buntsandstein, Harz Mountains, Germany). *Palaeogeogr. Palaeoclimatol. Palaeoecol.* 161, 435–458. [https://doi.org/10.1016/S0031-0182\(00\)00098-5](https://doi.org/10.1016/S0031-0182(00)00098-5).
- Paula-Santos, G.M., Babinski, M., Kuchenbecker, M., Caetano-Filho, S., Trindade, R.I., Pedrosa-Soares, A.C., 2015. New evidence of an Ediacaran age for the Bambuí Group in southern São Francisco craton (eastern Brazil) from zircon U-Pb data and isotope chemostratigraphy. *Gondwana Res.* 28, 702–720. <https://doi.org/10.1016/j.gr.2014.07.012>.
- Paula-Santos, G.M., Caetano-Filho, S., Babinski, M., Trindade, R.I., Guacaneme, C., 2017. Tracking connection and restriction of West Gondwana São Francisco Basin through isotope chemostratigraphy. *Gondwana Res.* 42, 280–305. <https://doi.org/10.1016/j.gr.2016.10.012>.
- Paulsen, T., Deering, C., Sliwinski, J., Bachmann, O., Guillong, M., 2017. Evidence for a spike in mantle carbon outgassing during the Ediacaran period. *Nat. Geosci.* 10, 930–934. <https://doi.org/10.1038/s41561-017-0011-6>.
- Pedrosa-Soares, A., De Campos, C.P., Noce, C., Silva, L.C., Novo, T., Roncato, J., Medeiros, S., Castañeda, C., Queiroga, G., Dantas, E., 2011. Late Neoproterozoic-Cambrian granitic magmatism in the Araçuaí orogen (Brazil), the Eastern Brazilian Pegmatite Province and related mineral resources. *Geol. Soc., London, Spl. Publ.* 350, 25–51. <https://doi.org/10.1144/SP350.3>.
- Peng, Y., Bao, H., Pratt, L.M., Kaufman, A.J., Jiang, G., Boyd, D., Wang, Q., Zhou, C., Yuan, X., Xiao, S., Loyd, S., 2014. Widespread contamination of carbonate-associated sulfate by present-day secondary atmospheric sulfate: evidence from triple oxygen isotopes. *Geology* 42, 815–818. <https://doi.org/10.1130/g35852.1>.
- Perrella Júnior, P., Uhlein, A., Uhlein, G.J., Sial, A.N., Pedrosa-Soares, A.C., Lima, O.N.B.d., 2017. Facies analysis, sequence stratigraphy and chemostratigraphy of the Sete Lagoas Formation (Bambuí Group), northern Minas Gerais State, Brazil: evidence of a cap carbonate deposited on the Januária basement high. *Braz. J. Geol.* 47, 59–77. <https://doi.org/10.1590/2317-4889201720160112>.
- Petrov, P.Y., Pokrovsky, B., 2020. Carbon isotope evidence of methanogenesis in sediments of the Dal'naya Taiga Group (Lower Vendian of the Patom Basin, Siberia). *Lithol. Min. Resour.* 55, 83–94. <https://doi.org/10.1134/S0024490220020066>.
- Pierre, C., Blanc-Valleron, M.M., Caqueneau, S., März, C., Ravelo, A.C., Takahashi, K., Alvarez Zarikian, C., 2016. Mineralogical, geochemical and isotopic characterization of authigenic carbonates from the methane-bearing sediments of the Bering Sea continental margin (IODP Expedition 323, Sites U1343–U1345). *Deep Sea Res. Part II* 125–126, 133–144. <https://doi.org/10.1016/j.dsr2.2014.03.011>.
- Planavsky, N.J., Bekker, A., Hofmann, A., Owens, J.D., Lyons, T.W., 2012. Sulfur record of rising and falling marine oxygen and sulfate levels during the Lomagundi event. *Proc. Natl. Acad. Sci.* 109, 18300–18305. <https://doi.org/10.1073/pnas.1120387109>.
- Pratt, B.R., 1998. Syneresis cracks: subaqueous shrinkage in argillaceous sediments caused by earthquake-induced dewatering. *Sed. Geol.* 117, 1–10. [https://doi.org/10.1016/S0037-0738\(98\)00023-2](https://doi.org/10.1016/S0037-0738(98)00023-2).
- Prave, A.R., Condon, D.J., Hoffmann, K.H., Tapster, S., Fallick, A.E., 2016. Duration and nature of the end-Cryogenian (Marinoan) glaciation. *Geology* 44, 631–634. <https://doi.org/10.1130/g38089.1>.
- Prokoff, A., Shields, G.A., Veizer, J., 2008. Compilation and time-series analysis of a marine carbonate $\delta^{18}\text{O}$, $\delta^{13}\text{C}$, $^{87}\text{Sr}/^{86}\text{Sr}$ and $\delta^{34}\text{S}$ database through Earth history. *Earth Sci. Rev.* 87, 113–133. <https://doi.org/10.1016/j.earscirev.2007.12.003>.
- Reis, H.L.S., Suss, J.F., 2016. Mixed carbonate-siliciclastic sedimentation in forebulge grabens: an example from the Ediacaran Bambuí group, São Francisco Basin, Brazil. *Sed. Geol.* 339, 83–103. <https://doi.org/10.1016/j.sedgeo.2016.04.004>.
- Reis, H.L.S., Suss, J.F., Fonseca, R.C.S., Alkmim, F.F., 2017. Ediacaran forebulge grabens of the southern São Francisco basin, SE Brazil: Craton interior dynamics during West Gondwana assembly. *Precamb. Res.* 302, 150–170. <https://doi.org/10.1016/j.precambres.2017.09.023>.
- Ries, J.B., Fike, D.A., Pratt, L.M., Lyons, T.W., Grotzinger, J.P., 2009. Superheavy pyrite ($\delta^{34}\text{S}_{\text{pyr}} > \delta^{34}\text{S}_{\text{CAS}}$) in the terminal Proterozoic Nama Group, southern Namibia: a consequence of low seawater sulfate at the dawn of animal life. *Geology* 37, 743–746. <https://doi.org/10.1130/g25775a.1>.
- Ripperdan, R.L., 2001. Stratigraphic variation in marine carbonate carbon isotope ratios. In: Valley, J.W., Cole, D.R. (Eds.), *Reviews in Mineralogy and Geochemistry: Stable Isotope Geochemistry*. The Mineralogical Society of America, Washington, D.C., pp. 637–662. <https://doi.org/10.2138/gsrmg.43.1.637>.
- Rodrigues, J.B., 2008. Proveniência de sedimentos dos grupos Canastra, Ibiá, Vazante e Bambuí: um estudo de zircões detriticos e idades modelo Sm-Nd. Ph.D. dissertation, Universidade de Brasília, Brazil, 128 pp.
- Rose, C.V., Swanson-Hysell, N.L., Husson, J.M., Poppick, L.N., Cottle, J.M., Schoene, B., Malooof, A.C., 2012. Constraints on the origin and relative timing of the Trezona $\delta^{13}\text{C}$ anomaly below the end-Cryogenian glaciation. *Earth Planet. Sci. Lett.* 319–320, 241–250. <https://doi.org/10.1016/j.epsl.2011.12.027>.
- Rothman, D.H., Hayes, J.M., Summons, R.E., 2003. Dynamics of the Neoproterozoic carbon cycle. *Proc. Natl. Acad. Sci.* 100, 8124–8129. <https://doi.org/10.1073/pnas.0832439100>.
- Sackett, W.M., Nakaparksin, S., Dalrymple, D., 1968. Carbon isotope effects in methane production by thermal cracking. In: Hobson, G.D., Speers, G.C. (Eds.), *Advances in Organic Geochemistry-1966*. Pergamon Press, New York, pp. 37–53.
- Sackett, W.M., 1978. Carbon and hydrogen isotope effects during the thermocatalytic production of hydrocarbons in laboratory simulation experiments. *Geochim. Cosmochim. Acta* 42, 571–580. [https://doi.org/10.1016/0016-7037\(78\)90002-9](https://doi.org/10.1016/0016-7037(78)90002-9).
- Sawaki, Y., Ohno, T., Tahata, M., Komiya, T., Hirata, T., Maruyama, S., Windley, B.F., Han, J., Shu, D., Li, Y., 2010. The Ediacaran radiogenic Sr isotope excursion in the

- Doushantuo Formation in the Three Gorges area, South China. *Precamb. Res.* 176, 46–64. <https://doi.org/10.1016/j.precamres.2009.10.006>.
- Schidlowski, M., 1987. Application of stable carbon isotopes to early biochemical evolution on Earth. *Annu. Rev. Earth Planet. Sci.* 15, 47–72. <https://doi.org/10.1146/annurev.ea.15.050187.000403>.
- Schobben, M., Stebbins, A., Ghaderi, A., Strauss, H., Korn, D., Korte, C., 2015. Flourishing ocean drives the end-Permian marine mass extinction. *Proc. Natl. Acad. Sci.* 112, 10298–10303. <https://doi.org/10.1073/pnas.1503755112>.
- Schrag, D.P., Higgins, J.A., Macdonald, F.A., Johnston, D.T., 2013. Authigenic carbonate and the history of the global carbon cycle. *Science* 339, 540–543. <https://doi.org/10.1126/science.1229578>.
- Schwab, V., Spangenberg, J.E., Grimalt, J.O., 2005. Chemical and carbon isotopic evolution of hydrocarbons during prograde metamorphism from 100°C to 550°C: Case study in the Liassic black shale formation of Central Swiss Alps. *Geochim. Cosmochim. Acta* 69, 1825–1840. <https://doi.org/10.1016/j.gca.2004.09.011>.
- Shen, B., Dong, L., Xiao, S., Lang, X., Huang, K., Peng, Y., Zhou, C., Ke, S., Liu, P., 2016. Molar tooth carbonates and benthic methane fluxes in Proterozoic oceans. *Nat. Commun.* 7, 10317. <https://doi.org/10.1038/ncomms10317>.
- Shields-Zhou, G.A., Hill, A.C., Macgabhann, B.A., 2012. The Cryogenian Period. In: Gradstein, F.M., Ogg, J.G., Schmitz, M.D., Ogg, G.M. (Eds.), *The Geologic Time Scale*. Elsevier, Boston, USA, pp. 393–411. <https://doi.org/10.1016/b978-0-444-59425-9.00017-2>.
- Shields, G., Stille, P., Brasier, M.D., Atudorei, N.V., 1997. Stratified oceans and oxygenation of the late Precambrian environment: a post glacial geochemical record from the Neoproterozoic of W. Mongolia. *Terra Nova* 9, 218–222. <https://doi.org/10.1111/j.1365-3121.1997.tb00016.x>.
- Shields, G.A., Brasier, M.D., Stille, P., Dorjnamjaa, D.-I., 2002. Factors contributing to high $\delta^{13}\text{C}$ values in Cryogenian limestones of western Mongolia. *Earth Planet. Sci. Lett.* 196, 99–111. [https://doi.org/10.1016/S0012-821X\(02\)00461-2](https://doi.org/10.1016/S0012-821X(02)00461-2).
- Shields, G.A., Mills, B.J.W., 2017. Tectonic controls on the long-term carbon isotope mass balance. *Proc. Natl. Acad. Sci.* 114, 4318–4323. <https://doi.org/10.1073/pnas.1614506114>.
- Shields, G.A., Mills, B.J.W., Zhu, M., Raub, T.D., Daines, S.J., Lenton, T.M., 2019. Unique Neoproterozoic carbon isotope excursions sustained by coupled evaporite dissolution and pyrite burial. *Nat. Geosci.* 12, 823–827. <https://doi.org/10.1038/s41561-019-0434-3>.
- Sial, A.N., Gaucher, C., Misi, A., Boggiani, P.C., Alvarenga, C.J.S.D., Ferreira, V.P., Pimentel, M.M., Pedreira, J.A., Warren, L.V., Fernández-Ramírez, R., Geraldés, M., Pereira, N.S., Chigliano, L., Cezario, W.D.S., 2016. Correlations of some Neoproterozoic carbonate-dominated successions in South America based on high-resolution chemostratigraphy. *Braz. J. Geol.* 46, 439–488. <https://doi.org/10.1590/2317-4889201620160079>.
- Siewers, F.D., 2003. Oolite and coated grains. In: Middleton, G.V., Church, M.J., Coniglio, M., Hardie, L.A., Longstaffe, F.J. (Eds.), *Encyclopedia of Sediments and Sedimentary Rocks*. Springer, Netherlands, Dordrecht, pp. 502–506. https://doi.org/10.1007/978-1-4020-3609-5_150.
- Simonet, B.R., Brenner, S., Peters, K., Kaplan, I., 1981. Thermal alteration of Cretaceous black shale by diabase intrusions in the Eastern Atlantic—II. Effects on bitumen and kerogen. *Geochim. Cosmochim. Acta* 45, 1581–1602. [https://doi.org/10.1016/0016-7037\(81\)90287-8](https://doi.org/10.1016/0016-7037(81)90287-8).
- Sperling, E.A., Wolock, C.J., Morgan, A.S., Gill, B.C., Kunzmann, M., Halverson, G.P., Macdonald, F.A., Knoll, A.H., Johnston, D.T., 2015. Statistical analysis of iron geochemical data suggests limited late Proterozoic oxygenation. *Nature* 523, 451–454. <https://doi.org/10.1038/nature14589>.
- Stiller, M., Rounick, J.S., Shasha, S., 1985. Extreme carbon-isotope enrichments in evaporating brines. *Nature* 316, 434–435. <https://doi.org/10.1038/316434a0>.
- Strauss, H., Des Marais, D.J., Hayes, J.M., Summons, R.E., 1992. The carbon-isotopic record. In: Schopf, J.W., Klein, C. (Eds.), *The Proterozoic Biosphere: A Multidisciplinary Study*. Cambridge University Press, Cambridge.
- Summons, R.E., Hayes, J.M., 1992. Principles of molecular and isotopic biogeochemistry. In: Schopf, J.W., Klein, C. (Eds.), *The Proterozoic Biosphere: A Multidisciplinary Study*. Cambridge University Press, Cambridge, pp. 83–93.
- Sun, X., Turchyn, A.V., 2014. Significant contribution of authigenic carbonate to marine carbon burial. *Nat. Geosci.* 7, 201–204. <https://doi.org/10.1038/ngeo2070>.
- Swanson-Hysell, N.L., Rose, C.V., Calmet, C.C., Halverson, G.P., Hurtgen, M.T., Maloof, A.C., 2010. Cryogenian glaciation and the onset of carbon-isotope decoupling. *Science* 328, 608–611. <https://doi.org/10.1126/science.1184508>.
- Talbot, M., Kelts, K., 1986. Primary and diagenetic carbonates in the anoxic sediments of Lake Bosumtwi, Ghana. *Geology* 14, 912–916. [https://doi.org/10.1130/0091-7613\(1986\)14<912:padcit>2.0.co;2](https://doi.org/10.1130/0091-7613(1986)14<912:padcit>2.0.co;2).
- Tavares, T.D., Martins, M.D.S., Alkmim, F.F., Lana, C., 2020. Detrital zircons from the Upper Três Marias Formation, São Francisco basin, SE Brazil: Record of foreland deposition during the Cambrian? *J. S. Am. Earth Sci.* 97, 102395. <https://doi.org/10.1016/j.jsames.2019.102395>.
- Tohver, E., Cawood, P.A., Rossello, E.A., Jourdan, F., 2012. Closure of the Clymene Ocean and formation of West Gondwana in the Cambrian: evidence from the Sierras Australes of the southernmost Rio de la Plata craton, Argentina. *Gondwana Res.* 21, 394–405. <https://doi.org/10.1016/j.jgr.2011.04.001>.
- Trindade, R.I., D'Agrella-Filho, M.S., Epof, I., Neves, B.B.B., 2006. Paleomagnetism of Early Cambrian Itabaiana mafic dikes (NE Brazil) and the final assembly of Gondwana. *Earth Planet. Sci. Lett.* 244, 361–377. <https://doi.org/10.1016/j.epsl.2005.12.039>.
- Trower, E.J., Lamb, M.P., Fischer, W.W., 2017. Experimental evidence that ooid size reflects a dynamic equilibrium between rapid precipitation and abrasion rates. *Earth Planet. Sci. Lett.* 468, 112–118. <https://doi.org/10.1016/j.epsl.2017.04.004>.
- Uhlein, G.J., Uhlein, A., Stevenson, R., Halverson, G.P., Caxito, F.A., Cox, G.M., 2017. Early to late ediacaran conglomeratic wedges from a complete foreland basin cycle in the southwest São Francisco Craton, Bambuí Group, Brazil. *Precamb. Res.* 299, 101–116. <https://doi.org/10.1016/j.precamres.2017.07.020>.
- Uhlein, G.J., Uhlein, A., Pereira, E., Caxito, F.A., Okubo, J., Warren, L.V., Sial, A.N., 2019. Ediacaran paleoenvironmental changes recorded in the mixed carbonate-siliciclastic Bambuí Basin, Brazil. *Palaeogeogr. Palaeoclimatol. Palaeoecol.* 517, 39–51. <https://doi.org/10.1016/j.palaeo.2018.12.022>.
- Valero-Garcés, B., Delgado-Huertas, A., Ratto, N., Navas, A., Edwards, L., 2000. Paleohydrology of Andean saline lakes from sedimentological and isotopic records, Northwest Argentina. *J. Paleolimnol.* 24, 343–359. <https://doi.org/10.1023/A:1008146122074>.
- Walter, M.R., Veevers, J.J., Calver, C.R., Gorjan, P., Hill, A.C., 2000. Dating the 840–544 Ma Neoproterozoic interval by isotopes of strontium, carbon, and sulfur in seawater, and some interpretative models. *Precamb. Res.* 100, 371–433. [https://doi.org/10.1016/S0301-9268\(99\)00082-0](https://doi.org/10.1016/S0301-9268(99)00082-0).
- Warren, L.V., Fairchild, T.R., Gaucher, C., Boggiani, P.C., Poire, D.G., Anelli, L.E., Inchausti, J.C., 2011. *Corumbella* and *in situ Cloudina* in association with thrombolites in the Ediacaran Itapucumi Group, Paraguay. *Terra Nova* 23, 382–389. <https://doi.org/10.1111/j.1365-3121.2011.01023.x>.
- Warren, L.V., Quaglio, F., Riccomini, C., Simões, M.G., Poiré, D.G., Strikis, N.M., Anelli, L.E., Strikis, P.C., 2014. The puzzle assembled: Ediacaran guide fossil *Cloudina* reveals an old proto-Gondwana seaway. *Geology* 42, 391–394. <https://doi.org/10.1130/g35304.1>.
- Warren, L.V., Quaglio, F., Simões, M.G., Gaucher, C., Riccomini, C., Poiré, D.G., Freitas, B.T., Boggiani, P.C., Sial, A.N., 2017. *Cloudina-Corumbella-Namacalathus* association from the Itapucumi Group, Paraguay: Increasing ecosystem complexity and tiering at the end of the Ediacaran. *Precamb. Res.* 298, 79–87. <https://doi.org/10.1016/j.precamres.2017.05.003>.
- Wehrmann, L.M., Risgaard-Petersen, N., Schrum, H.N., Walsh, E.A., Huh, Y., Ikehara, M., Pierre, C., D'Hondt, S., Ferdelman, T.G., Ravelo, A.C., Takahashi, K., Zarkian, C.A., 2011. Coupled organic and inorganic carbon cycling in the deep seafloor sediment of the northeastern Bering Sea Slope (IODP Exp. 323). *Chem. Geol.* 284, 251–261. <https://doi.org/10.1016/j.chemgeo.2011.03.002>.
- Wohlwend, S., Hart, M., Weissert, H., 2016. Chemostratigraphy of the Upper Albian to mid-Turonian Natih Formation (Oman) – how authigenic carbonate changes a global pattern. *Depos. Record* 2, 97–117. <https://doi.org/10.1002/dep2.15>.
- Wotte, T., Shields-Zhou, G.A., Strauss, H., 2012. Carbonate-associated sulfate: Experimental comparisons of common extraction methods and recommendations toward a standard analytical protocol. *Chem. Geol.* 326–327, 132–144. <https://doi.org/10.1016/j.chemgeo.2012.07.020>.
- Xiao, S., Narbonne, G.M., Zhou, C., Laflamme, M., Grazhdankin, D.V., Moczyłowska-Vidal, M., Cui, H., 2016. Toward an Ediacaran time scale: problems, protocols, and prospects. *Episodes* 39, 540–555. <https://doi.org/10.18814/epiugs/2016/v39i4/103886>.
- Xiao, S., Cui, H., Kang, J., McFadden, K.A., Kaufman, A.J., Kitajima, K., Fournelle, J.H., Valley, J.W., 2019. Using SIMS data to understand the role of authigenic carbonate in the origin of chaotic stratigraphic variations of carbon isotopes in the early Ediacaran Doushantuo Formation. Geological Society of America annual meeting, Phoenix, Arizona, USA. <https://doi.org/10.1130/abs/2019AM-335046>.
- Xiao, S., Cui, H., Kang, J., McFadden, K.A., Kaufman, A.J., Kitajima, K., Fournelle, J.H., Schwid, M., Nolan, M., Baele, J.-M., Valley, J.W., 2020. Using SIMS to decode noisy stratigraphic $\delta^{13}\text{C}$ variations in Ediacaran carbonates. *Precamb. Res.* 343, 105686. <https://doi.org/10.1016/j.precamres.2020.105686>.
- Yochelson, E.L., Stump, E., 1977. Discovery of early Cambrian fossils at Taylor Nunatak, Antarctica. *J. Paleontol.* 51, 872–875. <https://doi.org/10.2307/1303753>.
- Zhang, F., Xiao, S., Romaniello, S.J., Hardisty, D., Li, C., Melezhik, V., Pokrovsky, B., Cheng, M., Shi, W., Lenton, T.M., Anbar, A.D., 2019. Global marine redox changes drove the rise and fall of the Ediacara biota. *Geobiology* 17, 594–610. <https://doi.org/10.1111/gbi.12359>.
- Zhou, C., Bao, H., Peng, Y., Yuan, X., 2010. Timing the deposition of ^{17}O -depleted barite at the aftermath of Nantuo glacial meltdown in South China. *Geology* 38, 903–906. <https://doi.org/10.1130/g31224.1>.
- Zhou, C., Guan, C., Cui, H., Ouyang, Q., Wang, W., 2016. Methane-derived authigenic carbonate from the lower Doushantuo Formation of South China: implications for seawater sulfate concentration and global carbon cycle in the early Ediacaran ocean. *Palaeogeogr. Palaeoclimatol. Palaeoecol.* 461, 145–155. <https://doi.org/10.1016/j.palaeo.2016.08.017>.